

1977

# An Investigation Of Anomalous Scattering Of Laser Radiation By A Theta-pinch Plasma

Andrew Kam-hung Ng

Follow this and additional works at: <https://ir.lib.uwo.ca/digitizedtheses>

---

## Recommended Citation

Ng, Andrew Kam-hung, "An Investigation Of Anomalous Scattering Of Laser Radiation By A Theta-pinch Plasma" (1977). *Digitized Theses*. 1049.

<https://ir.lib.uwo.ca/digitizedtheses/1049>

This Dissertation is brought to you for free and open access by the Digitized Special Collections at Scholarship@Western. It has been accepted for inclusion in Digitized Theses by an authorized administrator of Scholarship@Western. For more information, please contact [tadam@uwo.ca](mailto:tadam@uwo.ca), [wlsadmin@uwo.ca](mailto:wlsadmin@uwo.ca).



National Library of Canada

Cataloguing Branch  
Canadian Theses Division

Ottawa, Canada  
K1A 0N4

Bibliothèque nationale du Canada

Direction du catalogage  
Division des thèses canadiennes

## NOTICE

The quality of this microfiche is heavily dependent upon the quality of the original thesis submitted for microfilming. Every effort has been made to ensure the highest quality of reproduction possible.

If pages are missing, contact the university which granted the degree.

Some pages may have indistinct print especially if the original pages were typed with a poor typewriter ribbon or if the university sent us a poor photocopy.

Previously copyrighted materials (journal articles, published tests, etc.) are not filmed.

Reproduction in full or in part of this film is governed by the Canadian Copyright Act, R.S.C. 1970, c. C-30. Please read the authorization forms which accompany this thesis.

**THIS DISSERTATION  
HAS BEEN MICROFILMED  
EXACTLY AS RECEIVED**

## AVIS

La qualité de cette microfiche dépend grandement de la qualité de la thèse soumise au microfilmage. Nous avons tout fait pour assurer une qualité supérieure de reproduction.

S'il manque des pages, veuillez communiquer avec l'université qui a conféré le grade.

La qualité d'impression de certaines pages peut laisser à désirer, surtout si les pages originales ont été dactylographiées à l'aide d'un ruban usé ou si l'université nous a fait parvenir une photocopie de mauvaise qualité.

Les documents qui font déjà l'objet d'un droit d'auteur (articles de revue, examens publiés, etc.) ne sont pas microfilmés.

La reproduction, même partielle, de ce microfilm est soumise à la Loi canadienne sur le droit d'auteur, SRC 1970, c. C-30. Veuillez prendre connaissance des formules d'autorisation qui accompagnent cette thèse.

**LA THÈSE A ÉTÉ  
MICROFILMÉE TELLE QUE  
NOUS L'AVONS REÇUE**

AN INVESTIGATION OF ANOMALOUS  
SCATTERING OF LASER RADIATION  
BY A THETA-PINCH PLASMA

by

Andrew Kam-Hung Ng

Department of Physics

Submitted in partial fulfillment  
of the requirements for the degree of  
Doctor of Philosophy

Faculty of Graduate Studies  
The University of Western Ontario  
London, Ontario  
October, 1976

© Andrew Kam-Hung Ng 1976.

## ABSTRACT

An experiment has been performed to observe the anomalous scattering of ruby laser radiation from a theta-pinch plasma. Measurement of the scattered spectra was achieved using a specially designed and developed multi-channel spectrometer system. This system consists of four individual channels with which one is able to not only scan simultaneously the red-shifted and the blue-shifted sides of the scattered spectrum, but, at the same time, also monitor the "shot-to-shot" variations in the plasma electron density and electron temperature. Two sets of  $90^\circ$ -scattering measurements are presented, one for a plasma discharge that was formed at an initial hydrogen filling pressure of 20 milliTorr (Case 1) and the other for a discharge formed at 50 milliTorr (Case 2). Photographic study using an image converter camera showed that, at the time scattering measurements were made, both discharges were macroscopically uniform and quiescent although the diameters of the two plasma columns differed by almost a factor of two. In both cases, the measured scattered spectra revealed anomalous structures which were not predicted by theory for a thermal plasma. These anomalies appeared as oscillations superimposed on the thermal spectrum and were symmetrical with respect to the incident wavelength. In Case 1, enhancement of approximately 100% in the

scattering cross section corresponding to the ion spectrum was also observed. The results were interpreted as an observation of non-thermal density fluctuations in the plasma. The anomalies seemed to be correlated with harmonics of the plasma frequency and were qualitatively similar to those reported in some measurements made on different arc plasmas which, like the theta-pinch plasma studied here, were cold, dense plasmas. This is of particular interest in the study of anomalous scattering of laser radiation by plasmas as it may be an indication of the fundamental nature of the phenomenon. The present results also suggested that the deviations from standard scattering theories were not correlated with the plasma approximation used in the theories and were not caused by macroscopic nonuniformities in the plasma.

## ACKNOWLEDGEMENTS

The author wishes to express his sincere thanks to Dr. P. K. John for his guidance and encouragement throughout the course of this investigation.

He also wishes to thank Dr. E. Brannen and Dr. T. D. Gaily for their valuable criticism and suggestions.

Special thanks are extended to Dr. D. R. Moorcroft for his enlightening discussions and suggestions in statistical analysis of experimental data, and to Dr. M. Crocker for providing a computer program which is most essential for the successful analysis of the experimental data.

Financial supports, in the form of Faculty of Graduate Studies Special Teaching Assistantships (1970-1971 and 1974-1976), a National Research Council of Canada Scholarship (1971-1974) and a Province of Ontario Graduate Fellowship (1974-1976), are gratefully acknowledged.

*To my wife Pauline*

## TABLE OF CONTENTS

	Page
CERTIFICATE OF EXAMINATION .....	ii
ABSTRACT .....	iii
ACKNOWLEDGEMENTS .....	v
TABLE OF CONTENTS .....	vii
LIST OF FIGURES .....	xi
LIST OF TABLES .....	xiv
CHAPTER 1 - INTRODUCTION .....	1
1-1 General Introduction .....	1
1-2 Objectives of Present Work .....	5
CHAPTER 2 - THEORY OF LIGHT SCATTERING BY A PLASMA .....	7
2-1 Introduction .....	7
2-2 Formulation of the Scattering Problem .....	7
2-3 The Electron Density Fluctuation .....	15
2-4 The Scattered Spectrum for a Maxwellian Plasma .....	18
CHAPTER 3 - THE LASER SCATTERING EXPERIMENT .....	26
3-1 The Plasma Source .....	26



	Page
3-2 Light Input System .....	28
3-2.1 The Ruby Laser .....	28
3-2.2 Focusing Optics .....	31
3-3 Light Collection System .....	35
3-3.1 Design Considerations .....	35
3-3.2 Collection Optics and the Spectrometer System .....	47
3-3.3 Optical Alignment .....	50
3-4 Detection System .....	52
3-4.1 Photomultipliers .....	52
3-4.2 Signal Recording .....	54
3-5 Calibration .....	56
3-5.1 Intensity Calibration by Rayleigh Scattering .....	56
3-5.2 Relative Transmission Calibrations in Channels 1 and 2 .....	59
3-5.3 Spectral Calibration .....	61
 CHAPTER 4 - PHOTOGRAPHIC STUDY OF THE THETA-PINCH PLASMA .....	   65
 CHAPTER 5 - RESULTS OF SCATTERING MEASUREMENTS .....	 73
5-1 The Scattering Measurements .....	73
5-2 Procedure for Data Analysis .....	77

	Page
5-3 The Scattered Spectra .....	79
5-3.1 Case 1: Initial Hydrogen Filling Pressure of 20 milliTorra.....	79
5-3.2 Case 2: Initial Hydrogen Filling Pressure of 50 milliTorra .....	83
CHAPTER 6 - DISCUSSIONS .....	88
6-1 Implications of the Experimental Results .....	88
6-1.1 The Anomalies in the Scattered Spectra .....	88
6-1.2 Comparison with Arc Plasmas ....	95
6-1.3 The Plasma Approximation .....	97
6-1.4 Macroscopic Plasma Structure ...	100
6-2 Other Considerations .....	101
6-2.1 Effect of Laser Radiation on the Plasma .....	101
6-2.2 Non-Maxwellian Velocity Distri- bution of Electrons in the Plasma .....	103
6-3 Summary and Conclusions .....	107
APPENDICES .....	111
Appendix A - Rayleigh Scattering Calibration .....	111

Appendix B - The Scattered Spectrum for a  
Plasma with Non-Maxwellian  
Electron Velocity

Distribution .....	115
REFERENCES .....	117
VITA .....	122

## LIST OF FIGURES

Figure	Description	Page
2-1	The geometry for the scattering of an electromagnetic wave by a plasma .....	8
2-2	Vector representation of the scattering process .....	12
2-3	The function $\Gamma_{\alpha}(x)$ for $\alpha=0, .0.5, 1, 2, 3,$ and $4$ .....	22
2-4	Transition of the scattered spectrum from incoherent scattering to coherent scattering .....	25
3-1	Schematics of the theta-pinch configuration .....	27
3-2	Arrangement of the vacuum and gas inlet systems for the theta-pinch .....	29
3-3	Component configuration of the Holobeam Series 600 ruby laser .....	30
3-4	The focusing optics .....	33
3-5	A simple arrangement for the collection optics .....	36
3-6	$S(k)$ as a function of $\alpha$ for $Z=1$ and $T_e=T_i$ .....	41
3-7	Curves of $n_r$ as a function of electron density and electron temperature .....	43
3-8	Curves of $\epsilon$ as a function of electron temperature and electron density .....	46
3-9	Details of the collection optics and the four-channel spectrometer system .....	48
3-10	The prism mount .....	51
3-11	Schematics of the voltage-divider for the photomultipliers .....	53
3-12	Schematics of the high voltage distribution network .....	55

Figure	Description	Page
3-13	Profile of Rayleigh scattered intensity from nitrogen gas at 85 Torr in channel 1 .....	57
3-14	Profile of Rayleigh scattered intensity from nitrogen gas at 85 Torr in channel 2 .....	58
3-15	Rayleigh scattered intensity as a function of nitrogen gas pressure in channel 3 .....	60
3-16	Optical arrangement for spectral calibration of channel 4 .....	63
3-17	Transmission profile of channel 4 .....	64
4-1	Optical arrangement for end-on photographic study of the theta-pinch plasma .....	66
4-2	Photographs showing the compression phase of the plasma during the ninth half cycle of the discharge formed at an initial hydrogen filling pressure of 20 milli-Torr .....	68
4-3	Photographs showing the compression phase of the plasma during the ninth half cycle of the discharge formed at an initial hydrogen filling pressure of 50 milli-Torr .....	70
5-1	Oscillographs of a typical set of laser scattering measurement .....	75
5-2	The red-shifted side of the scattered spectrum for Case 1 .....	80
5-3	The blue-shifted side of the scattered spectrum for Case 1 .....	81
5-4	The red-shifted side of the scattered spectrum for Case 2 .....	85
5-5	The blue-shifted side of the scattered spectrum for Case 2 .....	86
6-1	The red-shifted side of the non-thermal component of the scattered spectrum for Case 1 .....	91

Figure	Description	Page
6-2	The blue-shifted side of the non-thermal component of the scattered spectrum for Case 1 .....	92
6-3	The red-shifted side of the non-thermal component of the scattered spectrum for Case 2 .....	93
6-4	The blue-shifted side of the non-thermal component of the scattered spectrum for Case 2 .....	94
6-5	Calculated scattered spectra for a plasma in thermal equilibrium and for a non-Maxwellian plasma with two arbitrarily imposed secondary, cold, drifting electron components .....	104

LIST OF TABLES

Table	Description	Page
3-1	Description of the optical elements in Fig. 3-9 .....	49
6-1	Comparison between the theta-pinch plasma and some arc plasmas .....	96
6-2	Parameters of the plasmas considered in Fig. 6-5. ....	106

The author of this thesis has granted The University of Western Ontario a non-exclusive license to reproduce and distribute copies of this thesis to users of Western Libraries. Copyright remains with the author.

Electronic theses and dissertations available in The University of Western Ontario's institutional repository (Scholarship@Western) are solely for the purpose of private study and research. They may not be copied or reproduced, except as permitted by copyright laws, without written authority of the copyright owner. Any commercial use or publication is strictly prohibited.

The original copyright license attesting to these terms and signed by the author of this thesis may be found in the original print version of the thesis, held by Western Libraries.

The thesis approval page signed by the examining committee may also be found in the original print version of the thesis held in Western Libraries.

Please contact Western Libraries for further information:

E-mail: [libadmin@uwo.ca](mailto:libadmin@uwo.ca)

Telephone: (519) 661-2111 Ext. 84796

Web site: <http://www.lib.uwo.ca/>



## CHAPTER 1 INTRODUCTION

### 1-1 General Introduction.

Laser light scattering emerged as a potentially powerful technique in the study of laboratory plasmas<sup>(1)</sup> soon after it was shown that laser action in ruby crystal was possible<sup>(2)</sup>. A most important feature of such measurements is that they provide information on one of the most basic properties of a plasma, namely the auto-correlation function of the electron density fluctuation<sup>(3)</sup>. Furthermore, information may also be derived about the density and temperature of the plasma electrons and ions, velocity distribution function of the electrons<sup>(4,5)</sup>, collision processes<sup>(6)</sup>, magnetic fields in the plasma<sup>(7-11)</sup>, and about drifts<sup>(12-16)</sup> in plasmas.

Excellent overviews of laser light scattering on laboratory plasmas including outlines of scattering theory, general considerations and discussions of various scattering experiments are given by Evans and Katzenstein<sup>(3)</sup>; Ramsden<sup>(17)</sup>; Desilva and Goldenbaum<sup>(18)</sup>, and Kunze<sup>(19)</sup>. Work in scattering theory was pioneered by Salpeter<sup>(20)</sup>, Fejer<sup>(21)</sup>, Dougherty and Farley<sup>(22)</sup>, and Rosenbluth and Rostoker<sup>(23)</sup>. The entire theoretical scattering field is reviewed at length by Bernstein et al<sup>(24)</sup>.

While many experimental results agreed with the theory for thermal plasmas, some of them indicated considerable deviations of the electron density fluctuations from their thermal level. For example, deviations were evident in the scattered spectra obtained from theta-pinch plasmas by Evans, Forrest and Katzenstein<sup>(25)</sup>, and Seimon and Benford<sup>(26)</sup> although they have not been commented on by the authors. On the other hand, there were several observations specifically reporting deviations or anomalous features in the scattered spectra. These can be broadly classified into two categories according to the type of plasmas studied in the experiments, namely arc plasmas and theta-pinch plasmas. Observations in the first category can be further subdivided into three groups. In the first group, scattering measurements were made on magnetically stabilized hydrogen arc plasmas. Ringler and Nodwell<sup>(27)</sup> first reported enhancements of the scattering cross section at the central frequency and at the plasma frequency, as well as some indication of enhancement at harmonics of the plasma frequency. In a later measurement<sup>(28)</sup>, they observed not only enhancements at harmonics of the plasma frequency but also, at a particular gas pressure, enhancement at all frequencies. Spectra obtained by Ludwig and Mahn<sup>(11)</sup> revealed enhancements at multiples of half the plasma frequency and the anomaly was independent of the orientation of the scattering wave vector with respect to that of the magnetic field. Yet, measurements with progressively

higher spectral resolutions<sup>(29)</sup> showed that the deviations consisted of seemingly unsystematic, fine structures of modulations. In the second group, scattered spectra were measured from magnetically confined high current helium arc plasmas. Neufeld<sup>(30)</sup> reported enhancement at the central frequency and an unclear indication of enhancement at the plasma frequency whereas results obtained by Meyer and Potocnik<sup>(31)</sup> showed a definite enhancement at the plasma frequency. In the third group, scattering measurements were made on a high current carbon arc plasma by Churchland and Nodwell<sup>(32)</sup>. The spectra showed enhancements at multiples of quarter of the plasma frequency. In the second category, only two observations have been reported. In the scattered spectra obtained by Gondhalekar, Kronast and Benesch<sup>(33)</sup>, two anomalies were observed: (i) an anomalous blue shift of the entire spectrum, and (ii) in one of the spectra, an apparent "dip" in each of the red-shifted and blue-shifted sides of the spectrum and in the other spectrum, an apparent "dip" in the red-shifted side alone. On the other hand, a "peak" or enhancement was observed in the scattered spectrum obtained by John, Irisawa and Ng<sup>(34)</sup>.

Thus, the anomalies observed in the spectra of laser radiation scattered from plasmas seem varied. Properties of the anomalies are also unclear. In particular, spectrally resolved measurements of both sides of the scattered spectra were made only in the experiment of Gondhalekar et

4

a) (33)\*. However, results of their measurements show that the deviations were symmetrical about the central frequency in one spectrum and asymmetrical in the other. The symmetry property of the anomalous scattering phenomenon, therefore, had yet to be studied. Furthermore, the few measurements made on theta-pinch plasmas are insufficient to allow for a comparison of the anomalies in the scattered spectra measured on theta-pinch plasmas to that on arc plasmas. Such a comparison is of interest as it may provide information on the dependence of the anomalies on plasma device or a particular excitation mechanism.

Evidently, much more work needs to be done before the anomalous scattering phenomenon can be explained. It should be pointed out that understanding of the phenomenon is of great significance in plasma studies not only from the diagnostic point of view, but also from the standpoint of basic understanding of plasma dispersion theory and of non-thermal processes within the plasma.

---

\* In the experiment of Churchland and Nodwell (32), only the frequency integrated intensity in each side of the spectrum was measured as a check for symmetry.

1-2 Objectives of Present Work.

Initiated by the preliminary observation of anomalous scattering of laser radiation from a theta-pinch plasma<sup>(34)</sup>, the present work was conceived as the first phase of a formal investigation of the phenomenon. Hence, the primary objectives of the project included (i) the design and development of the appropriate instrumentation and (ii) the study of some of the properties of the anomalous scattering phenomenon.

The main problem in instrumentation lay in the design of a spectrometer system to be used in  $90^\circ$ -scattering measurements on a theta-pinch plasma. As required by the experimental conditions, the system has to satisfy the following basic criteria.

- (1) Since  $90^\circ$ -scattering measurements yield relatively broad spectra, the system must be usable over a large spectral interval.
- (2) The spectral resolution of the system should be sufficiently high so that anomalous structures or deviations can be resolved.
- (3) The system must allow the measurement of both sides of the scattered spectrum. If point-to-point scanning technique is employed, the two sides should be scanned simultaneously so that the resulting spectral profiles are derived from the same set of scattering measurements.

- (4) All scattering measurements must be made on the same plasma volume.

Furthermore, for scanning measurements of the scattered spectra, specific instrumentation will also be required for monitoring the "shot-to-shot" variations in the plasma discharge.

As for the investigation of the anomalous scattering phenomenon, an attempt will be made to provide information on the following:

- (1) symmetry property of the anomalies in the scattered spectra,
- (2) correlation between the anomalies observed in this experiment and that observed in measurements obtained from arc plasmas,
- (3) possible correlation between the observed deviations from scattering theory and the plasma approximation which is used in the theory, and
- (4) possible dependence of the anomalous scattering phenomenon on the the macroscopic structures of the plasma.

## CHAPTER 2

### THEORY OF LIGHT SCATTERING BY A PLASMA

#### 1-1 Introduction.

In this chapter, the theory of light scattering by a plasma is outlined so as to illustrate the physical meaning of the scattered spectrum and to provide a basis of comparison for the experimental data. In Section 2-2, the basic formulation of the scattering process is described, which shows that the scattered spectrum is a measure of the spectrum of electron density fluctuation, or, electron plasma waves. Calculation of the density fluctuation is described in Section 2-3. The "dressed test particle" approach is followed as it provides a clear physical picture of the various contributions to the total density fluctuation. In Section 2-4, results of the scattering theory for a case of practical interest is described, namely, a Maxwellian plasma in which the velocity distribution of the electrons and that of the ions are Maxwellian although the electron and ion temperatures may differ.

#### 2-2 Formulation of the Scattering Problem.

The geometry for the scattering of an electromagnetic wave by a plasma is shown in Fig. 2-1. We wish to consider

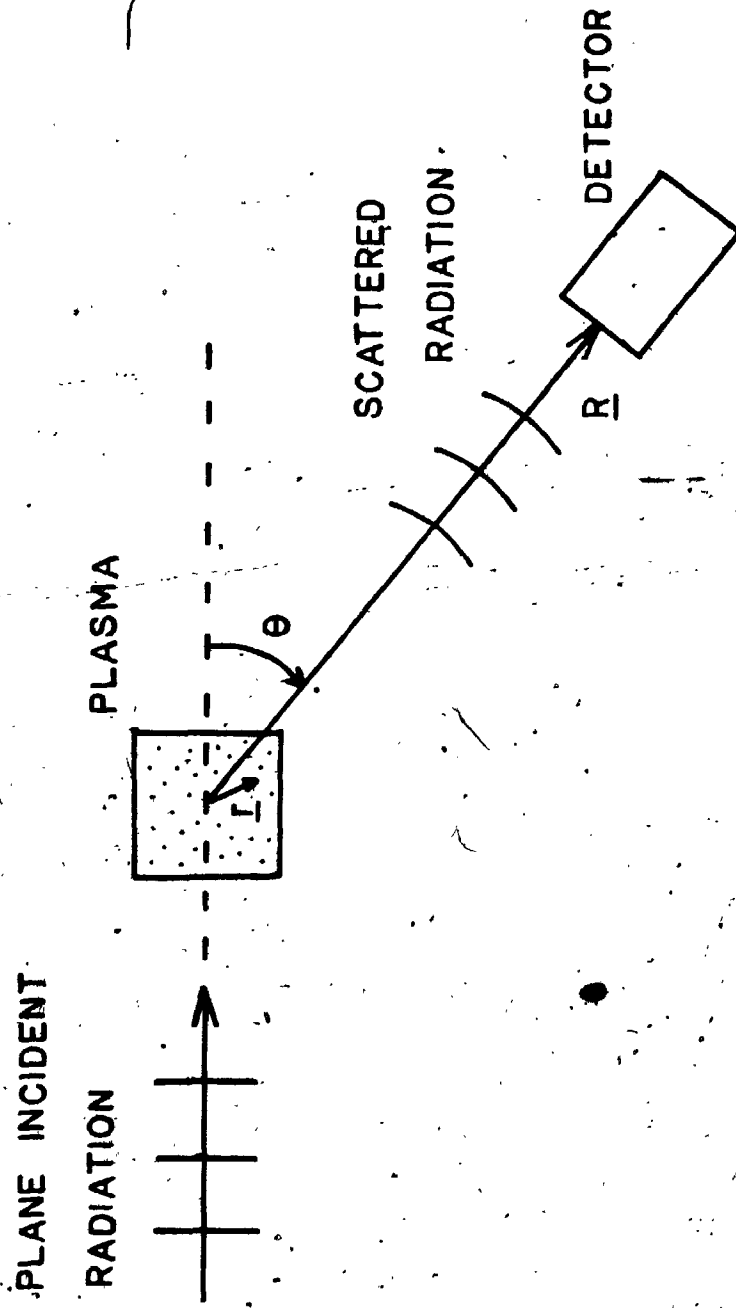


Fig. 2-1 The geometry for the scattering of an electromagnetic wave by a plasma.



the re-radiation by an electron under the influence of the electric field of a monochromatic plane wave of amplitude  $E_0$ , wave vector  $\underline{k}_0$  and frequency  $\omega_0$ . It is assumed that the motion of the electron remains at all times nonrelativistic so that the Lorentz force exerted by the magnetic radiation field can be ignored. Quantum mechanical effects are also neglected. Since only a very small part of the incident radiation is scattered, we can use the first-Born approximation and write the total field at  $\underline{r}_j$  as

$$\underline{E} \approx E_0 \cos(\underline{k}_0 \cdot \underline{r}_j - \omega_0 t)$$

The acceleration of the electron under the action of this radiation field can then be written as

$$\ddot{\underline{r}}(t) = - \left( \frac{e}{m} \right) E_0 \cos\{\underline{k}_0 \cdot \underline{r}_j(t) - \omega_0 t\}$$

where  $e$  and  $m$  are the electron charge and mass respectively.

At the position  $\underline{R}$  of the detector, the vector and the scalar potentials of the electromagnetic field radiated by an electron describing an orbit  $\underline{r}(\underline{t})$  are given by the Liénard-Wiechert potentials<sup>(35)</sup>

$$\underline{A}(\underline{R}, t) = \frac{-(e/c) \dot{\underline{r}}(t^*)}{|\underline{R} - \underline{r}(t^*)| - (1/c) \dot{\underline{r}}(t^*) \cdot \{\underline{R} - \underline{r}(t^*)\}}$$

$$\phi(\underline{R}, t) = \frac{-e}{|\underline{R} - \underline{r}(t^*)| - (1/c) \dot{\underline{r}}(t^*) \cdot \{\underline{R} - \underline{r}(t^*)\}}$$

where the retarded time  $t^*$  is given by

$$t^* \approx t - \frac{R}{c} + \frac{\underline{R} \cdot \underline{r}(t-R/c)}{R c} \quad \text{for } |R| \gg |\underline{r}|.$$

The scattered electromagnetic fields are given in terms of these potentials by

$$\underline{B} = \nabla_R \times \underline{A}$$

$$\underline{E} = -\nabla_R \phi - \left(\frac{1}{c}\right) \frac{\partial \underline{A}}{\partial t}$$

Accordingly, for the  $j^{\text{th}}$  electron,

$$\begin{aligned} \underline{B}_j(\underline{R}, t) &\approx \left(\frac{e}{c^2}\right) \frac{\underline{R} \times \ddot{\underline{r}}_j(t^*)}{R^2} \\ &\approx - \left(\frac{e}{mc^2}\right) \left(\frac{\underline{R} \times \underline{E}_0}{R^2}\right) \times \\ &\quad \cdot \cos\{\underline{k}_0 \cdot \underline{r}_j(t-R/c) = \omega_0 \left(t - \frac{R}{c} + \frac{\underline{R} \cdot \underline{r}_j(t-R/c)}{R c}\right)\} \\ &= - \left(\frac{e}{mc^2}\right) \left(\frac{\underline{R} \times \underline{E}_0}{R^2}\right) \times \\ &\quad \cos\{\underline{k} \cdot \underline{r}_j(t-R/c) - \omega_0(t-R/c)\} \end{aligned}$$

where

$$\underline{k} = \underline{k}_0 - \left(\frac{\omega_0}{c}\right) \frac{\underline{R}}{R}$$

is the differential wave vector of the scattered wave, or simply, the scattering wave vector. The quantity  $(\omega_0/c)(\underline{R}/R)$

is just the propagation vector of the scattered wave. Its magnitude is equal to  $|\underline{k}_0|$ , neglecting Compton effect.

This is justified in the limit of  $h\nu \ll mc^2$  which is strongly satisfied for radiation in the optical spectrum. As shown in Fig. 2-2, the magnitude of  $\underline{k}$  is given by

$$\underline{k} = 2 \left( \frac{\omega_0}{c} \right) \sin\left(\frac{\theta}{2}\right)$$

For an assembly of  $N$  electrons, the total scattered field can then be written as

$$\underline{B}(\underline{R}, t) = -\left(\frac{e^2}{mc^2}\right) \left(\frac{R \times \underline{E}_0}{R^2}\right) \sum_{j=1}^N \cos\{\underline{k} \cdot \underline{r}_j(t-R/c) - \omega_0(t-R/c)\} \quad (2-1)$$

The scattered field of the ions would be given by a similar expression substituting the ion mass and charge. Scattering by ions can therefore be neglected since the fields are three orders of magnitude smaller because of the greater ion mass.

By means of the Wiener-Khinchine theorem<sup>(36)</sup>, the power spectrum of the scattered radiation is given by

$$I(\underline{k}, \omega_s) = \frac{1}{\pi} \int_{-\infty}^{\infty} d\tau e^{i\omega_s \tau} \left(\frac{c}{4\pi}\right) \langle \underline{B}(\underline{R}, t) \underline{B}(\underline{R}, t+\tau) \rangle$$

(2-2)

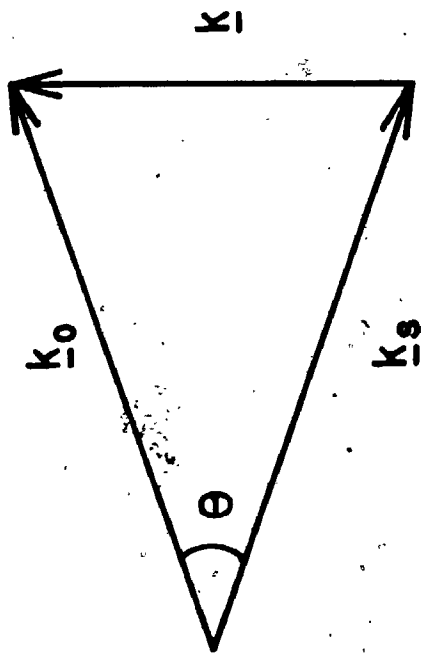


Fig. 2-2 Vector representation of the scattering process.

where  $\langle \rangle$  indicates either time averaging over the variable  $t$  or, equivalently, averaging over the ensemble of collections of electrons which are macroscopically identical. Substituting Eq.(2-1) into Eq.(2-2) and simplifying,

$$I(\underline{k}, \omega_s) = \frac{c}{4\pi} \left( \frac{e^2}{mc^2} \right)^2 \left( \frac{R \times E_0}{R^2} \right) \times \\ \frac{1}{2\pi} \int_{-\infty}^{\infty} d\tau e^{i\omega_s \tau} \langle \sum_{l,j} \cos\{\underline{k} \cdot |\underline{r}_l(t) - \underline{r}_j(t+\tau)| - \omega_0 \tau\} \rangle$$

Furthermore, the density  $n(\underline{r}, t)$  of a collection of  $N$  point electrons is

$$n(\underline{r}, t) = \sum_{j=1}^N \delta\{\underline{r} - \underline{r}_j(t)\}$$

whose Fourier transform is given by

$$n(\underline{k}, t) = \sum_j \exp\{i\underline{k} \cdot \underline{r}_j(t)\}$$

It can be shown that (3).

$$\langle n(\underline{k}, t) n^*(\underline{k}, t+\tau) e^{-i\omega_0 \tau} \rangle = \langle \sum_{l,j} \cos\{\underline{k} \cdot |\underline{r}_l(t) - \underline{r}_j(t+\tau)| - \omega_0 \tau\} \rangle$$

so that

$$I(\underline{k}, \omega) = \frac{c}{4\pi} \left( \frac{e^2}{mc^2} \right) \left( \frac{R \times E_0}{R^2} \right) \times \frac{1}{2\pi} \int_{-\infty}^{\infty} d\tau e^{i\omega \tau} \langle n(\underline{k}, t) n^*(\underline{k}, t+\tau) \rangle$$

where  $\omega = \omega_s - \omega_0$  is the shift in frequency with respect to the laser frequency.

Following the usual specification of a scattering process, a differential scattering cross section  $\sigma(\underline{k}, \omega)$  is defined by

$$I(\underline{k}, \omega) d\omega d\Omega = N I_0 \sigma(\underline{k}, \omega) d\omega d\Omega \quad (2-3)$$

where  $N$  is the total number of scattering centres,  $I_0 = (c/4\pi)E_0^2$  is the incident intensity and  $d\Omega$  is the solid angle. Accordingly, the scattering cross section is given by

$$\begin{aligned} \sigma(\underline{k}, \omega) &= \left(\frac{e^2}{mc^2}\right) \sin^2 \gamma \times \frac{1}{2\pi N} \int_{-\infty}^{\infty} d\tau e^{i\omega\tau} \langle n(\underline{k}, t) n^*(\underline{k}, t+\tau) \rangle \\ &= \sigma_T S(\underline{k}, \omega) \end{aligned} \quad (2-4)$$

where  $\gamma$  is the angle between  $\underline{E}_0$  and  $\underline{R}$ ,  $\sigma_T = (e^2/mc^2)\sin^2 \gamma$  is the well-known Thomson cross section for the scattering of an electromagnetic wave by a free electron and  $S(\underline{k}, \omega)$  is the dynamic form factor (also generally referred to as the scattered spectrum) defined as

$$S(\underline{k}, \omega) = \frac{1}{2\pi N} \int_{-\infty}^{\infty} d\tau e^{i\omega\tau} \langle n(\underline{k}, t) n^*(\underline{k}, t+\tau) \rangle \quad (2-5)$$

Therefore, from the spectrum of scattered radiation, a most fundamental property of plasmas can be studied, namely, the charged particle correlation. Furthermore,  $S(\underline{k}, \omega)$  can be equivalently expressed as (24)

$$S(\underline{k}, \omega) = \frac{1}{2\pi N} \lim_{t' \rightarrow \infty} \frac{\langle |n(\underline{k}, \omega)|^2 \rangle}{2 t'} \quad (2-6)$$

where  $t'$  is the observation time. Accordingly, the scattered spectrum is in fact a measure of the spectrum of electron density fluctuation in the plasma.

### 2-3 The Electron Density Fluctuation.

In the usual formulation of plasma kinetic theory, it is assumed that the state of an infinite, homogeneous plasma can be described in terms of a single particle distribution  $f_e(\underline{r}, \underline{v}, t)$  for the electrons and another such distribution  $f_i(\underline{r}, \underline{v}, t)$  for the ions. For simplicity, only one ion species of mass  $M$  and charge  $Ze$  is considered. For a collisionless plasma and in the absence of externally imposed fields, the Boltzmann equations for these distribution functions are

$$\frac{\partial f_e}{\partial t} + \underline{v} \cdot \nabla f_e - \frac{e}{m} \underline{E}(\underline{r}, t) \cdot \nabla_{\underline{v}} f_e = 0$$

$$\frac{\partial f_i}{\partial t} + \underline{v} \cdot \nabla f_i - \frac{Ze}{M} \underline{E}(\underline{r}, t) \cdot \nabla_{\underline{v}} f_i = 0$$

The internal electric field is given by Poisson's equation

$$\nabla \cdot \underline{E} = 4\pi e \int \{Zf_i(\underline{r}, \underline{v}, t) - f_e(\underline{r}, \underline{v}, t)\} d\underline{v}$$

This set of equations are nonlinear. They are linearized and solved by a perturbation procedure neglecting second and higher order terms in  $f_e$  and  $f_i$ .

In the Landau theory of plasma oscillation, these linearized equations are solved as an initial-value problem; that is, the time evolution of the system is traced from an initial state whose configuration is arbitrary but whose velocity distributions are specified. The time variations of  $f_e$  and  $f_i$  as the state evolves permit the calculation of the autocorrelation function of the density fluctuation. This approach was employed by Salpeter<sup>(20)</sup> and Fejer<sup>(21)</sup>.

An alternative approach is the superposition of "dressed test particles" used by Rosenbluth and Rostoker<sup>(23)</sup>. The distribution functions  $f_e$  and  $f_i$  are assumed to be time independent. A particle in the plasma is taken as a test particle with mass  $m_j$ , charge  $q_j$ , velocity  $\underline{v}_{0j}$  and position vector  $\underline{r}_{0j}$ . The test particle will act to polarize the plasma and therefore carry a screening cloud with it. Clearly, this action corresponds to the establishment of a pair correlation. The electron density fluctuation or the screening cloud associated with the test particle is given by<sup>(3)</sup>

$$n_j(\underline{k}, t) = \left( \frac{-G_e(v_{0j})}{1 - G_e(v_{0j}) - G_i(v_{0j})} \right) \frac{q_j}{e} \exp\{i\mathbf{k} \cdot (\underline{r}_{0j} + \underline{v}_{0j}t)\}$$

where



$$G_e(v_{oj}) = \frac{4\pi e^2}{m k^2} \int \frac{\underline{k} \cdot \nabla_{\underline{v}} f_{e0}(\underline{v})}{\underline{k} \cdot (\underline{v} - \underline{v}_{oj})} d\underline{v} \quad (2-7)$$

$$G_i(v_{oj}) = \frac{4 Z^2 e^2}{M k^2} \int \frac{\underline{k} \cdot \nabla_{\underline{v}} f_{i0}(\underline{v})}{\underline{k} \cdot (\underline{v} - \underline{v}_{oj})} d\underline{v} \quad (2-8)$$

and  $f_{e0}$ ,  $f_{i0}$  are the spatially homogeneous distribution functions of the electrons and ions respectively. The total electron density fluctuation is obtained by summing the individual contributions  $n_j(\underline{k}, t)$  over all of the particles of plasma in which the role of the test particle is played by each particle in turn. In addition, the "self-fluctuation" of the test particle itself must be included if it is an electron. This "self-fluctuation" is the fluctuation in the mean number density that arises from the discreteness of the particles themselves. Thus, the total density fluctuation of the plasma is

$$\begin{aligned} n(\underline{k}, t) &= \sum_{\substack{j=1 \\ \text{electrons}}}^N n_j(\underline{k}, t) + \sum_{l=1}^{N/Z} n_l(\underline{k}, t) \\ &+ \sum_{\substack{j=1 \\ \text{electron} \\ \text{self-fluctuation}}}^N \exp\{i \underline{k} \cdot (\underline{r}_{oj} + \underline{v}_{oj} t)\} \\ &= \sum_{j=1}^N \left[ 1 + \frac{G_e(v_{oj})}{1 - G_e(v_{oj}) - G_i(v_{oj})} \right] \exp\{i \underline{k} \cdot (\underline{r}_{oj} + \underline{v}_{oj} t)\} \\ &- Z \sum_{l=1}^{N/Z} \left[ \frac{G_e(v_{ol})}{1 - G_e(v_{ol}) - G_i(v_{ol})} \right] \exp\{i \underline{k} \cdot (\underline{r}_{ol} + \underline{v}_{ol} t)\} \end{aligned}$$

From this, the autocorrelation function  $\langle n(\underline{k}, t) n^*(\underline{k}, t+\tau) \rangle$  can be calculated and the dynamic form factor can be obtained (3),

$$S(\underline{k}, \omega) = \frac{1}{N} \sum_{j=1}^N \left| \frac{1 - G_i(v_{0j})}{1 - G_e(v_{0j}) - G_i(v_{0j})} \right|^2 \delta(\omega + \underline{k} \cdot \underline{v}_{0j}) \\ + Z^2 \sum_{l=1}^{N/Z} \left| \frac{G_e(v_{0l})}{1 - G_e(v_{0l}) - G_i(v_{0l})} \right|^2 \delta(\omega + \underline{k} \cdot \underline{v}_{0l})$$

The sums can then be evaluated by converting them to integrals over configuration and velocity space weighted by the zero-order distribution functions. Denoting  $F_e(v)$  and  $F_i(v)$  as the zero-order distribution functions for the component of velocity along the  $\underline{k}$  direction, we obtain

$$S(\underline{k}, \omega) = \left| \frac{1 - G_i(\omega/k)}{1 - G_e(\omega/k) - G_i(\omega/k)} \right|^2 F_e(\omega/k) \\ + Z \left| \frac{G_e(\omega/k)}{1 - G_e(\omega/k) - G_i(\omega/k)} \right|^2 F_i(\omega/k) \quad (2-9)$$

#### 2-4 The Scattered Spectrum for a Maxwellian Plasma.

Next, we consider the case of a Maxwellian plasma in which the zero-order velocity distribution functions of the electrons and ions are Maxwellian although the electron and

ion temperatures may be different. Accordingly, we may take for  $f_{e0}$  and  $f_{i0}$  the expressions

$$f_{e0}(\underline{v}) = \left( \frac{n_e}{v_e^3 \pi^{3/2}} \right) \exp\left\{-\left(\frac{v}{v_e}\right)^2\right\} \quad (2-10)$$

$$f_{i0}(\underline{v}) = \frac{n_e}{Z} \left( \frac{1}{v_i^3 \pi^{3/2}} \right) \exp\left\{-\left(\frac{v}{v_i}\right)^2\right\} \quad (2-11)$$

where  $n_e$  is the electron density and  $v_e, v_i$  are respectively the mean thermal speeds of the electrons and the ions, defined as

$$v_e = \left( \frac{2KT_e}{m} \right)^{1/2}$$

$$v_i = \left( \frac{2KT_i}{M} \right)^{1/2}$$

where  $T_e$  and  $T_i$  are the electron and ion temperatures respectively and  $K$  is the Boltzmann constant. Introducing the dimensionless frequency variables defined as  $x_e = \omega/kv_e$  and  $x_i = \omega/kv_i$ , the screening integrals of Eq.(2-7) and Eq.(2-8) can be evaluated as

$$G_e = -\alpha^2 W(x_e) \quad (2-12)$$

$$G_i = -Z \left( \frac{T_e}{T_i} \right) \alpha^2 W(x_i) \quad (2-13)$$

where the scattering parameter  $\alpha = 1/k\lambda_D$  and the Debye length

$$\lambda_D = (KT_e / 4\pi n_e e^2)^{1/2}, \text{ and}$$

$$W(x) = 1 - 2xe^{-x^2} \int_0^x e^{p^2} dp - i\pi^{1/2} x e^{-x^2}$$

Thus, substituting equations (2-10) to (2-13) into Eq. (2-9), we obtain for a Maxwellian plasma,

$$S(\underline{k}, \omega) d\omega = \left| \frac{1 + Z\alpha^2 \left(\frac{T_e}{T_i}\right) W(x_i)}{1 + \alpha^2 W(x_e) + \alpha^2 Z \left(\frac{T_e}{T_i}\right) W(x_i)} \right|^2 \frac{\exp(-x_e^2)}{\pi^{1/2}} dx_e$$

$$+ Z \left| \frac{-\alpha^2 W(x_e)}{1 + \alpha^2 W(x_e) + \alpha^2 Z \left(\frac{T_e}{T_i}\right) W(x_i)} \right|^2 \frac{\exp(-x_i^2)}{\pi^{1/2}} dx_i$$

(2-14)

For values of the electron-ion temperature ratio that are not too large and  $\{(m/M)(T_i/T_e)\}^{1/2} \ll 1$ , the dynamic form factor can be written, using an approximation due to Salpeter<sup>(20)</sup>, as the sum of two terms, each of which is a function of either  $x_e$  or  $x_i$  alone. Accordingly,

$$S(\underline{k}, \omega) d\omega = \left| \frac{1}{1 + \alpha^2 W(x_e)} \right|^2 \frac{\exp(-x_e^2)}{\pi^{1/2}} dx_e$$

$$+ Z \left( \frac{\alpha^2}{1 + \alpha^2} \right) \left| \frac{1}{1 + \alpha^2 W(x_i)} \right|^2 \frac{\exp(-x_i^2)}{\pi^{1/2}} dx_i$$

$$= \Gamma_\alpha(x_e) dx_e + Z \left( \frac{\alpha^2}{1 + \alpha^2} \right) \Gamma_\beta(x_i) dx_i \quad (2-15)$$

where

$$\beta^2 = Z \left( \frac{\alpha^2}{1 + \alpha^2} \right) \frac{T_e}{T_i}$$

$$\Gamma_\alpha(x) = \frac{\exp(-x^2)}{|1 + \alpha^2 W(x)|^2}$$

The first term in Eq.(2-15) is usually referred to as the "electron component" or "electron spectrum" and the second term is the so-called "ion component" or "ion spectrum". The detailed shape of the scattered spectrum depends upon the values of  $\alpha$  and  $\beta$ . Fig. 2-3 shows the function  $\Gamma_\alpha(x)$  for  $\alpha=0, 0.5, 1, 2, 3$  and  $4$ . It follows from Eq.(2-15) that the total scattering cross section  $S(\underline{k}) = \int_{-\infty}^{\infty} S(\underline{k}, \omega) d\omega$  can also be written as the sum of an electron term and an ion

$$S(\underline{k}) = S_e(\underline{k}) + S_i(\underline{k}) \quad (2-16)$$

where

$$S_e(\underline{k}) = \frac{1}{1 + \alpha^2} \quad (2-17)$$

$$S_i(\underline{k}) = \frac{Z \alpha^4}{(1 + \alpha^2) \{1 + \alpha^2 (1 + Z T_e / T_i)\}} \quad (2-18)$$

$$S(\underline{k}) = \frac{1 + \alpha^2 (1 + Z T_e / T_i) + Z \alpha^4}{(1 + \alpha^2) \{1 + \alpha^2 (1 + Z T_e / T_i)\}} \quad (2-19)$$

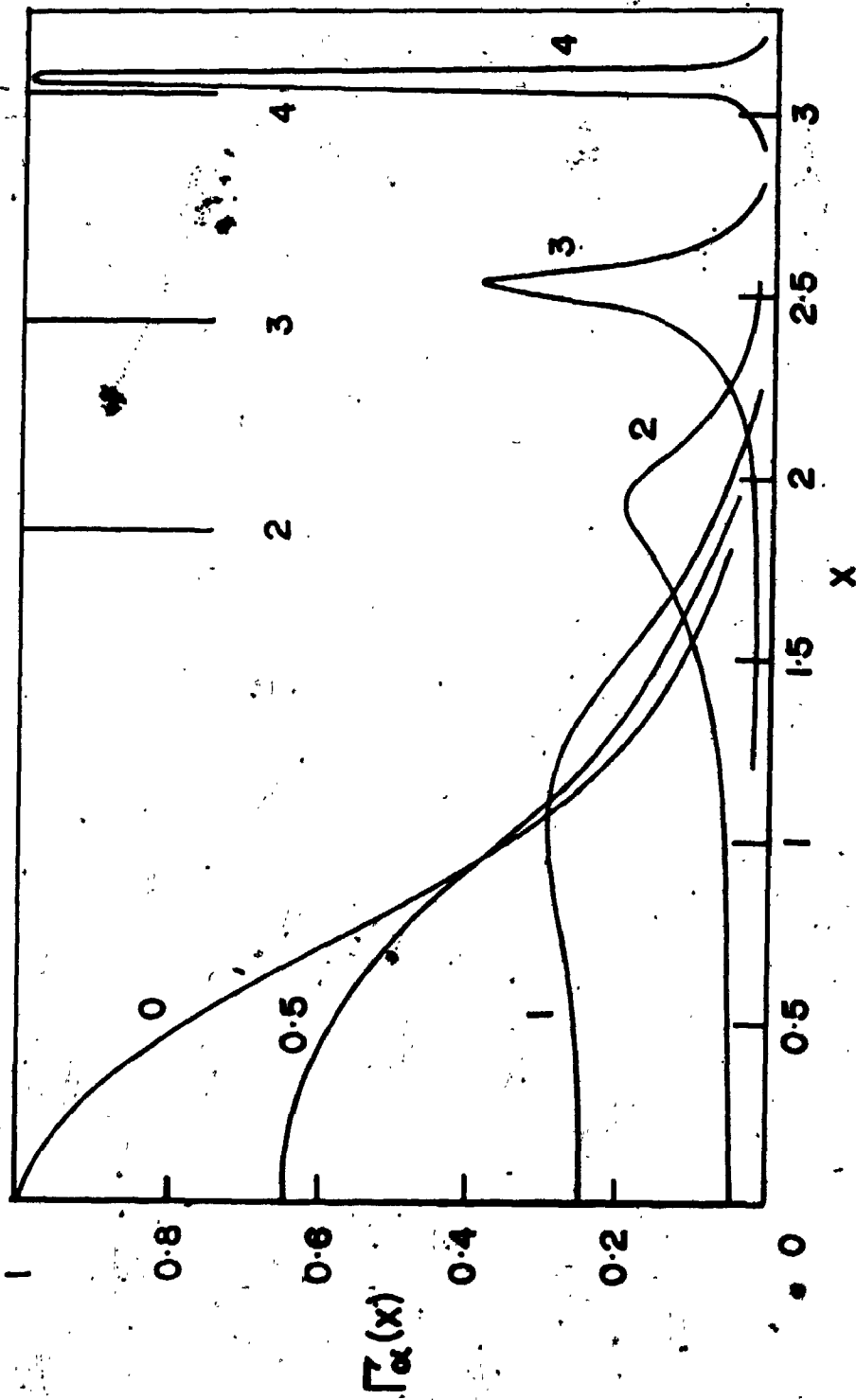


Fig. 2-3 The function  $\Gamma_{\alpha}(x)$  for  $\alpha=0, 0.5, 1, 2, 3, \text{ and } 4$ .  
 ( E.E. Salpeter, Phys. Rev. 120, 1528 (1960) )

It follows then, for  $\alpha \ll 1$  (that is,  $1/k \ll \lambda_D$ ),  $S(\underline{k}) \approx S_e(\underline{k})$  and the scattered intensity is almost exclusively in the electron component with  $S_i(\underline{k}) \approx 0$ . The scattered spectrum approximates a Gaussian function

$$S(\underline{k}, \omega) = \frac{1}{\pi^{1/2} kv_e} \exp\left\{-\left(\frac{\omega}{kv_e}\right)^2\right\} \quad (\alpha \ll 1)$$

Clearly, this is symmetrical with respect to the incident frequency with a half width consistent with the thermal velocity of the electrons. In this short wavelength limit, scattering is due to non-interacting electrons and is called "incoherent" scattering.

As  $\alpha$  approaches unity and beyond, the scattered spectrum begins to show both the electron as well as the ion components. In the limit of  $\alpha \gg 1$  (that is,  $1/k \gg \lambda_D$ ),  $S_e(\underline{k}) \approx 1/\alpha^2$  whereas  $S_i(\underline{k}) \approx 1/2$ . The electron component then becomes two weak satellite lines located symmetrically with respect to the incident frequency at  $\pm\omega_0$  given by

$$\omega_0 \approx \omega_p \left(1 + \frac{3}{\alpha^2}\right)^{1/2}$$

which is the well-known Bohm and Gross dispersion relation for longitudinal plasma waves<sup>(61)</sup>. The shape of the satellite line can be approximated by a Lorentzian function and the width is determined by Landau damping<sup>(62)</sup>. The ion spectrum becomes a relatively intense line centered around

the incident frequency. The shape of the ion line depends on  $\beta$  and hence on  $(T_e/T_i)^{1/2}$ . For values of  $\beta$  less than unity, the ion spectrum approaches a Gaussian function with a half width determined by the ion temperature. Thus, in this long wavelength limit, the scattered spectrum reflects highly correlated electron motions. Scattering is due to lightly damped plasma waves and those electrons shielding the ions. This is referred to as "coherent", "collective" or "cooperative" scattering. The transition of the scattered spectrum from incoherent scattering to coherent scattering is shown in Fig. 2-4.

For comparison with experimental data, the theoretical profiles can be calculated from Eq. (2-9), Eq. (2-14) or Eq. (2-15).



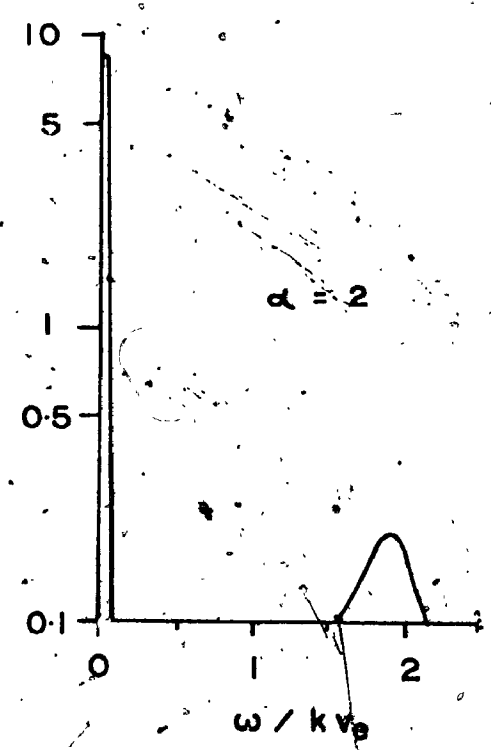
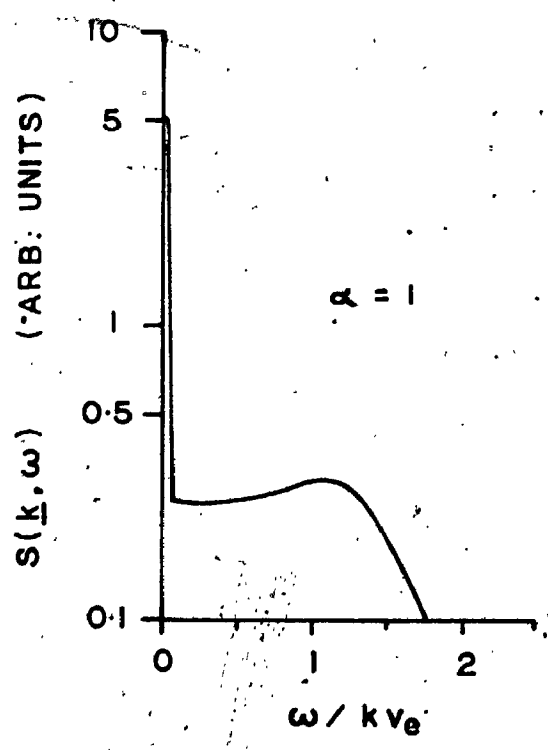
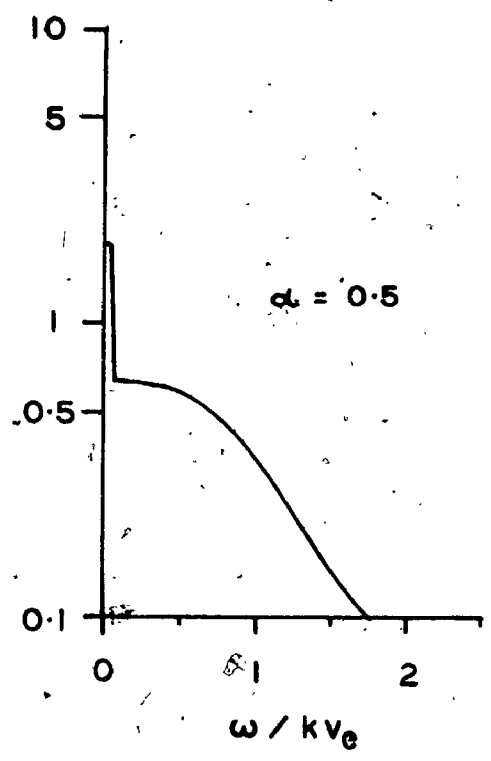
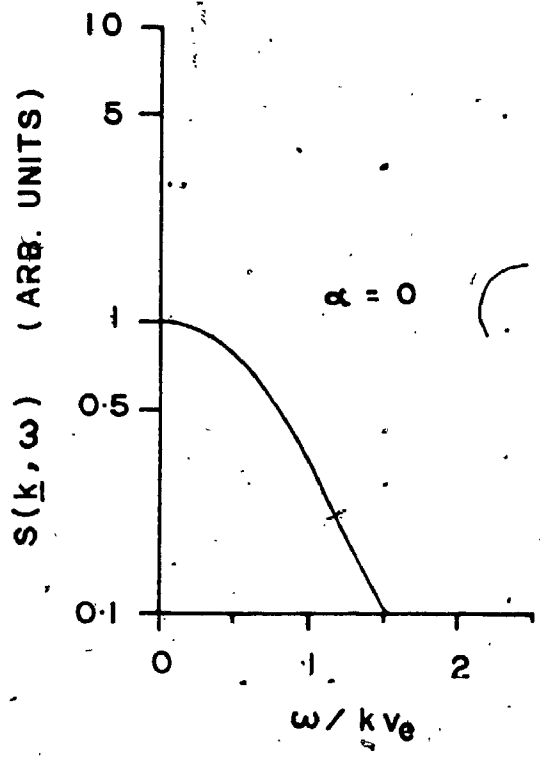
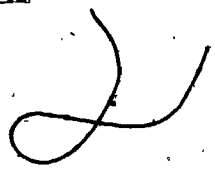


Fig. 2-4 Transition of the scattered spectrum from incoherent scattering to coherent scattering.



## CHAPTER 3

### THE LASER SCATTERING EXPERIMENT

#### 3-1 The Plasma Source.

In this experiment, the plasma studied was produced in a theta-pinch<sup>(37)</sup>. A schematic diagram of the theta-pinch configuration is shown in Fig. 3-1. In essence, the system consists of a low-inductance capacitor connected in parallel to a single turn brass coil which encircles a discharge vessel containing hydrogen gas. The theta-pinch coil is 10.2 cm long with inner and outer diameters of 4.6 cm and 7.1 cm respectively. The capacitor is a 0.75  $\mu$ F, 10 nH Jobe capacitor which is rated for a maximum charging voltage of 40 KV. It was charged by a 50 KV, 16 mA, constant current Universal Voltronics type BAX 50-16-NRC power supply. The capacitor discharge was triggered by a spark gap switch using a pulse from a 15 KV trigger generator through an isolation transformer. A simple form of such a transformer is a six-turn coil of RG 8/U coaxial cable with each turn having a diameter of approximately 15 cm. The inner conductor of the cable was used as the primary coil and the outer one as the secondary coil.

For all scattering measurements, the plasma was formed by a 0.34 KJ ( 30 KV ) discharge. The discharge current exhibited damped harmonic oscillations with ringing period

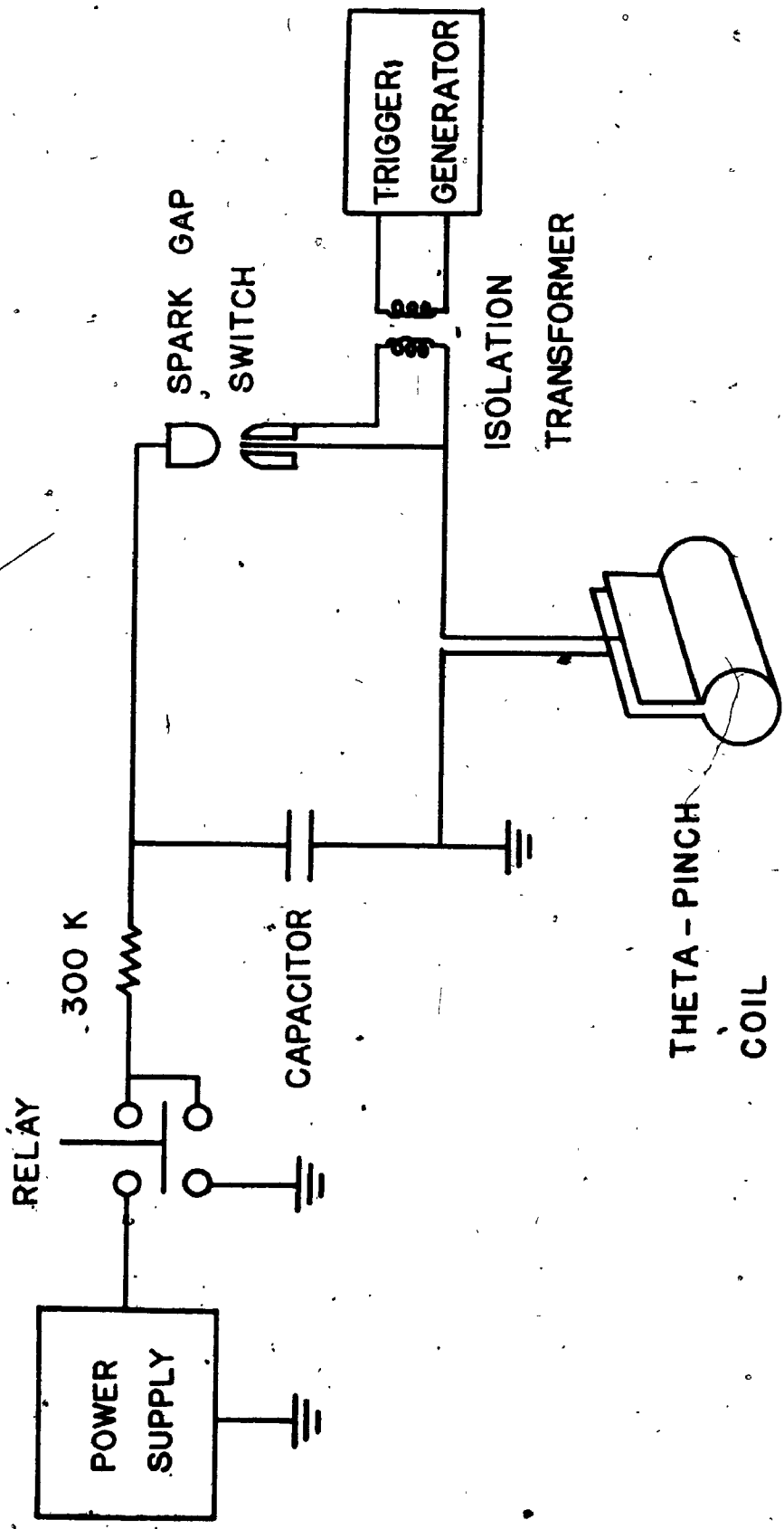


Fig. 3-1 Schematics of the theta-pinch configuration.

of 2  $\mu$ sec. Peak value of the discharge current was estimated to be 70 Kiloamperes with a corresponding axial magnetic field of approximately 9 Kilogauss.

The discharge vessel was a pyrex glass tube with nominal outer diameter of 4.4 cm and wall thickness of 1.6 mm. It was coupled to an aluminum tube at each end, forming a scattering chamber. This chamber will be described in detail in the next section. The arrangement of the vacuum and gas inlet systems for the scattering chamber is shown in Fig. 3-2. A Welch Duo-Seal rotary pump provided an initial vacuum of about  $10^{-2}$  Torr. An ultimate vacuum of about  $10^{-5}$  Torr was obtained with the additional Speedivac oil diffusion pump, model F. 203.

### 3-2 Light Input System.

#### 3-2.1 The Ruby Laser<sup>(38)</sup>

The heart of the light input system is a Holobeam Series 600 ruby laser system capable of providing a 300 MW pulse ( 19 nsec full width half maximum ) of 6943 Å coherent radiation. Component configuration of the laser is shown in Fig. 3-3. The system uses a 15.2 cm long and 1.3 cm diameter ruby laser rod as the active element and employs a Pockel's cell<sup>(39)</sup> for giant pulse Q-switching.

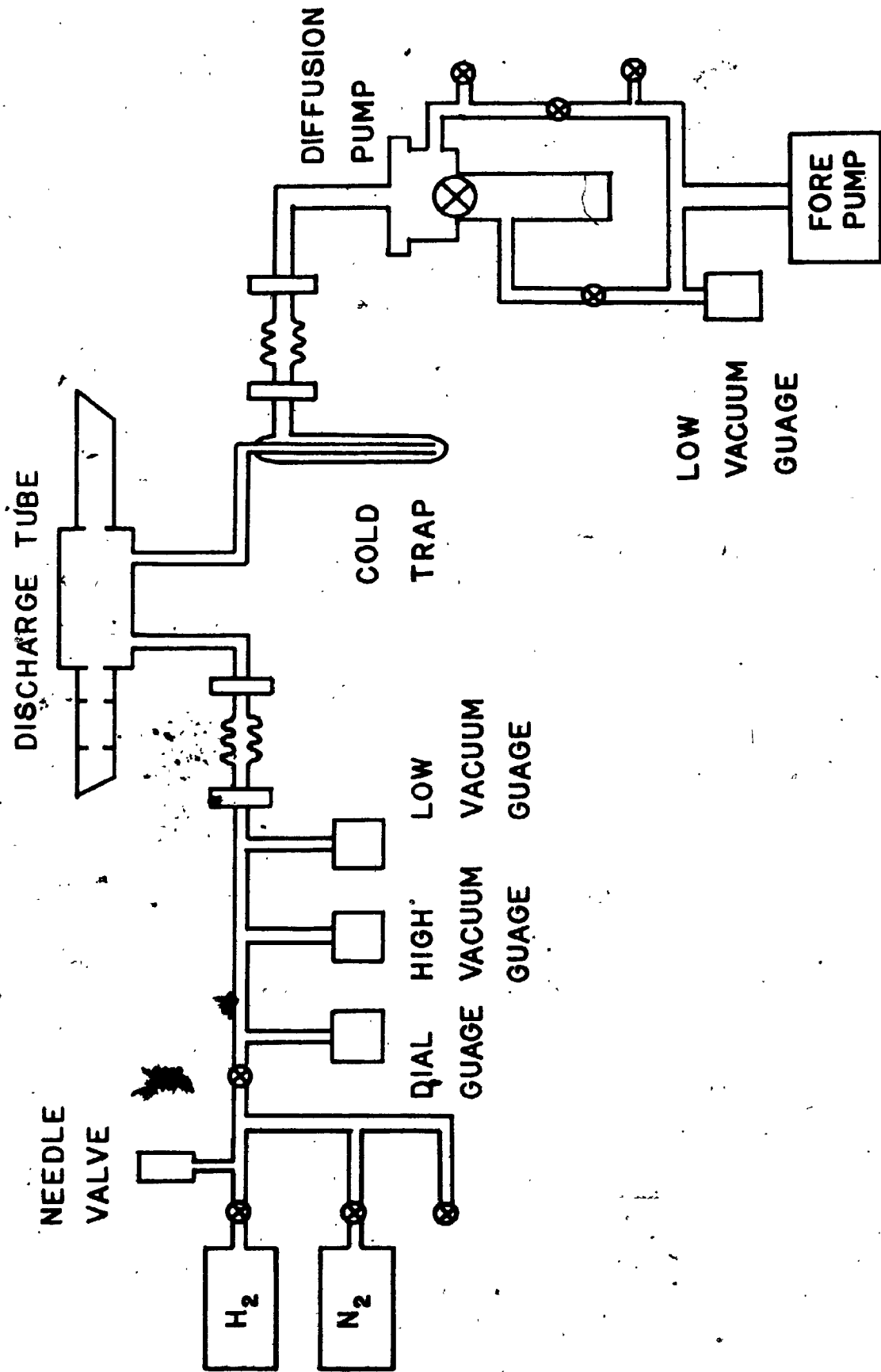


Fig. 3-2 Arrangement of the vacuum and gas inlet systems for the theta-pinch.

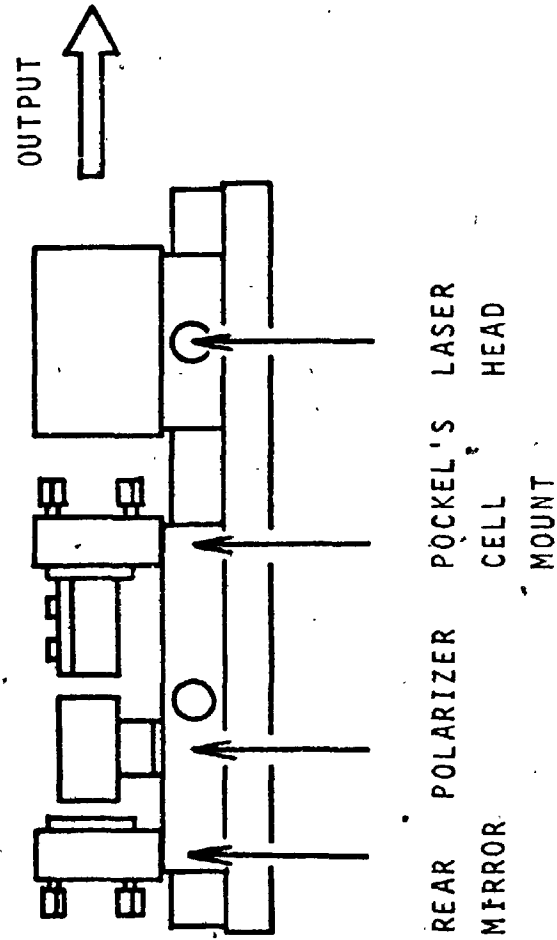


Fig. 3-3 Component configuration of the Holobeam Series 600 ruby laser.

The beam diameter is restricted to 1.1 cm by a ground glass aperture located between the laser head and the Pockel's cell. Divergence of the beam is less than 3 milliradians ( full width, half-power ).

For all the scattering measurements made, the laser system was only operated to give a light pulse of peak power of about 60 MW ( 30 nsec full width half-maximum ). Polarization of the laser beam was set normal to the scattering plane defined by the incident and scattered wave vectors. Synchronization of the laser pulse and the theta-pinch plasma discharge was regulated by a special delay circuit built into the control of the laser system, which provided a pulse of +25 volts at a time variable between 1-25  $\mu$ sec before the laser pulse.

### 3-2.2 Focusing Optics.

The function of the focusing optics is two-fold. First, it must reduce excessive divergence of the laser beam, thus suppressing the amount of stray light ( that is, light scattered into the collection optics that does not originate from the desired plasma scattering volume ). Second, it must focus the laser beam into the selected plasma volume.

The initial problem of divergence selection was handled by focusing the beam through a small aperture. Stray, off-axis rays were blocked by this focal plane stop as the beam diverged to the next element. The only limitation on such a method is the maximum power density that air can withstand at atmospheric pressure before it is ionized<sup>(40)</sup>. Fig. 3-4 shows the optical elements of the focusing system. The first lens  $L_1$  after the laser head is a 402 mm focal length plano-convex lens fitted with a stop having an aperture approximately 20% larger than the laser beam diameter. The laser beam was focused onto an aperture  $A_1$  of 1.2 mm diameter and light rays with a divergence greater than 3 milliradians were filtered off at this stop. The beam was recollimated by lens  $L_2$  ( focal length 385 mm ) and then focused by lens  $L_3$  ( focal length 1269 mm ) to a spot of 4.0 mm at the centre of the theta-pinch coil.

The converging beam entered the theta-pinch discharge tube through a glass window and into an aluminum baffled chamber. The Brewster angle of the window assured maximum transmission of the input beam. Three baffles were used in the aluminum chamber, each having a diameter of 1.5 cm. They prevented multiple or grazing reflections of stray light off the window or chamber walls from getting into the collection optics. Further reduction of spurious reflections from the chamber walls is usually achieved by blackening the chamber. A different approach has been adopted



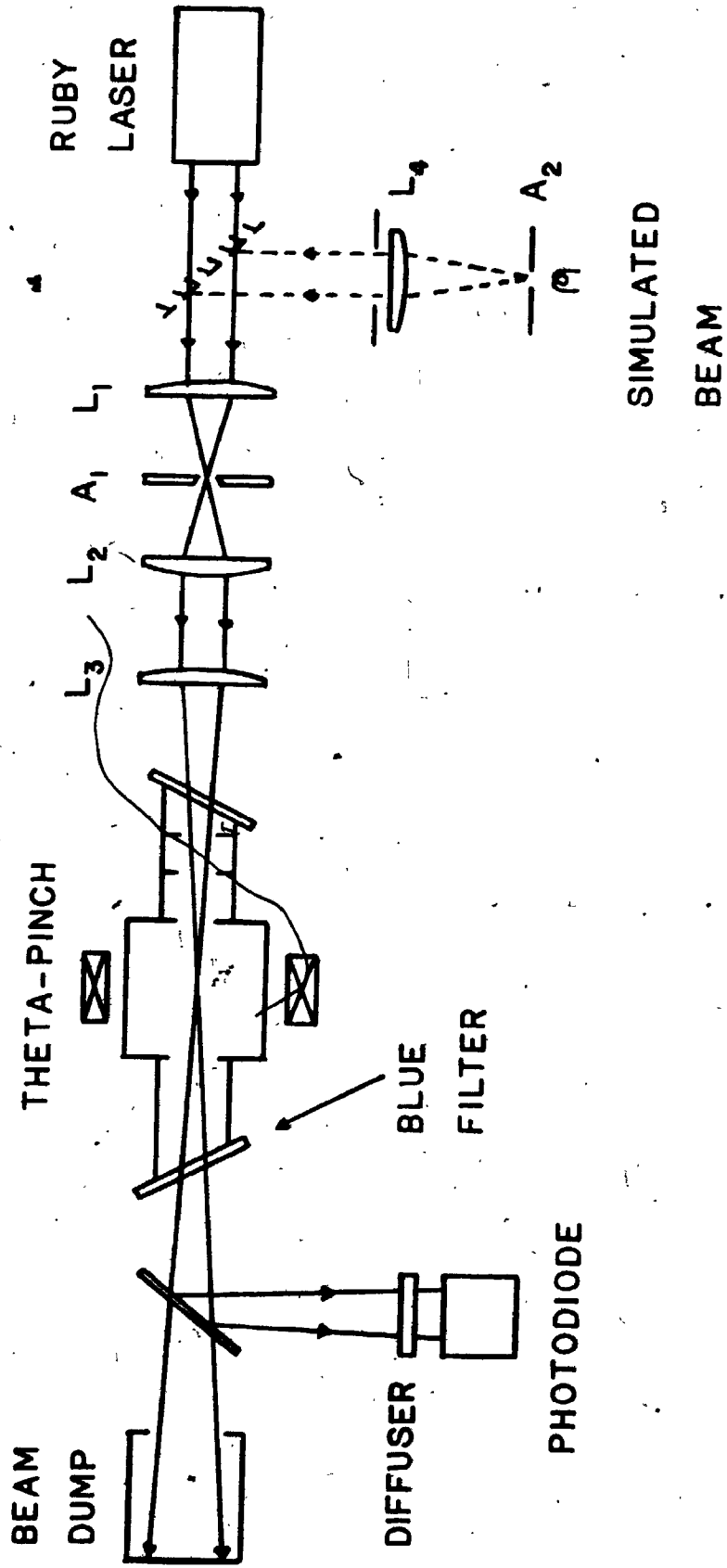



Fig. 3-4 The focusing optics.

here: the aluminum tube was coarsely threaded inside, forming minute light traps and baffles throughout the inside tube wall.

The laser beam, after traversing the plasma, passed through another chamber and was absorbed in a piece of blue filter glass ( Chance Pilkington OB 10 filter ) set at the Brewster angle to reduce reflection. The chamber was also an aluminum tube, coarsely threaded inside. Only one baffle was used as an added precaution in the event that some light might be scattered from the filter surface. The small percentage of light that was not absorbed by the blue filter was partially reflected onto an E. G. & G. SGD 100 photodiode which monitored the laser pulse and served to normalize the stray light and plasma or Rayleigh scattered light signals.

Both the input and exit window were located as far away as possible from the plasma discharge tube to keep them as clean as possible. Dust that settled on the input window was especially detrimental since any light scattered before the focus would reduce the power on the target and was often collected as stray light. The window was removed and cleaned as often as necessary. Since dust or imperfections in the focusing lenses would also scatter light out of the laser beam, it was necessary to place the whole focusing system in a blackened cardboard tunnel with



black paper baffles along the side of the light path.

Alignment of the focusing optics was made using a simulated beam with a steady light source as shown in Fig. 3-4, which had the same diameter and beam divergence as the laser beam.

### 3-3 Light Collection System.

Once the laser beam is focused into the scattering volume, it remains to collect, spectrally analyse, detect and record the small portion ( typically  $10^{-13}$  ) of the incident laser beam that is Thomson scattered into a selected angle. The light collection system is composed of (a) the collection optics and (b) the dispersing instruments.

#### 3-3.1 Design Considerations.

The function of the collection optics is to gather light scattered from a selected plasma volume, at a fixed scattering angle, within a small solid angle. A simple arrangement is shown in Fig. 3-5. The desired plasma scattering volume is imaged by a pair of plano-convex lenses  $L_1$  and  $L_2$  onto a focal plane stop  $A_2$  which also serves as the entrance aperture of a dispersing instrument. An aperture  $A_1$  placed at the first lens limits the cone of scattered light collected ( solid angle  $d\Omega$  ), thus

## THETA-PINCH

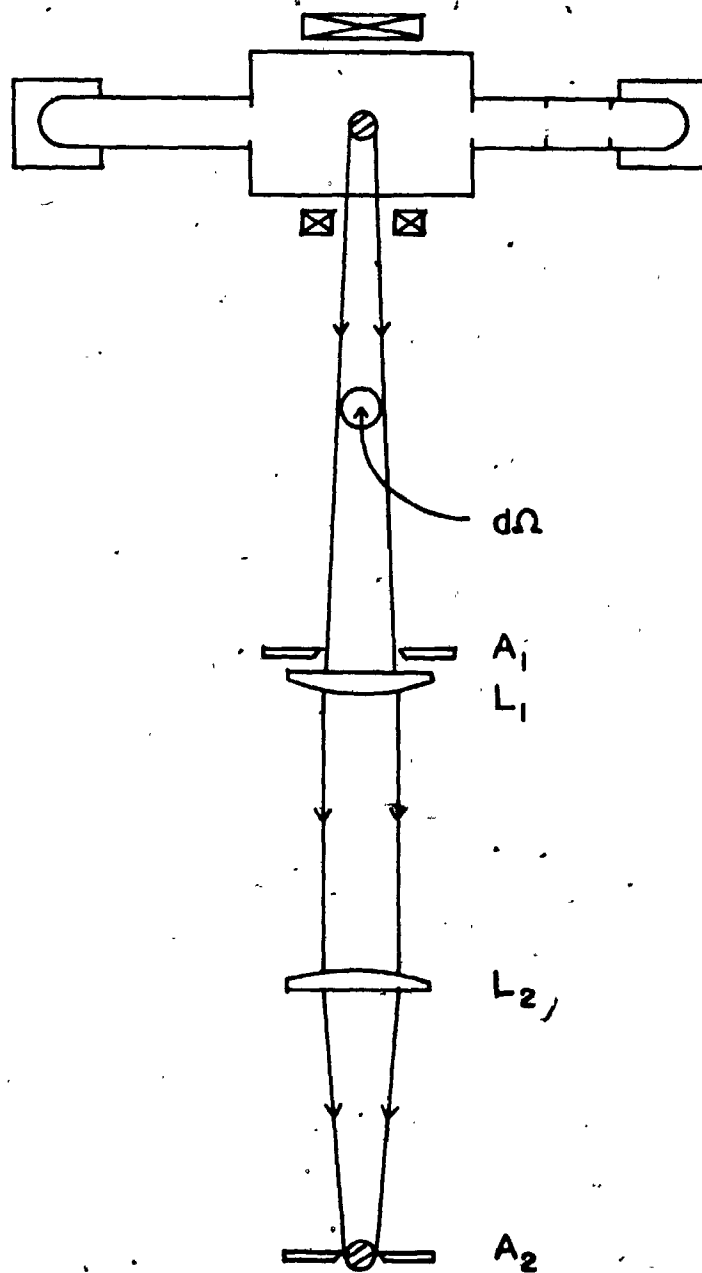


Fig. 3-5 A simple arrangement for the collection optics.

37  
geometrically defining the scattering wave vector  $k$  with a finite spread.

Spectral analysis of the scattered light can be made by either (a) simultaneously recording the complete or a major part of the scattered spectrum using a multichannel spectrometer system,<sup>(41,42)</sup> or (b) scanning the spectrum point-to-point using a single dispersing instrument. For measurements on pulsed plasmas, the first method has the distinct advantage of being unaffected by non-reproducibility of the plasma since the spectrum can be recorded in a single measurement. However, spectral resolution is limited by the number of channels and each channel may not be collecting light from the same region of the plasma scattering volume<sup>(41)</sup>. Signal strength may present a problem as the scattered intensity is distributed among all channels<sup>(41)</sup>. Cost and ease of operation are other limiting factors. On the other hand, instrumentation for scanning operation is relatively simple and inexpensive. Spectral resolution is basically limited by the dispersing element used. However, as a large number of scattering measurements is required to yield the scattered spectrum, the method is particularly vulnerable to non-reproducibility of the plasma. If such a method is to be used for measurements on pulsed plasmas that are not perfectly reproducible, a more valid measurement would require close monitoring of the plasma condition at the time of scattering and only those

scattering measurements from plasmas with comparable parameters should be compiled.

In the present work, scattering measurements were made at  $90^\circ$  and the resulting scattered spectrum was relatively broad. However, spectral resolution of the order of  $6 \text{ \AA}$  was required in order to detect anomalies in the spectrum. These and the further requirement that both the red-shifted and the blue-shifted sides of the spectrum be measured simultaneously dictated the use of scanning technique.

For scanning operation, the dispersing instrument can be a grating monochromator, a Fabry-Perot etalon or a tunable interference filter<sup>(43)</sup>. The Fabry-Perot etalon and the interference filter have a light gathering power of at least an order of magnitude greater than grating monochromator<sup>(44)</sup>. For a resolution as high as  $1-2 \text{ \AA}$ , the interference filter is preferable to the etalon, as it is relatively inexpensive, easy to operate, and covers a large spectral range. Interference filters with good transmission characteristics (peak transmission greater than 50%) and narrow bandwidth ( $\sim 1.5 \text{ \AA}$ ) are now readily available.

It was pointed out earlier that for scanning measurements, it is necessary to monitor the plasma condition at the time of scattering if the plasma discharge is not

perfectly reproducible as is usually the case. In a  $90^\circ$ -scattering measurement, the relevant plasma parameters are the electron density and the electron temperature. For effective and meaningful monitoring of these parameters, it is essential that they are measured simultaneously with the scattering measurements and in the same plasma region from which scattering measurements are made. Thus, it is preferable to incorporate such monitoring measurements as part of the scattering measurement. The scattered radiation will be distributed among four channels, one each for scanning the red-shifted and the blue-shifted sides of the scattered spectrum, one for monitoring the electron density and one for monitoring the electron temperature.

From equations (2-3), (2-4) and (2-19) of Chapter 2, the frequency integrated scattered intensity is

$$I(\underline{k}) = n_e V_s \sigma_T I_0 S(\underline{k})$$

where

$$S(\underline{k}) = \frac{1 + \alpha^2(1 + ZT_e/T_i) + Z\alpha^4}{(1 + \alpha^2) \{1 + \alpha^2(1 + ZT_e/T_i)\}}$$

For  $Z=1$  and  $T_e=T_i$ ,

$$S(\underline{k}) = \frac{1 + 2\alpha^2 + \alpha^4}{(1 + \alpha^2)(1 + 2\alpha^2)}$$

Fig. 3-6 shows  $S(\underline{k})$  as a function of  $\alpha$  for  $Z=1$  and  $T_e=T_i$ . Even at extreme variations of  $\alpha$ ,  $S(\underline{k})$  will only change by a factor of two. On the other hand,  $I(\underline{k})$  is directly proportional to the electron density. Thus, it is clear that  $I(\underline{k})$  can be used to monitor changes in the electron density. Experimentally, the total scattered radiation is detected through a dispersing instrument with a large but finite bandpass. If  $\Psi_T(\omega)$  is the instrumental function of the density monitoring channel, normalized to unity at peak transmission and  $T_T$  is the absolute percentage peak transmission, the measured total intensity will be

$$\begin{aligned} I_T(\underline{k}) &= \int_{-\infty}^{\infty} I(\underline{k}, \omega) \Psi_T(\omega) T_T d\omega \\ &= n_e V_S \sigma_T I_0 T_T \int_{-\infty}^{\infty} S(\underline{k}, \omega) \Psi_T(\omega) d\omega \end{aligned} \quad (3-1)$$

Providing  $\Psi_T(\omega)$  has a sufficiently large bandwidth,  $I_T(\underline{k})$  will show similar dependence on electron density and  $\alpha$  as  $I(\underline{k})$ . Furthermore, for absolute measurement of electron density,  $I_T(\underline{k})$  can be calibrated using Rayleigh scattering measurements ( Appendix A ). The intensity of Rayleigh scattered light from a neutral gas of pressure  $P_0$  at temperature  $T_0$  is

$$I_R^e(P_0) = \left( \frac{P_0}{k T_0} \right) V_S \sigma_R I_0 T_T(\lambda_0) \quad (3-2)$$

where  $T_T(\lambda_0)$  is the transmission at the laser wavelength.



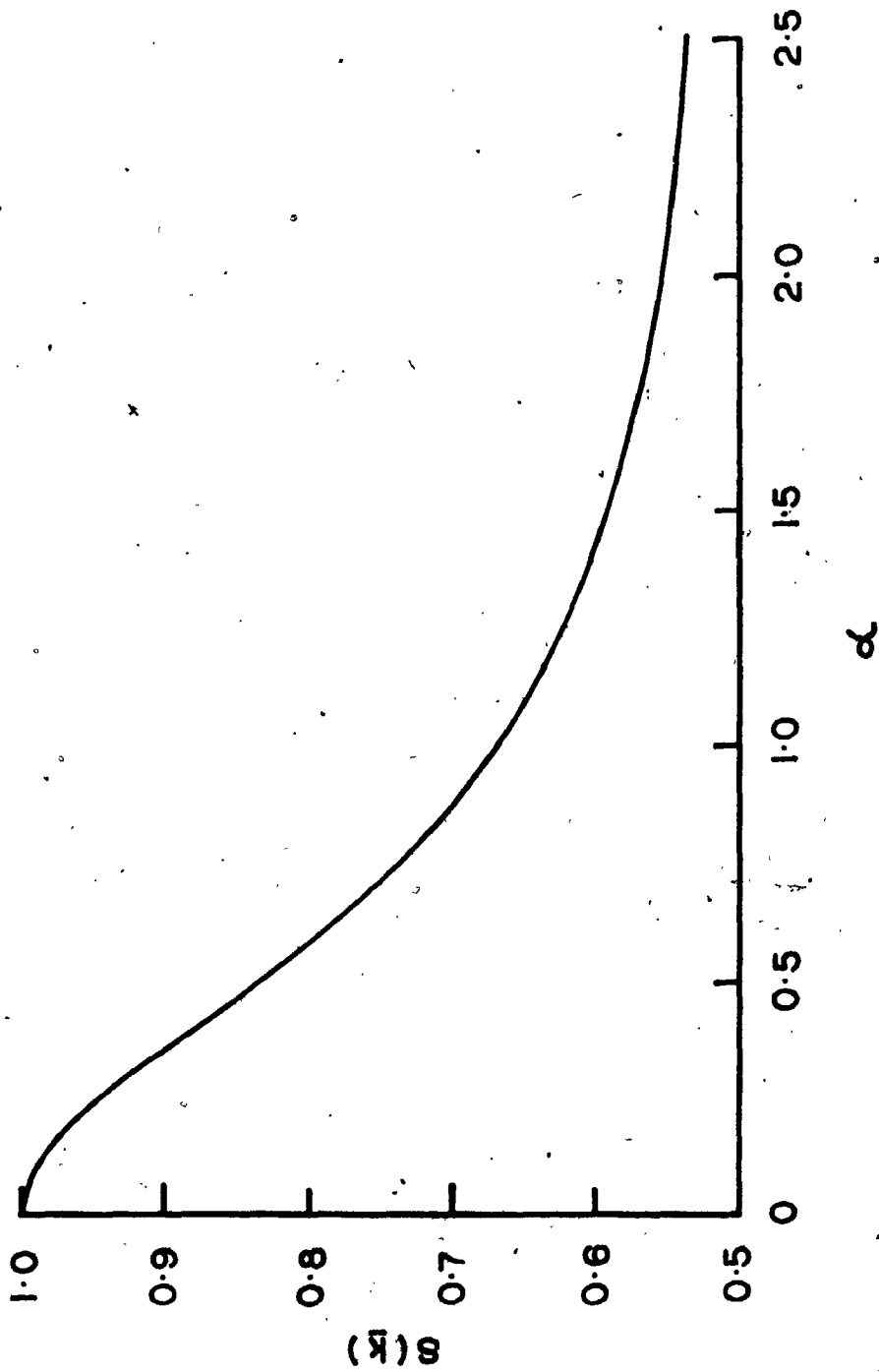


Fig. 3-6  $S(k)$  as a function of  $\alpha$  for  $Z=1$  and  $T_e=T_i$ .

and  $K$  is the Boltzmann constant. Hence,

$$\frac{I_T(\underline{k})}{I_R(P_0)} = n_e \left( \frac{\sigma_T}{\sigma_R} \right) \left( \frac{KT_0}{P_0} \right) \left( \frac{T_T}{T_T(\lambda_0)} \right) \int_{-\infty}^{\infty} S(\underline{k}, \omega) \Psi_T(\omega) d\omega \quad (3-3)$$

An electron density calibration factor  $\eta$  can then be defined as

$$\eta \equiv n_e \int_{-\infty}^{\infty} S(\underline{k}, \omega) \Psi_T(\omega) d\omega \quad (3-4A)$$

$$= \left( \frac{I_T(\underline{k})}{I_R(P_0)} \right) \left( \frac{\sigma_R}{\sigma_T} \right) \left( \frac{P_0}{KT_0} \right) \left( \frac{T_T(\lambda_0)}{T_T} \right) \quad (3-4B)$$

The integral can be computed for various combinations of electron densities and temperatures. Fig. 3-7 shows the computed variation of  $\eta$  with density and temperature for an interference filter with peak transmission at 6948 Å and bandwidth of 140 Å. Comparison of the experimentally determined value of  $\eta$  with these curves will then yield a density measurement.

To monitor changes in the plasma electron temperature, one notes that the value of the dynamic form factor at the centre of the spectrum, for  $T_e = T_i$ , is given by (3)

$$S_{\alpha \ll 1}(\underline{k}, 0) = \frac{c}{2\pi^{1/2}} \left( \frac{1}{\lambda_0 \sin(\theta/2)} \right)^2 \left( \frac{m}{KT_e} \right)^{1/2}$$

for  $\alpha \ll 1$ , and

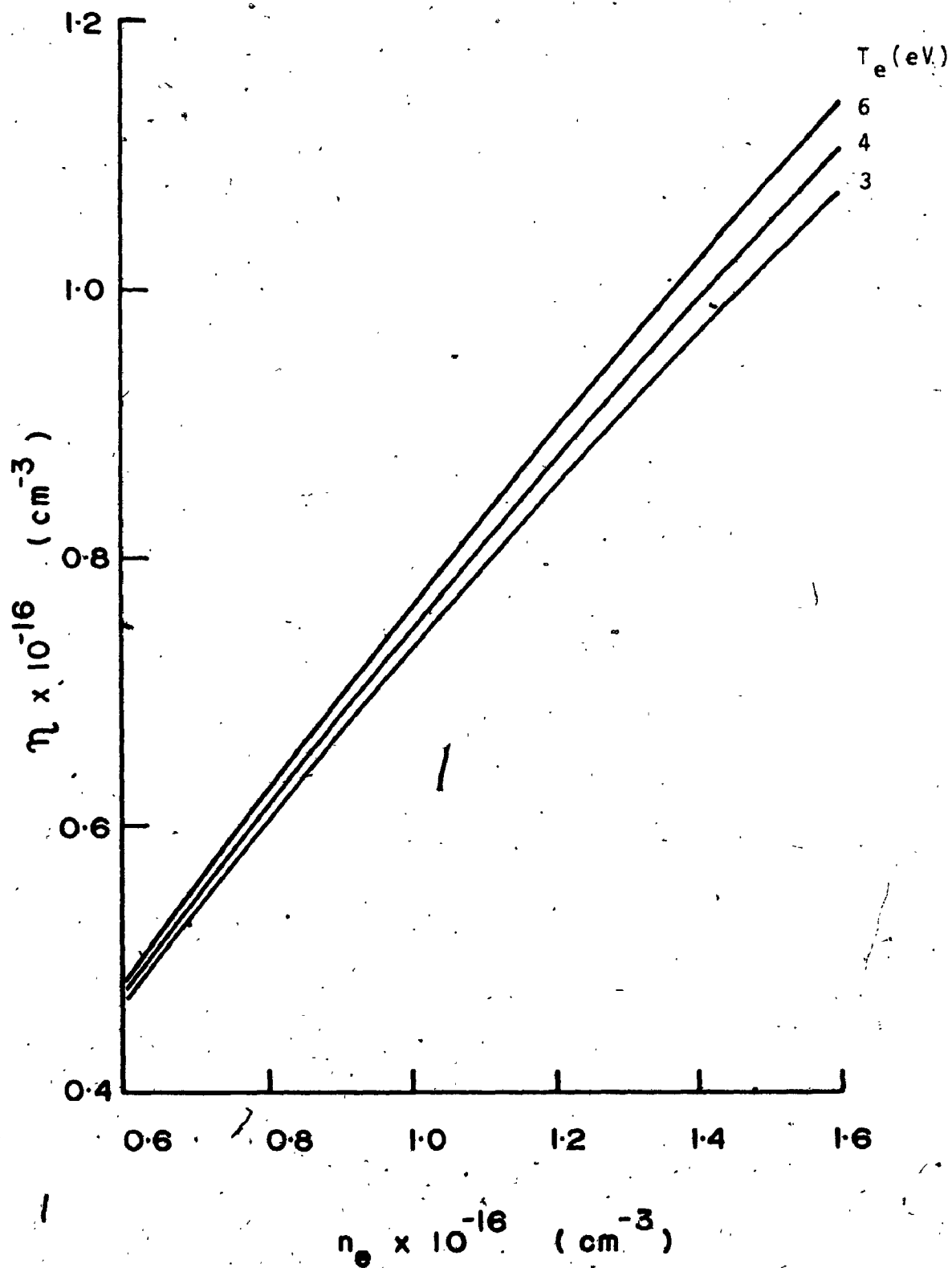


Fig. 3-7 Curves of  $\eta$  as a function of electron density and electron temperature.

$$S_{\alpha \gg 1}(\underline{k}, 0) = \frac{1}{2} \left( \frac{M}{m} \right)^{1/2} S_{\alpha \ll 1}(\underline{k}, 0)$$

for  $\alpha \gg 1$ , where  $c$  is the velocity of light,  $\lambda_0$  is the laser wavelength,  $\theta$  is the scattering angle,  $T_e$  is the electron temperature,  $T_i$  is the ion temperature, and  $m, M$  are the masses of the electron and ion respectively. Thus, the intensity in a narrow bandwidth of the scattered spectrum centred about the incident frequency has a temperature dependence and may be used to monitor the electron temperature. If  $\Psi_{\Delta}(\omega)$  is the instrumental function for the temperature monitoring channel, normalized to unity at peak transmission and  $T_{\Delta}$  is the absolute percentage peak transmission, the intensity of scattered light measured in this channel is

$$\begin{aligned} I_{\Delta}(\underline{k}) &= \int_{-\infty}^{\infty} I(\underline{k}, \omega) \Psi_{\Delta}(\omega) T_{\Delta} d\omega \\ &= n_e V_s \sigma_T I_0 T_{\Delta} \int_{-\infty}^{\infty} S(\underline{k}, \omega) \Psi_{\Delta}(\omega) d\omega \end{aligned} \quad (3-5)$$

It is clear that  $I_{\Delta}(\underline{k})$  alone cannot satisfactorily monitor changes in electron temperature since it is also directly proportional to electron density. To eliminate the density dependence, one can consider the ratio

$$\frac{I_{\Delta}(\underline{k})}{I_T(\underline{k})} = \frac{T_{\Delta}}{T_T} \frac{\int_{-\infty}^{\infty} S(\underline{k}, \omega) \Psi_{\Delta}(\omega) d\omega}{\int_{-\infty}^{\infty} S(\underline{k}, \omega) \Psi_T(\omega) d\omega} \quad (3-6)$$

An electron temperature calibration factor  $\xi$  can thus be

defined as

$$\xi \equiv \frac{\int_{-\infty}^{\infty} S(\underline{k}, \omega) \Psi_{\Delta}(\omega) d\omega}{\int_{-\infty}^{\infty} S(\underline{k}, \omega) \Psi_{T}(\omega) d\omega} \quad (3-7A)$$

$$= \left( \frac{I_{\Delta}(\underline{k})}{I_{T}(\underline{k})} \right) \cdot \left( \frac{T_{T}}{T_{\Delta}} \right) \quad (3-7B)$$

Sensitivity of  $\xi$  to changes in electron temperature depends upon the bandwidth of  $\Psi_{\Delta}(\omega)$  and the experimental temperature regime. In general, it may be improved by narrowing the bandwidth of  $\Psi_{\Delta}(\omega)$  at the sacrifice of the measured intensity. Fig. 3-8 shows the computed variation of  $\xi$  with electron temperature and electron density for a temperature monitoring channel with bandwidth of 15 Å and centred at 6941 Å. Furthermore, absolute measurement of electron temperature can be obtained from the measured value of  $\xi$ .

In the above discussion, a thermal plasma has been assumed. However, the general formulation of the technique and in particular, the calibration factors as defined in equations (3-4A), (3-4B), (3-7A) and (3-7B) are valid for all plasmas. For measurements on non-thermal plasmas, applicability of the method depends upon the knowledge of the dynamic form factor  $S(\underline{k}, \omega)$  characterizing the plasma. It should also be pointed out that caution should be exercised in deriving electron density and temperature values from the experimentally determined values of  $n_e$  and  $\xi$ .

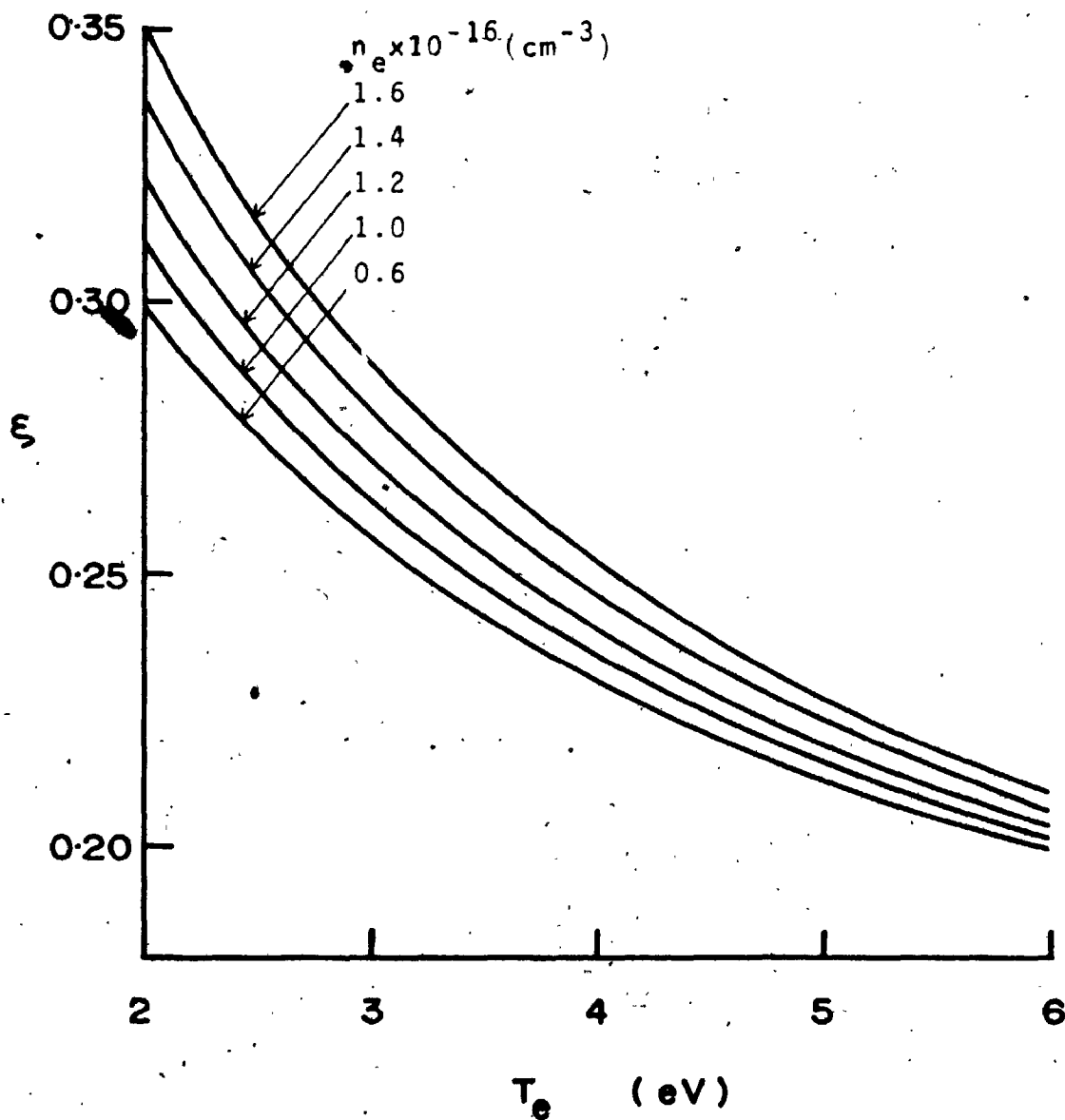


Fig. 3-8 Curves of  $\xi$  as a function of electron temperature and electron density.

Enhancements in the scattered intensity must be taken into account in the analysis.

### 3-3.2 Collection Optics and the Spectrometer System

Fig. 3-9 shows details of the collection optics and a four-channel spectrometer system. Parameters of the optical elements are listed in Table 3-1. Light scattered at 90° was collected in a solid angle of  $6.7 \times 10^{-3}$  steradians corresponding to a scattering wave vector  $k$  of  $1.28 \times 10^5 \text{ cm}^{-1} \pm 4\%$ . Only a region of diameter 2.5 mm in the plasma was imaged onto the entrance apertures of the four channels of the spectrometer system. Use of a common collection lens  $L_1$  ensured that all channels measured light scattered from the same plasma volume.

Each channel of the spectrometer system was basically an interference filter spectrometer. Channels 1 and 2 were used for scanning the red-shifted and the blue-shifted sides of the scattered spectrum respectively. Narrow band-pass filters which were tunable by rotation were used. By highly collimating the beam incident on the filter ( half-angle beam divergence less than 6 milliradians ), the instrumental widths of channels 1 and 2 were limited to about 6 Å and 5 Å respectively. Channel 3 was the electron density monitor for which a fixed-position, broadband inter-

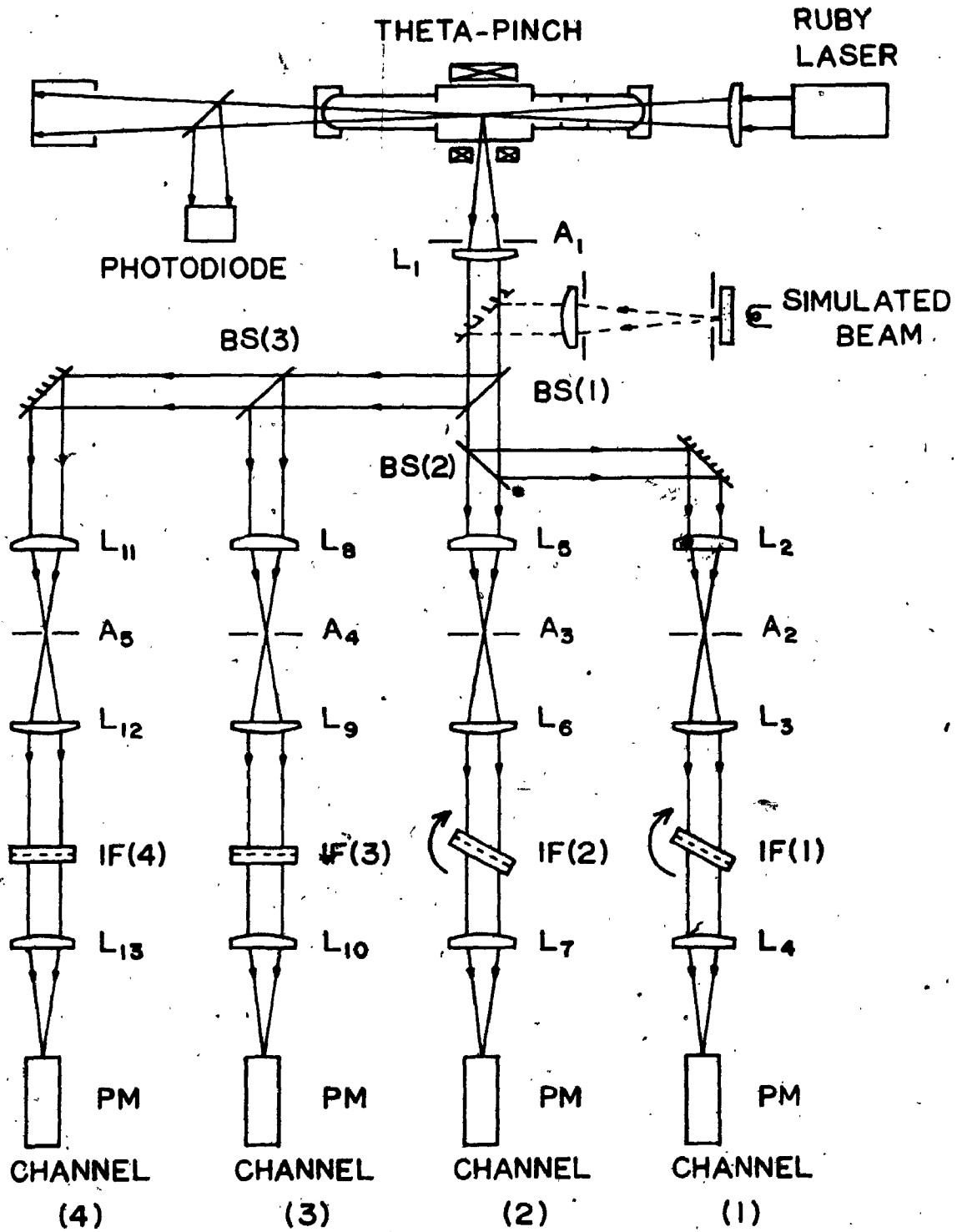


Fig. 3-9 Details of the collection optics and the four-channel spectrometer system.



Table 3-1 Description of the optical elements in Fig. 3-9.

Lens L <sub>1</sub>	: Focal length 110 mm.
Lens L <sub>2</sub>	: Focal length 300 mm.
Lens L <sub>3</sub>	: Focal length 575 mm.
Lens L <sub>4</sub>	: Focal length 225 mm.
Lens L <sub>5</sub>	: Focal length 230 mm.
Lens L <sub>6</sub>	: Focal length 466 mm.
Lens L <sub>7</sub>	: Focal length 115 mm.
Lens L <sub>8</sub>	: Focal length 254 mm.
Lens L <sub>9</sub>	: Focal length 254 mm.
Lens L <sub>10</sub>	: Focal length 120 mm.
Lens L <sub>11</sub>	: Focal length 483 mm.
Lens L <sub>12</sub>	: Focal length 45 mm.
Lens L <sub>13</sub>	: Focal length 45 mm.
Aperture A <sub>1</sub>	: Diameter 18.0 mm.
Aperture A <sub>2</sub>	: Diameter 6.8 mm.
Aperture A <sub>3</sub>	: Diameter 5.1 mm.
Aperture A <sub>4</sub>	: Diameter 5.7 mm.
Aperture A <sub>5</sub>	: Diameter 10.8 mm.
IF(1)*	: Interference filter, $\lambda_0 = 7025 \text{ \AA}$ , bandwidth 3 $\text{\AA}$ .
IF(2)*	: Interference filter, $\lambda_0 = 6946 \text{ \AA}$ , bandwidth 4 $\text{\AA}$ .
IF(3) <sup>©</sup>	: Interference filter, $\lambda_0 = 6948 \text{ \AA}$ , bandwidth 140 $\text{\AA}$ .
IF(4)*	: Interference filter, $\lambda_0 = 6941 \text{ \AA}$ , bandwidth 10 $\text{\AA}$ .
BS(1) <sup>†</sup>	: Dielectric 70/30 beam splitter.
BS(2) <sup>†</sup>	: Dielectric 45/55 beam splitter.
BS(3) <sup>†</sup>	: Dielectric 35/65 beam splitter.

\* Supplied by Infrared Industries, Waltham, Massachusetts.

© Supplied by Corion Corporation, Holliston, Massachusetts.

† Supplied by Rolyn Optics, Arcadia, California.

ference filter of bandwidth  $140 \text{ \AA}$  was used at normal incidence. With the incident beam highly collimated ( half-angle beam divergence of 11 milliradians ), the effective instrumental function of the channel was essentially that of the filter. Channel 4 was used to monitor the electron temperature and the optical arrangement was similar to that of channel 3. By coupling a readily available interference filter to a beam incident normally with a small divergence ( half-angle beam divergence of 0.12 radian ), the effective instrumental width of the channel was approximately  $15 \text{ \AA}$ .

Both the collection optics and the spectrometer system were enclosed in blackened cardboard tunnels which were kept as light tight as possible.

### 3-3.3 Optical Alignment.

Coupling of the laser input system to the scattered light collection system was made using a small right-angle prism placed at the centre of the theta-pinch discharge tube. Fig. 3-10 shows a diagram of the aluminum prism-mount. Diameters of the tubes were matched to that of the baffles at each end of the pyrex glass discharge tube for centering the prism on the axis of the theta-pinch coil. The simulated laser beam ( Fig. 3-4 ) reflected from the

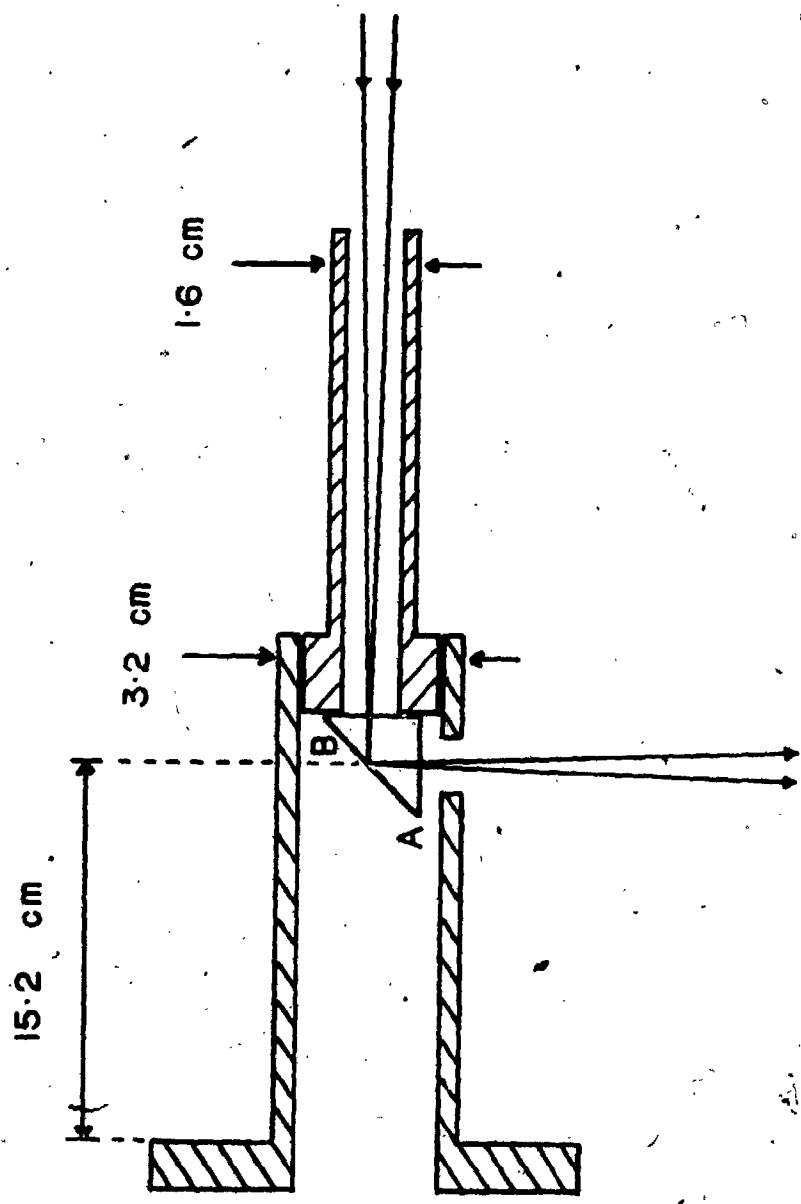


Fig. 3-10 The prism mount.

face AB of the prism then represented the  $90^\circ$ -scattered beam and was used for alignment of the collection optics. Once the entrance apertures of the four channels of the spectrometer system were properly located, the rest of the spectrometer optics were aligned using a simulated scattered beam ( Fig. 3-9 ) off a steady light source.

### 3-4 Detection System.

#### 3-4.1 Photomultipliers.

Light emerging from the interference filter in each channel of the spectrometer system was focused onto a photomultiplier tube ( RCA, 7265 with S-20 spectral response ). The photomultipliers were housed in aluminum cylinders along with their voltage-divider bases. Fig. 3-11 shows the schematics of the voltage-divider which was a variation of that given in the RCA 7265 data sheet<sup>(45)</sup>. Capacitors were used in the final dynode stages to keep a constant potential across the dynodes even though large currents may flow between them. The voltage-divider current needed only be sufficient to provide the average anode current for the photomultiplier; the high peak currents required during large amplitude light pulses were supplied by the capacitors. The principal limitation on current output is space charge at the last few dynodes. This was overcome by

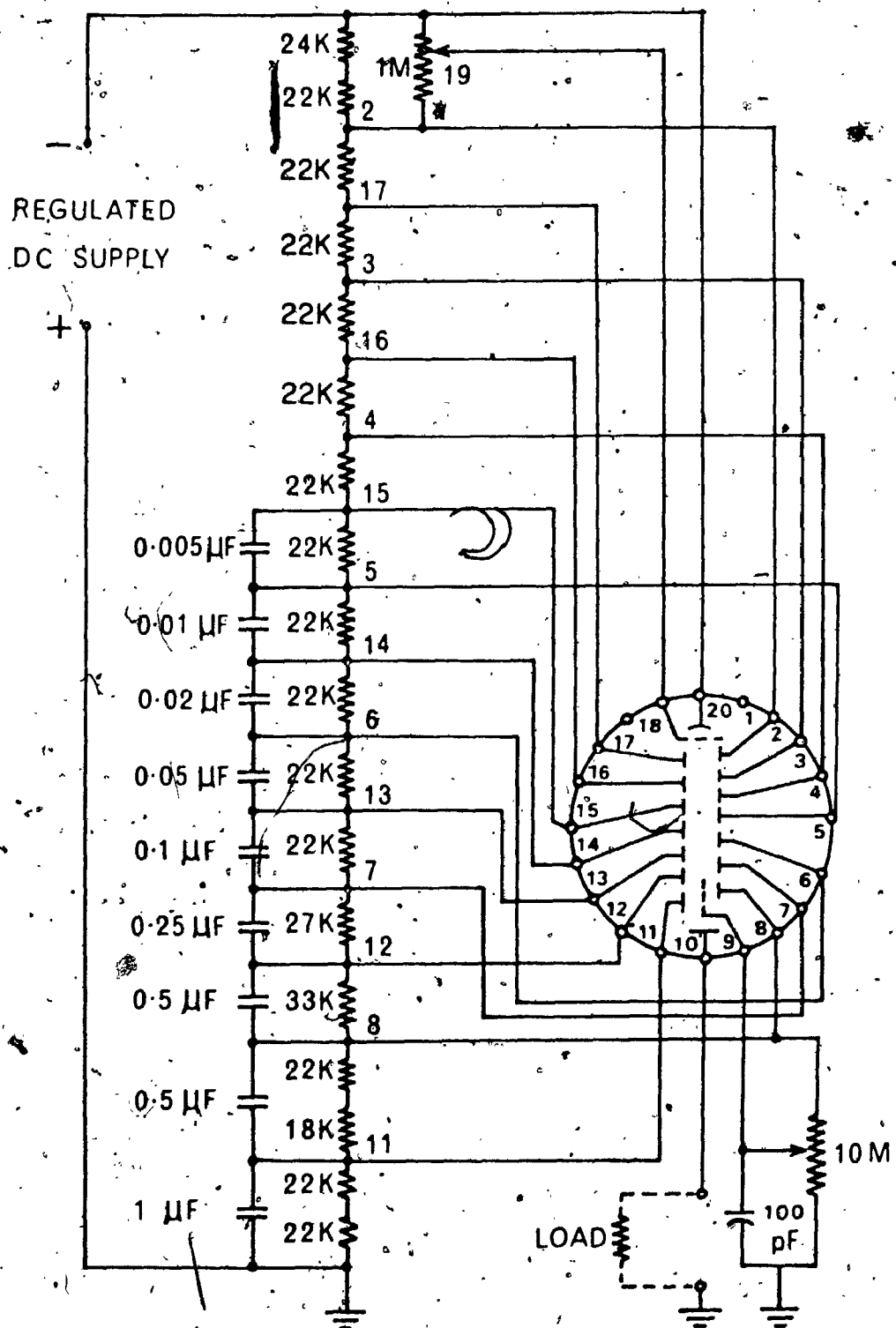


Fig. 3-11 Schematics of the voltage-divider for the photomultipliers.

increasing the potential difference across the last few stages by using a tapered voltage-divider rather than an equal-volt-per-stage divider.

High voltages for the photomultipliers were supplied by two Fluke 415B 30 mA, 3 KV power supplies (voltage regulation better than 0.1%) through a high voltage distribution network. Schematics of the network are shown in Fig. 3-12. It consisted of two identical branches, one for each of the power supplies. Three voltage-dividers were provided in each branch and the output voltages could be varied independently. Since four photomultipliers were used in this experiment, only two dividers in each branch were used.

#### 3-4.2 Signal Recording.

Signals from the four photomultipliers were carried on RG 62-U coaxial cables into two Tektronix Type 555 dual beam oscilloscopes. Each cable was terminated with a  $91\Omega$  resistor terminator cap (Amphenol 35650-91) and plugged into a Tektronix Type L preamplifier. The signal from the photodiode laser monitor was carried on an RG 58/U coaxial cable into a Tektronix Type 543B single beam oscilloscope. The cable was terminated with a  $51\Omega$  resistor terminator cap (Amphenol 35650-51) and plugged into a Tektronix Type K

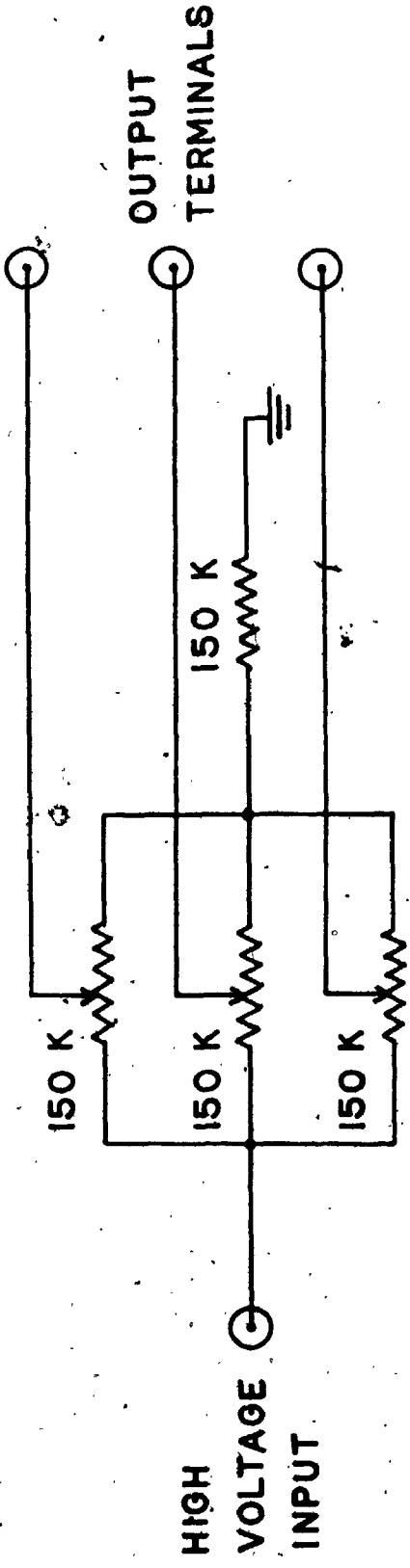
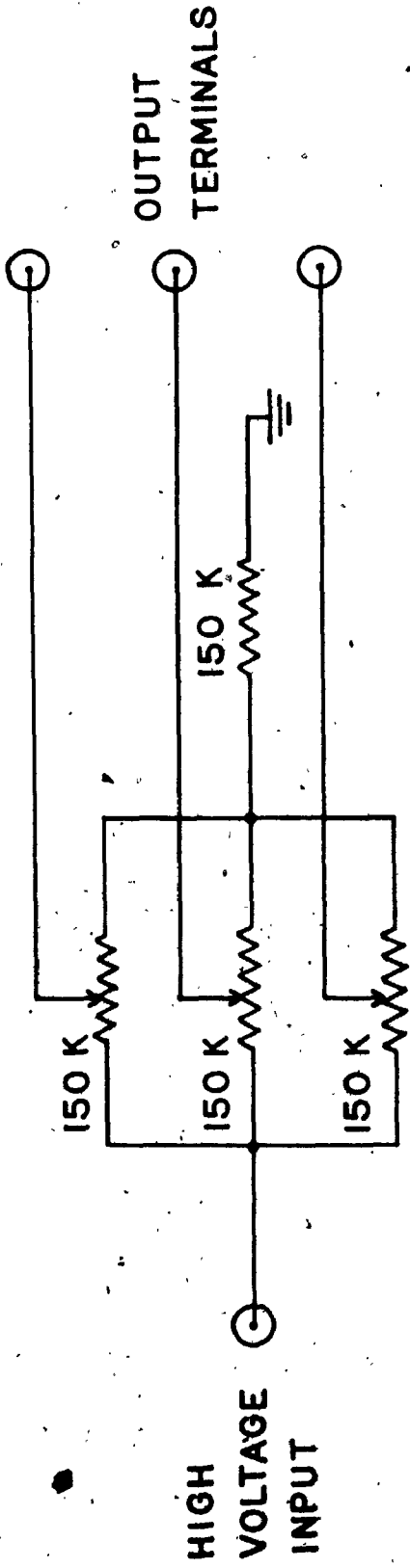


Fig. 3-12 Schematics of the high voltage distribution network.

preamplifier. All signal traces were photographed on Polaroid type 410 high-speed recording film using Tektronix C-12 cameras.

### 3-5 Calibration.

#### 3-5.1 Intensity Calibration by Rayleigh Scattering.

After all the optics were aligned, calibration of the various channels of the spectrometer system were made in situ, first using Rayleigh scattered light from nitrogen gas at pressures between 30 and 100 Torr.

For channels 1 and 2, profiles of the true Rayleigh scattered light ( with stray light level subtracted ) were measured and they are shown in Fig. 3-13 and Fig. 3-14 respectively. To determine the spectral width and shape of the instrumental function for each of these channels at the laser wavelength, a smooth curve was fitted to the experimental data as indicated by the solid curves in figures 3-13 and 3-14. The integrated intensity under the Rayleigh scattered profile further served as an intensity calibration for measurement of electron density ( Appendix A ).

In channels 3 and 4, only the total Rayleigh scattered intensities were measured. Since the measurements were



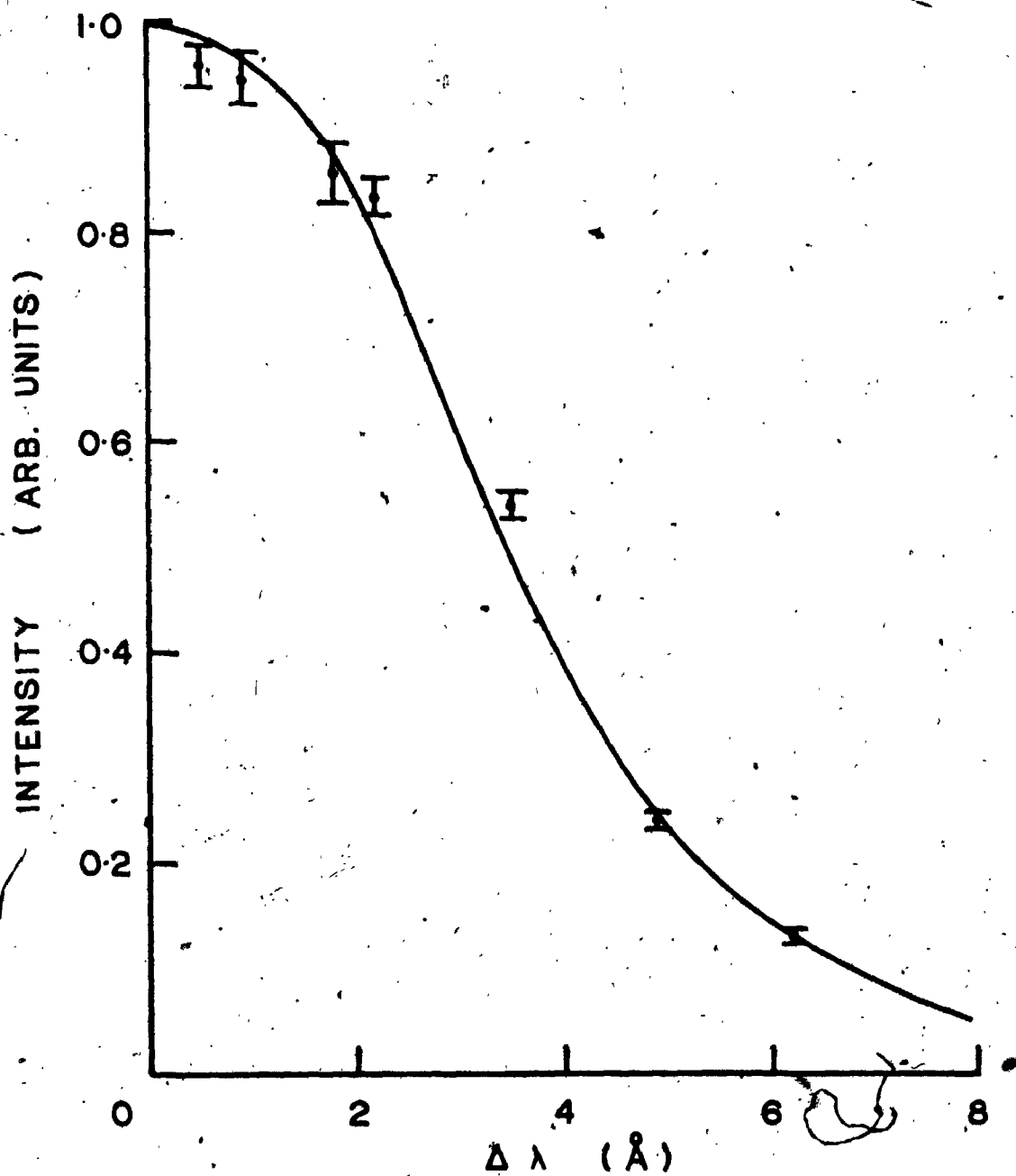


Fig. 3-13 Profile of Rayleigh scattered intensity from nitrogen gas at 85 Torr in channel 1.

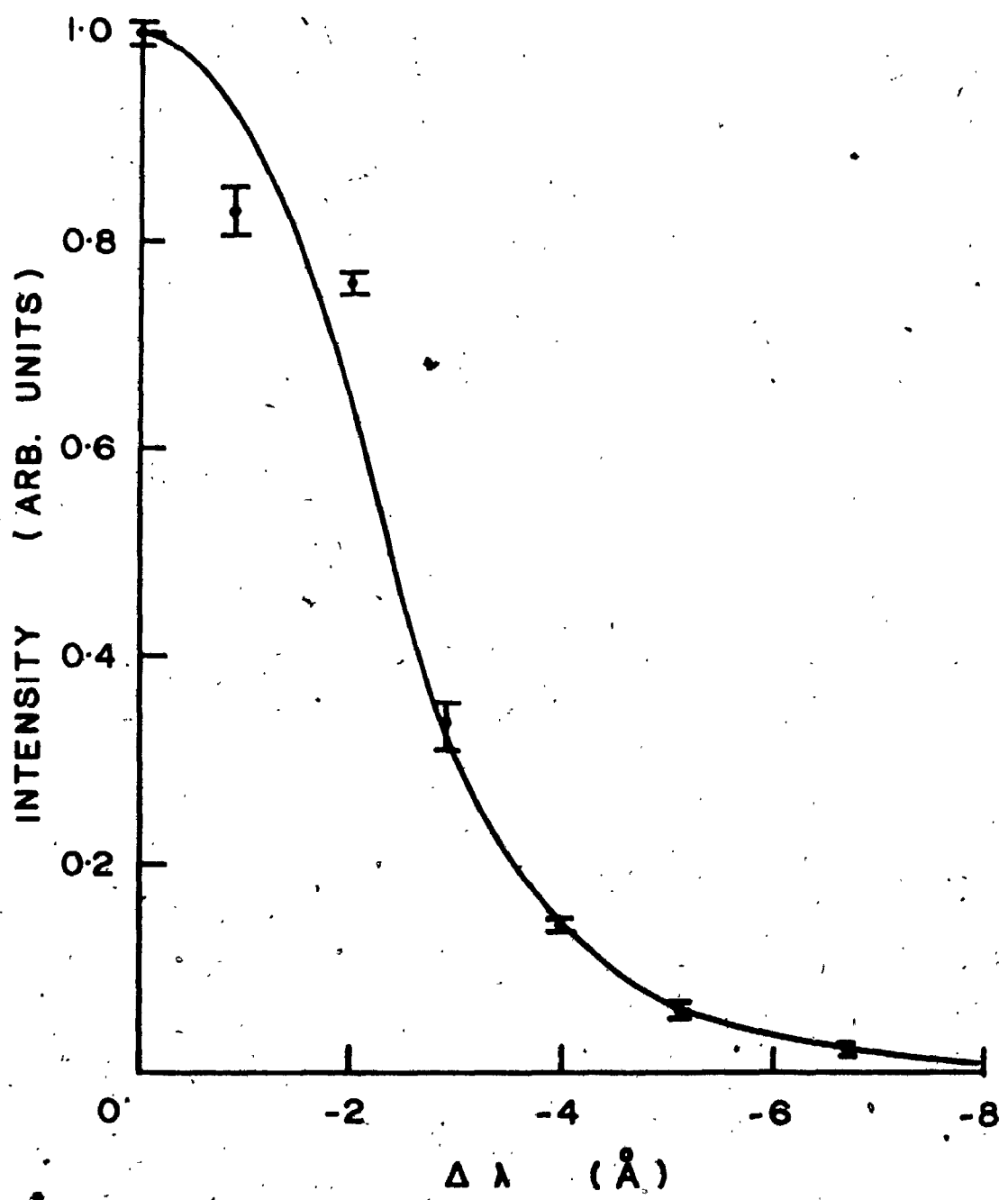


Fig. 3-14 Profile of Rayleigh scattered intensity from nitrogen gas at 85 Torr in channel 2.

made simultaneously, the ratio of the Rayleigh scattered signals yielded a calibration of the relative transmission of the two channels at the laser wavelength, that is,  $T_T(\lambda_0)/T_\Delta(\lambda_0)$ . The ratio of their peak transmissions,  $T_T/T_\Delta$ , can then be determined with a further knowledge of their instrumental profiles. For channel 3, the Rayleigh scattered intensity was also used to calibrate the Thomson scattered intensity for measurement of electron density ( Appendix A ).

It is important to note that presence of dust particles in the scattering volume will falsify a Rayleigh calibration. The problem can be minimized by using low filling pressures so that heavy particles will settle rapidly, and by waiting after the filling gas has been introduced for dust to settle. As a precaution, linear variation of the Rayleigh scattered signals with filling pressure was checked. For example, the Rayleigh scattered intensity as a function of nitrogen pressure in channel 3 is shown in Fig. 3-15.

### 3-5.2 Relative Transmission Calibration in Channels 1 and 2.

For each of the scanning channels 1 and 2, the relative transmission of the dispersing instrument over the

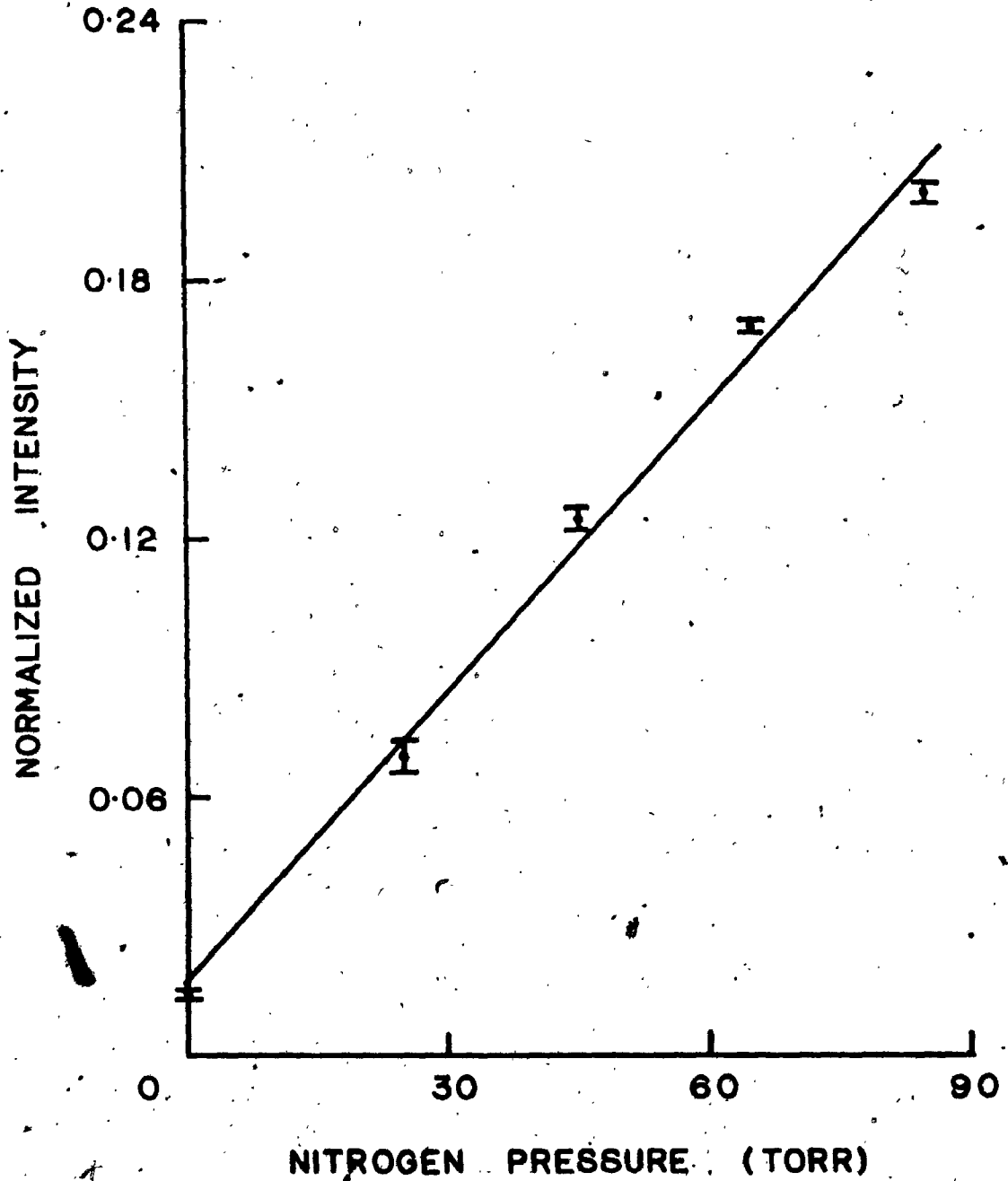


Fig. 3-15. Rayleigh scattered intensity as a function of nitrogen gas pressure in channel 3.

wavelength range of the scattered spectrum was measured using a General Radio Strobotac Type 1531A as light source. The spectrum of the strobe light was initially measured using a Heath EU-700 monochromator at a resolution of 1 Å. The strobe then replaced the steady light source of the simulated scattered beam ( Fig. 3-8 ) and was operated at 100 RPM. Each of the interference filters in channels 1 and 2 was rotated to cover a wavelength interval of 100 Å. The spectra of light transmitted were then compared to the source spectrum. Within the required spectral interval, transmission of each channel was constant.

### 3-5.3 Spectral Calibration.

For channels 1 and 2 where the wavelength of peak transmission of the interference filters was varied by rotation of the filters, wavelength calibration as a function of angle of incidence was obtained as follows. The interference filter equation<sup>(46)</sup> gives

$$\lambda_{\theta} = \lambda_N \left( 1 - \frac{\sin^2 \theta}{n^2} \right)^{1/2}$$

where  $\lambda_{\theta}$  is the wavelength of peak transmission at an angle of incidence  $\theta$ ,  $\lambda_N$  is that at normal incidence and  $n$  is the effective index of refraction of the filter. Measurements were made for two known values of  $\lambda_{\theta}$  so that values of  $\lambda_N$

and  $n$  are obtained experimentally. Ruby laser radiation at  $6943 \text{ \AA}$ , scattered from nitrogen gas by Rayleigh scattering, conveniently served as a wavelength standard for calibration of both channels 1 and 2. Furthermore, it was found that within a spectral range of about  $100 \text{ \AA}$  on both sides of the laser wavelength, two spectral lines were present in the spectrum of strobe light; one at  $6903 \pm 1 \text{ \AA}$  and the other at  $6992 \pm 1 \text{ \AA}$ . The appropriate spectral line was then used to complete the calibration of each of the two channels.

Spectral calibration of channel 3 was not required. As mentioned earlier, the very small divergence of the beam incident on the broadband interference filter ensured that the channel would assume an instrumental function the same as that of the filter<sup>(47)</sup>.

Since the intensity distribution of the strobe light was uniform within the wavelength interval covered by channel 4, the strobe was used as a calibration light source providing a simulated scattered beam ( Fig. 3-8 ). The light emerging from the interference filter in channel 4 was spectrally analysed using an interference filter spectrometer as shown in Fig. 3-16. The transmission profile of channel 4 thus measured is shown in Fig. 3-17. The solid line is a smooth curve fitted to the experimental data.

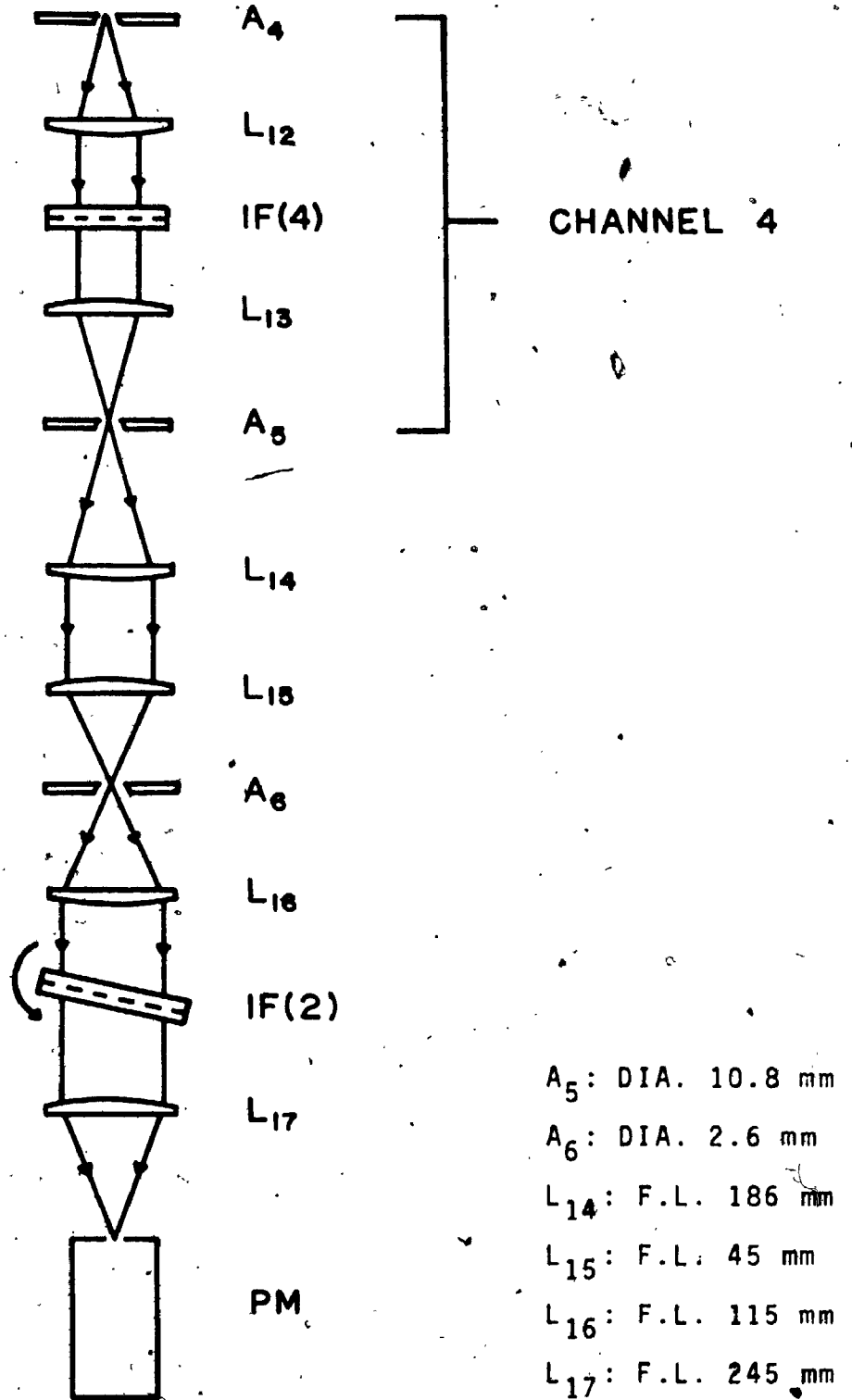


Fig. 3-16 Optical arrangement for spectral calibration of channel 4.

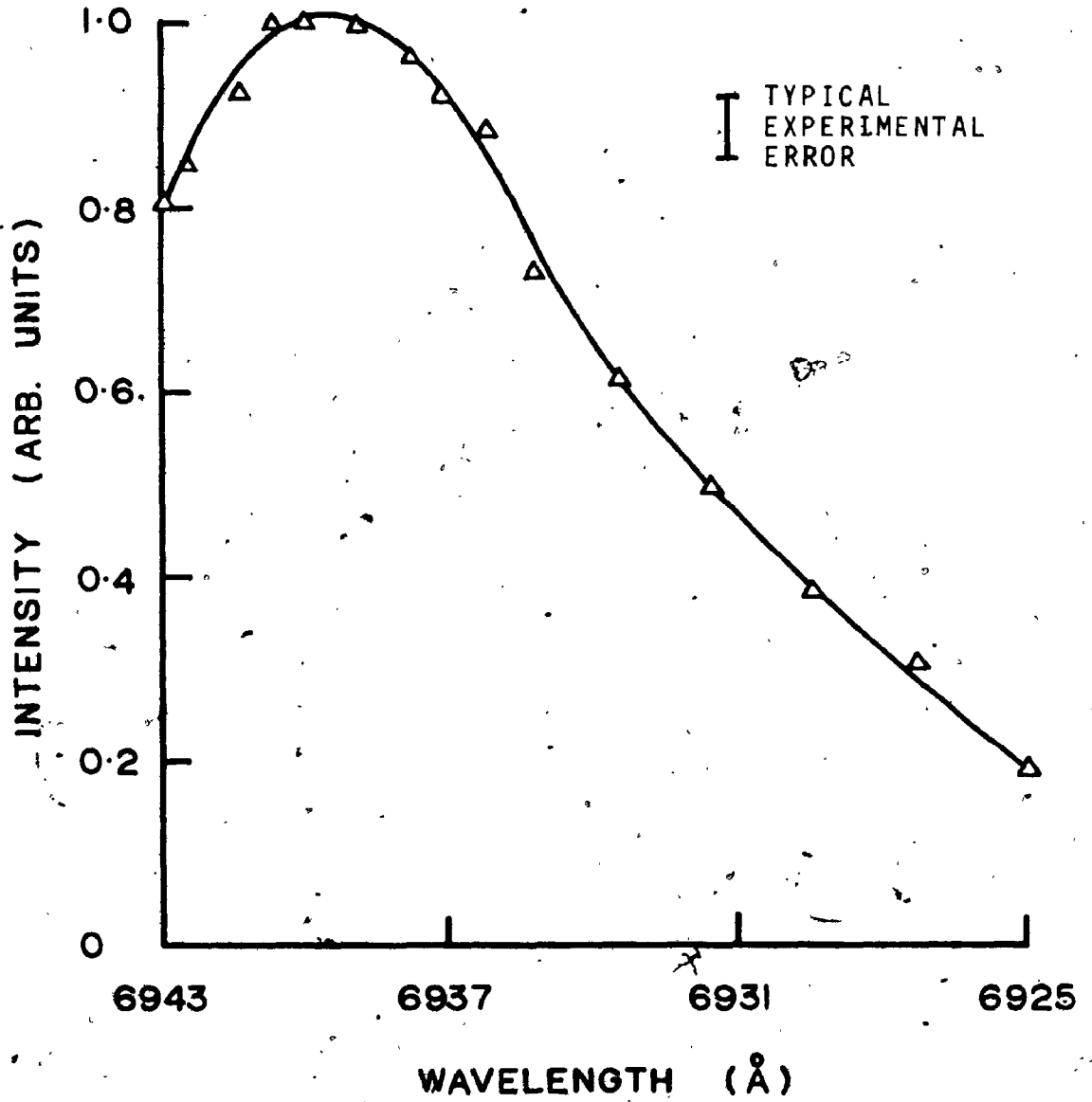


Fig. 3-17 Transmission profile of channel 4.



## CHAPTER 4

### PHOTOGRAPHIC STUDY OF THE THETA-PINCH PLASMA

Before scattering measurements were made, the dynamics and macroscopic structure of the theta-pinch plasma were studied using an image converter camera<sup>(48)</sup>. The primary purpose was to look for discharges which were macroscopically quiescent and homogeneous, and in particular, free from irregularities or non-uniformities such as flute instability<sup>(49)</sup> or plasma segmentation<sup>(50)</sup> which have been observed in some theta-pinch plasmas.

Fig. 4-1 shows the optical arrangement for end-on photographic study of the theta-pinch plasma. The exit chamber on which the blue filter glass was mounted ( Fig. 3-4 ), was removed and replaced by a glass window. The mid-plane of the theta-pinch discharge tube was first imaged by a pair of plano-convex lenses  $L_1$  and  $L_2$  onto a focal-plane stop A. The image of the plasma at A was then photographed using an Abtronics Model 2HS image converter camera with a phosphor screen having P11 spectral response. Overall demagnification due to the collection and camera optics was by a factor of 2.2.

The theta-pinch was discharged at 30 KV<sub>0</sub> at several

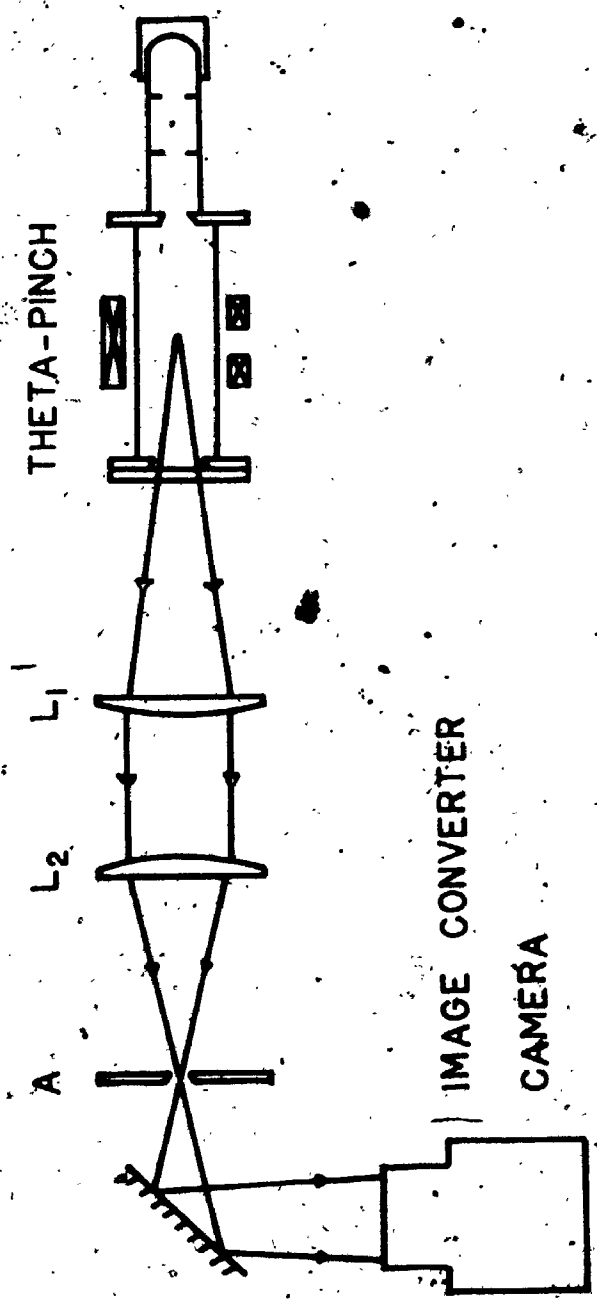
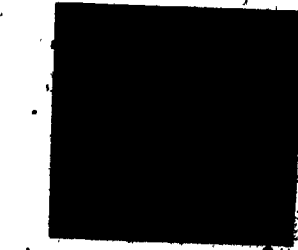


Fig. 4-1 Optical arrangement for end-on photographic study of the theta-pinch plasma.

initial hydrogen filling pressures between 20 to 200 milliTorr. Framing pictures of the plasma at various stages of development in the course of the discharge were taken. In particular, Fig. 4-2 and Fig. 4-3 show respectively the compression phases of the plasma during the ninth half cycle of the discharge formed at an initial hydrogen filling pressure of 20 milliTorr and that of the discharge formed at 50 milliTorr. Exposure time of each photograph was 0.01  $\mu$ sec and the time indicated with the photograph was measured from the beginning of the half cycle. In both cases, maximum compression of the plasma occurred at 0.50  $\mu$ sec. A qualitative picture of the degree of uniformity and the approximate spatial extent of the plasma was obtained from the observed luminosity. It should be noted that because of deterioration in the photocathode in the camera, sensitivity of the photocathode surface was not uniform even across a small area used in the experiment. Consequently, the region of the photocathode corresponding to the lower part of the photograph was more sensitive than that corresponding to the upper part.

From the photographs in Fig. 4-2 and Fig. 4-3, it is observed that at both filling pressures, breakdown of the gas appeared near the tube wall and the resulting plasma sheath was compressed uniformly to the axis of the theta-pinch coil. The compressed plasma showed a uniform and almost circular cross section. There was no indication of

Fig. 4-2 Photographs showing the compression phase of the plasma during the ninth half cycle of the discharge formed at an initial hydrogen filling pressure of 20 milliTorr.



0.60



0.50



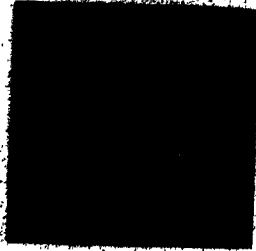
0.45



0.30



0.20



$\mu$  sec

Fig. 4-3 Photographs showing the compression phase of the plasma during the ninth half cycle of the discharge formed at an initial hydrogen filling pressure of 50 milliTorr.



0



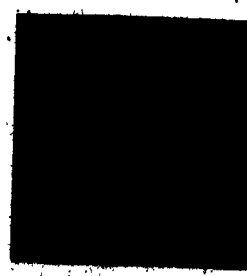
0.10



0.30



0.40



0.50



0.60

$\mu$  sec.

the presence of flute instability or plasma segmentation. At maximum compression, diameter of the luminous plasma filament in the case of 20 milliTorr was approximately 5.5 mm and that in the case of 50 milliTorr was about 9.9 mm. Since all scattering measurements would be made at the time of maximum compression of the plasma and the diameter of the focused spot of the laser beam at the centre of the theta-pinch discharge tube was 4 mm, it may be assumed that the plasma within the scattering volume was macroscopically quiescent and uniform for these two cases.



## CHAPTER 5

### RESULTS OF SCATTERING MEASUREMENTS

#### 5-1 The Scattering Measurements. C

Two sets of scattering data are presented here. The first one was obtained from a plasma formed at a hydrogen filling pressure of 20 milliTorr, which will be referred to as Case 1 and the second one was obtained from a plasma formed at a hydrogen pressure of 50 milliTorr, referred to as Case 2. In both cases, the laser pulse was timed to coincide with the maximum magnetic compression in the ninth half cycle of the discharge ( 9.5  $\mu$ sec after the initiation of the discharge ).

In making scanning measurements in channels 1 and 2, a special precaution was taken. For Case 1, the scanning was made symmetrically about the laser wavelength. For example, when channel 1 was set to measure the scattered intensity at  $+10 \text{ \AA}$ , channel 2 was set for measurements at approximately  $-10 \text{ \AA}$ . Whereas for Case 2, scanning of the red-shifted and the blue-shifted sides of the scattered spectrum was made randomly. That is, when channel 1 was measuring the scattered intensity at a certain wavelength shift on the red-shifted side, channel 2 was not always measuring the scattered intensity corresponding to the same wavelength shift on the blue-shifted side. Adopting such a

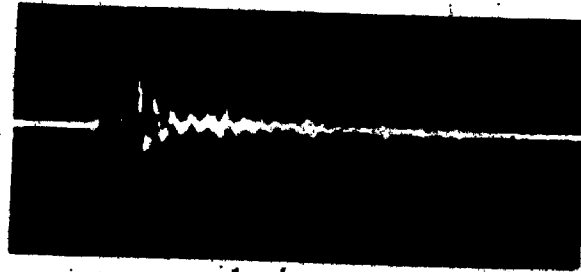
procedure, any observed symmetry in each of the scattered spectra ( Case 1 and Case 2 ) and in particular, any observed structures or deviations that are symmetrical about the laser wavelength are unlikely to be results of instrumental effects or random fluctuations.

In each set of scattering measurements, about 250 single measurements were made. For Case 1, variations of approximately 20% in the plasma electron density and electron temperature were observed at the time of scattering and for Case 2, variations of about 30% were observed. These variations were mainly due to non-reproducibility of the plasma discharge. Consistency between the measured scattered signals in the scanning channels and the signals measured from the electron density and temperature monitors was checked by repeating scanning measurements at the same wavelength shifts but at different times during the course of the experiment.

Fig. 5-1 shows the oscillographs of the laser monitor signal and the signals in the various channels of the spectrometer system obtained in a typical scattering measurement, the sharp spikes being the laser signals. The scattered signal in each channel of the spectrometer was a combined signal of Thomson scattered light and laser stray light and the latter was subtracted to yield the true Thomson scattered signal.

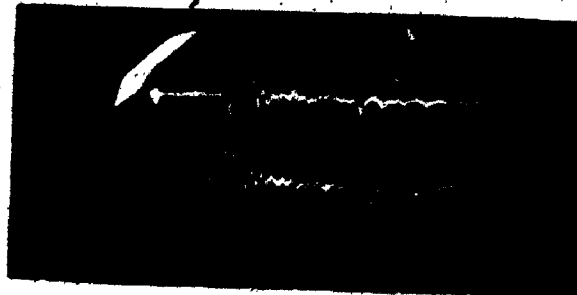
Fig. 5-1 Oscillographs of a typical set of  
laser scattering measurement.

LASER  
MONITOR



0.5 V/DIV.

CHANNEL 1



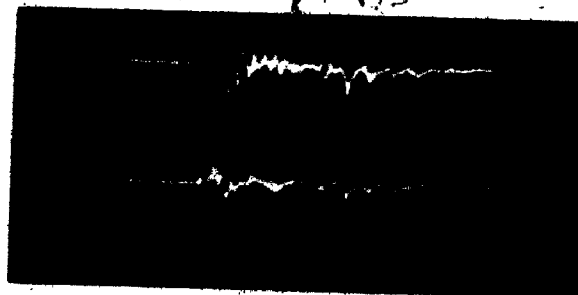
0.5 V/DIV.

CHANNEL 2



0.2 V/DIV.

CHANNEL 3



0.2 V/DIV.

CHANNEL 4



0.5 V/DIV.

ALL SWEEP : 2  $\mu$ SEC/DIV.

## 5-2. Procedure for Data Analysis.

From the discussion in Section 2-4 of Chapter 2, it is clear that the shape of the scattered spectrum is determined by the scattering parameter  $\alpha$  whereas the spectral width is determined by the electron temperature in the case of the electron spectrum, or by the ion temperature for the ion spectrum. Therefore, in general, scattered spectra are obtained by best fitting of theoretical profiles to the experimental data by varying three parameters, namely the  $\alpha$  parameter, the electron temperature and the constant which normalizes the scattering data for comparison with the theoretical profiles\*.

However, for the two sets of scattering measurements presented, the accuracy in the electron density measurement which was obtained from Rayleigh scattering calibration of the total scattered intensity measured in the density monitoring channel was estimated to be better than  $\pm 15\%$ . Such a measurement can thus be used to reduce the number of variables in the best fit analysis. Accordingly, the following procedure for data analysis was devised. First, the electron density was determined from the density monitor. Using such a density value, a theoretical profile was best

---

\* Note that  $\alpha \equiv 1/k\lambda_D = (1/k)(4\pi n_e e^2 / KT_e)^{1/2}$ , so that for the three parameters,  $\alpha$ ,  $T_e$  and  $n_e$ , only two of them are independent parameters.

fitted to the experimental data by varying the electron temperature ( or equivalently, the  $\alpha$  parameter ) and the normalization constant. Only data points corresponding to wavelength shifts sufficiently large so that they contained negligible contribution from the ion spectrum were used in the best fit analysis because (i) the primary interest in this work is to measure the electron spectrum and (ii) since the ion spectral profile was a rapidly changing function of wavelength shifts, the few points measured near the laser wavelength could not accurately represent the ion profile. A value for the electron temperature was then obtained from the best fit profile. As pointed out in Section 3-3.1, non-thermal density fluctuations in the plasma can cause enhancements in the scattering cross section, especially in the ion spectrum. Such enhanced scattering will introduce errors in the electron density measurement provided by the density monitor and must be accounted for. Thus, the best fit profile was extrapolated to the laser wavelength and compared with the measured data. Observed enhancements in the ion spectrum and the electron spectrum were taken into account and a new density value was obtained from the density monitor, with which the best fit analysis was performed again. By repeating the process, a self-consistent set of density and temperature values was obtained. As a further check, the density thus determined was compared with that obtained from Rayleigh scattering calibration of the integrated scattered intensity in the

electron spectrum, and the temperature value was compared with that determined from the temperature monitor with the effect of enhanced scattering again taken into account.

There is, however, one limitation with regard to the validity of such a procedure for analysing the scattering data. The method cannot detect the existence, if any, of a uniform enhancement of scattering cross section at all wavelength shifts ( or frequency shifts ). Such an enhancement will invalidate the electron density measurement determined from the density monitor. Only one observation of uniform enhancement of scattering cross section has been reported<sup>(28)</sup> in the literature, but no explanation or further elaboration has been given. Under the circumstances, we do not understand the cause of such an anomalous scattering phenomenon and we would therefore consider it only as an uncertainty in our present method of data analysis.

### 5-3 The Scattered Spectra.

#### 5-3.1 Case 1: Initial Hydrogen Filling Pressure of 20 milliTorr.

The scattered spectrum measured on a plasma formed at an initial hydrogen filling pressure of 20 milliTorr is presented in Fig. 5-2 and Fig. 5-3. Fig. 5-2 shows the red-

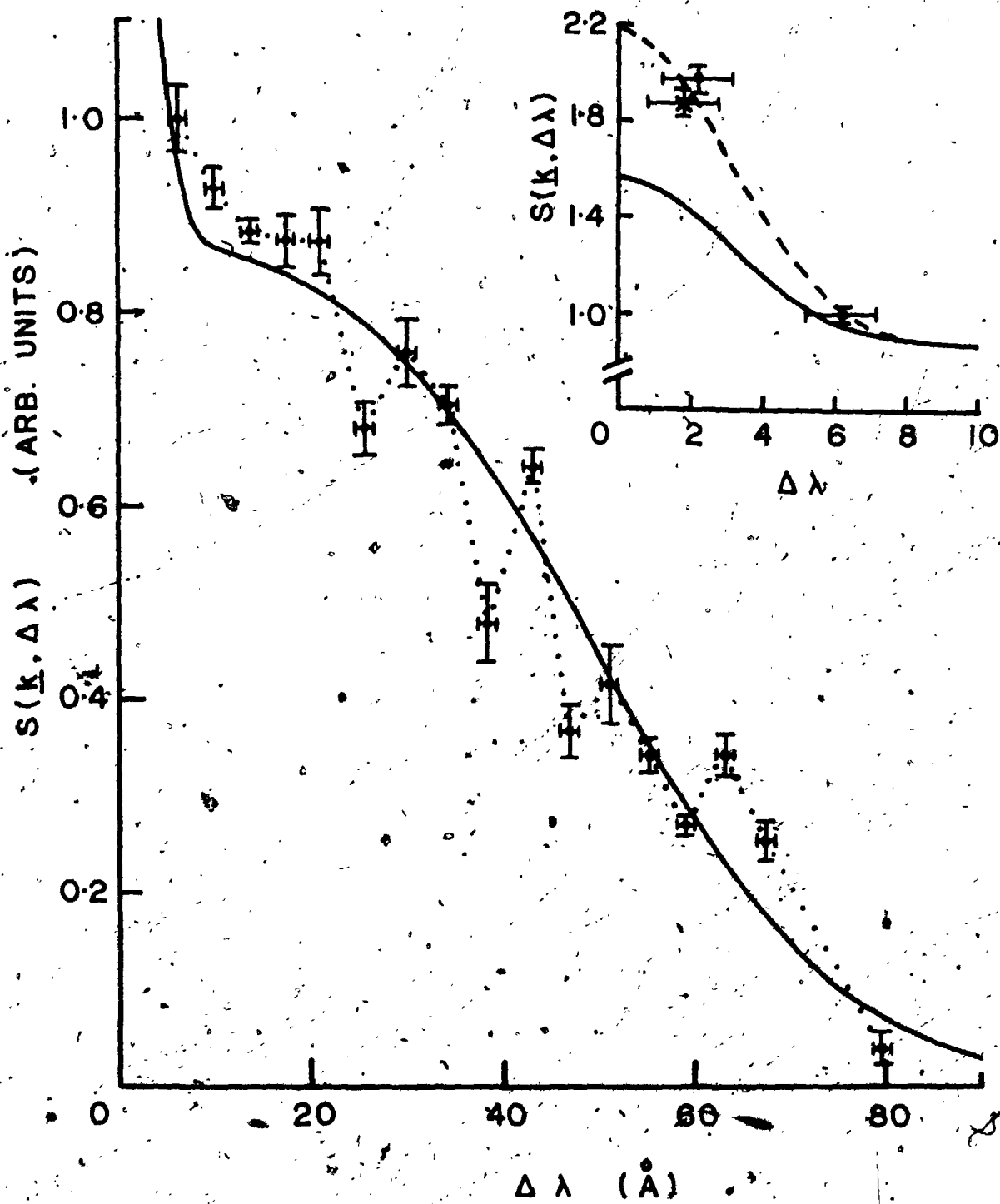


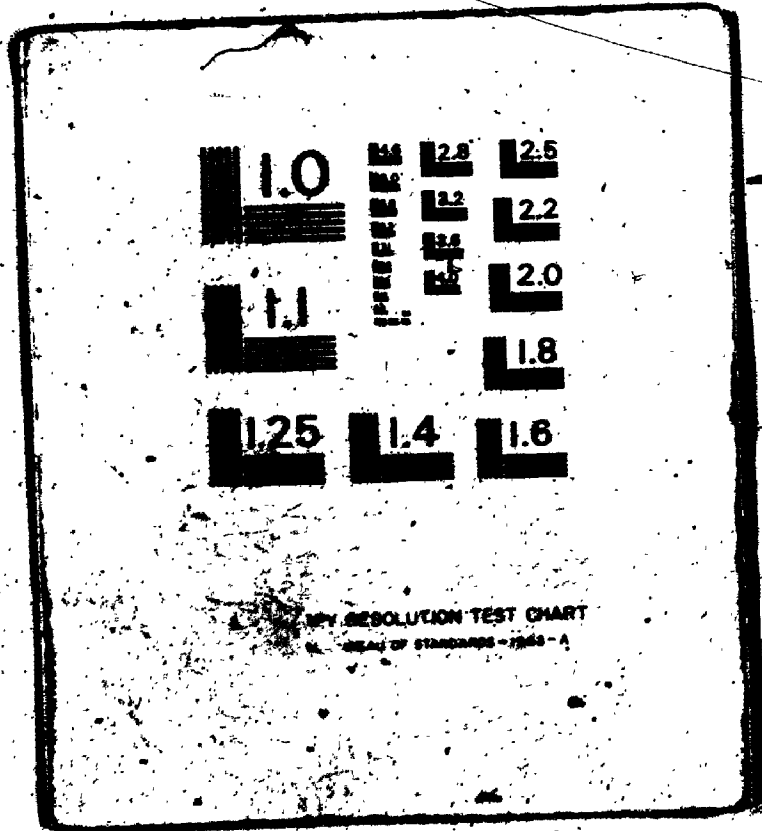
Fig. 5-2 The red-shifted side of the scattered spectrum for Case 1.



# 2

OF/DE

# 2



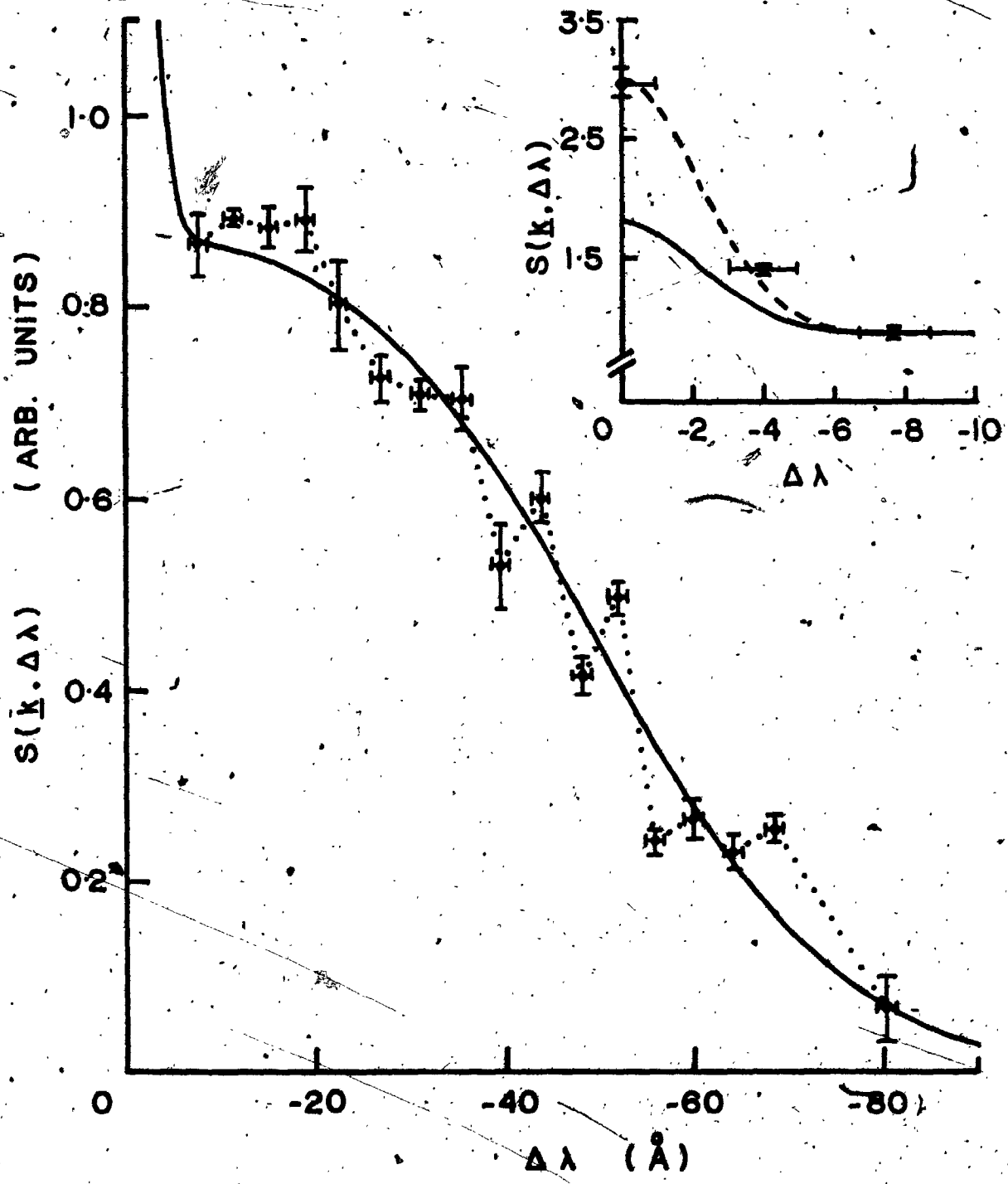


Fig. 5-3 The blue-shifted side of the scattered spectrum for Case 1.

shifted side of the scattered spectrum measured in channel 1 of the spectrometer system and Fig. 5-3 shows the blue-shifted side measured in channel 2. The data point x in the insert of Fig. 5-2 was actually measured at the indicated wavelength shift on the blue-shifted side. However, because of the different instrumental functions of channels 1 and 2, this data point cannot be presented in Fig. 5-3. The spectrum was compiled from about 120 single scattering measurements corresponding to variations of  $\pm 7\%$  in the plasma electron density and electron temperature. Each data point represents the average of a minimum of five measurements. The error bar in the ordinate corresponds to one standard deviation whereas the error bar in the abscissa represents the estimated accuracy in wavelength calibration. At the laser wavelength, laser stray light signals were approximately 40% of the true Thomson scattered signals for both channels 1 and 2. It is seen that the data points in each side of the spectrum do not fall on a smooth curve and even before any comparison is made with theoretical profiles, it is apparent that, by simply joining consecutive data points (as indicated by the dotted lines in the figures), the measured spectrum contains many features.

The plasma electron density as determined from the density monitor by Rayleigh scattering calibration of the Thomson scattered intensity was  $(1.40 \pm 0.14) \times 10^{16} \text{ cm}^{-3}$ .

Best fit analysis of the measured scattered spectrum using this value of density yielded an electron temperature of  $(5.1_{-0.2}^{+0.3})$  eV for  $\alpha=0.55\pm 0.04$ . The electron density determined from the integrated scattered intensity under each half of the spectral profile was  $(1.38\pm 0.19)\times 10^{16}$  cm<sup>-3</sup> whereas the electron temperature obtained from the temperature monitor was  $(5.2_{-1.4}^{+2.8})$  eV. Thus, all results were in agreement within the stated error.

The solid lines in Figures 5-2 and 5-3 are theoretical curves which have been convoluted with the appropriate instrumental profiles, for  $\alpha=0.55$ ,  $n_e=1.4\times 10^{16}$  cm<sup>-3</sup> and  $T_e=5.1$  eV. Deviations from the thermal spectrum are evident in both the red-shifted and the blue-shifted sides and appear as a fine structure of oscillations as indicated by the dotted lines. For the scattered spectrum near the laser wavelength as shown in the inserts of Figures 5-2 and 5-3, the dashed lines were obtained by raising the ion profile to best fit the experimental data. Enhancement of approximately 100% in the ion spectrum was observed.

### 5-3.2 Case 2: Initial Hydrogen Filling Pressure of 50 mill-Torr.

The red-shifted and the blue-shifted sides of the scattered spectrum measured on a plasma formed at an

initial hydrogen filling pressure of 50 milliTorr are shown in Fig. 5-4 and Fig. 5-5 respectively. For compilation of the scattered spectrum, about 110 single scattering measurements were selected for which the variations in the plasma electron density and electron temperature were within  $\pm 10\%$ . Each data point is an average of a minimum of five measurements with the error bars defined as in the previous section. At the laser wavelength, the magnitude of laser stray light signals was about the same as that of the true Thomson scattered signals. Again, as shown by the dotted lines which were obtained by joining consecutive data points, it is seen that many features are present in the measured spectrum.

Rayleigh scattering calibration of the scattered intensity measured in the density monitor yielded a plasma electron density of  $(7.7 \pm 1.1) \times 10^{15} \text{ cm}^{-3}$ . Using this value of density, a best fit analysis of the measured scattered spectrum gave an electron temperature of  $(5.1 \pm 0.3) \text{ eV}$  and  $\alpha = 0.41 \pm 0.04$ . The electron density determined from the integrated intensity under the spectral profile was  $(7.8 \pm 1.3) \times 10^{15} \text{ cm}^{-3}$  and the electron temperature determined from the temperature monitor was  $(4.6^{+2.6}_{-1.2}) \text{ eV}$ . All results were again in agreement within the stated error.

The solid lines in Fig. 5-4 and Fig. 5-5 are the theoretical curves that have been convoluted with the

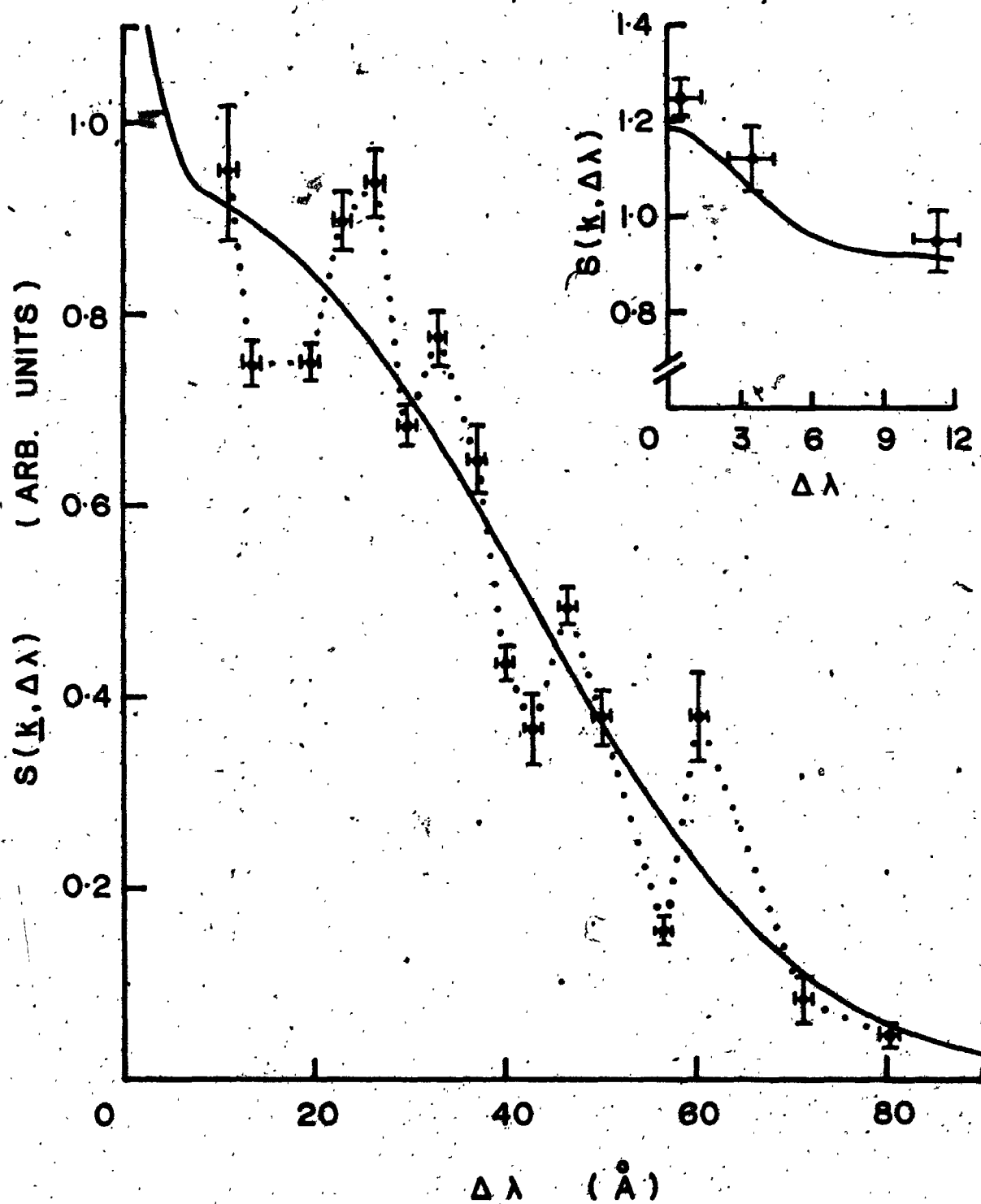


Fig. 5-4 The red-shifted side of the scattered spectrum for Case 2.

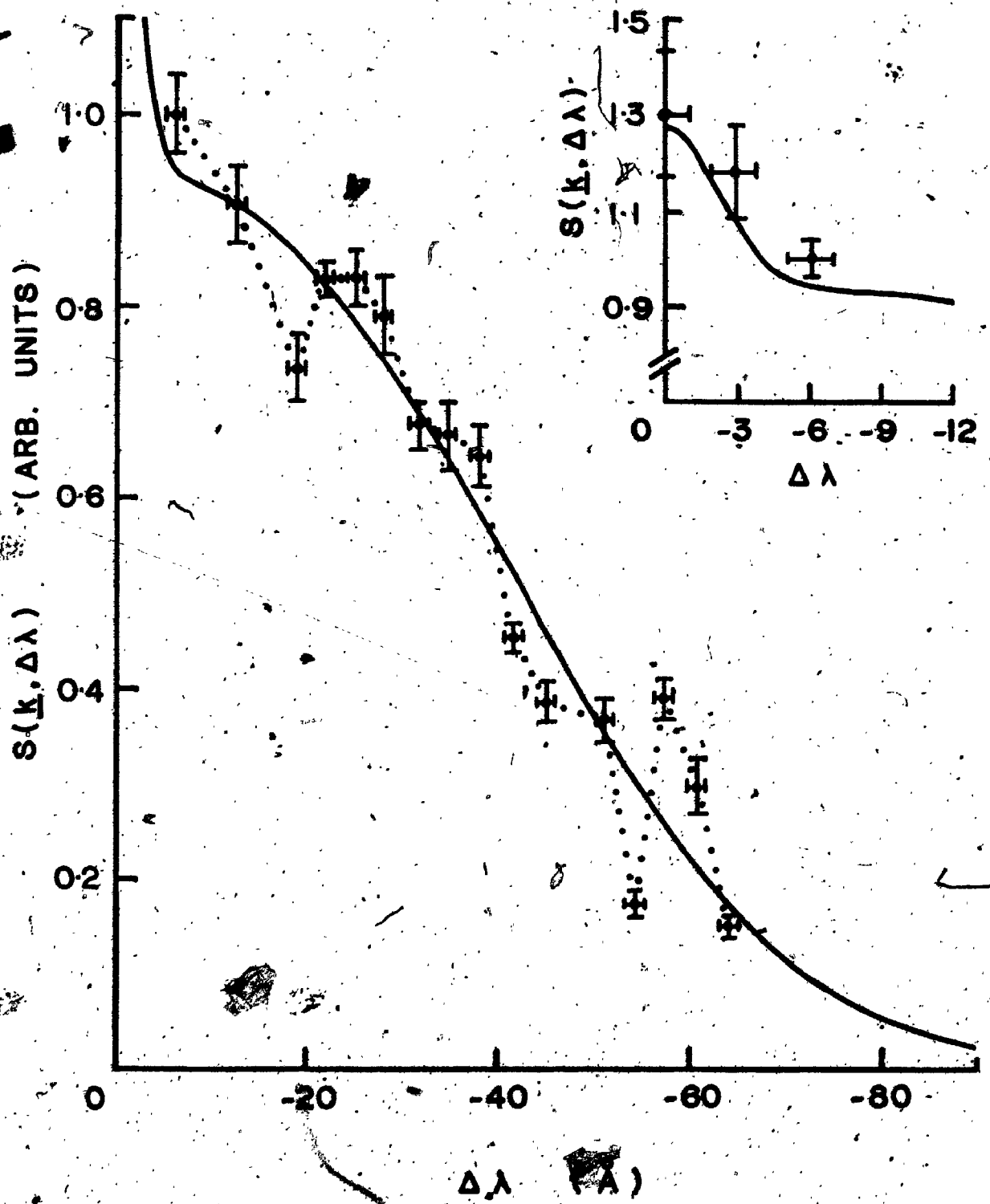


Fig. 5-5 The blue-shifted side of the scattered spectrum for Case 2.

appropriate instrumental profiles, for  $\alpha=0.41$ ,  $n_e=7.7 \times 10^{15}$   $\text{cm}^{-3}$  and  $T_e=5.1$  eV. Deviations in the form of a fine structure of oscillations ( indicated by the dotted lines in the figures ) superimposed on the thermal profile, were also observed. However, as shown in the inserts of the figures, there was no significant enhancement in the ion spectrum.



## CHAPTER 6 DISCUSSIONS

### 6-1 Implications of the Experimental Results.

#### 6-1.1 The Anomalies in the Scattered Spectra.

In the  $90^{\circ}$ -scattered spectra measured from two theta-pinch plasmas ( Case 1 and Case 2 ), anomalous deviations from the thermal profiles were observed. Results of the present analysis show that the anomalies in the electron spectrum contained both positive and negative deviations relative to the thermal level and consequently, there was no significant change in the corresponding scattering cross section.

As shown in figures 5-2, 5-3, 5-4 and 5-5, the general feature of the anomalous deviations was symmetrical about the laser wavelength. However, in both spectra, the fine structures of oscillations seemed to be more pronounced in the red-shifted side than that in the blue-shifted side in spite of the approximately equal spectral resolutions of the scanning channels 1 and 2. The significance or cause of this apparent, small degree of asymmetry was not understood.

The experimental results also show that in the

scattered spectral profile for Case 1, appearance of the anomalous deviations in the electron spectrum was accompanied by an approximately 100% enhancement in the ion spectrum whereas in the spectral profile of Case 2, only deviations in the electron spectrum was evident. It is, therefore, suggestive that the anomalies in the electron and the ion components of the scattered spectra are independent. Kegel<sup>(51,52)</sup> has shown that for a plasma whose electron distribution function consists of two Maxwellian components, namely a background electron component and a small fraction ( for example, 5-10% ) of electrons with a much lower temperature ( for example,  $10^{-2}$  of the temperature of the background component ), appreciable enhancements in the ion spectrum will occur. However, for the plasma discharges studied in this experiment, the electron-electron equipartition time<sup>(53)</sup> was of the order  $10^{-11}$  sec. In the time scale of the scattering measurements, which was about 30 nsec ( duration of the laser pulse ), the existence of a secondary component of cold electrons is unlikely. Furthermore, as the detailed profile of the ion spectrum was not measured, quantitative analysis cannot be performed.

As the scattered spectrum is also a measure of the spectrum of electron density fluctuations ( Eq. 2-6 ), the present results can be interpreted as an experimental observation of non-thermal density fluctuations or waves in the plasma. One further notes that the anomalous deviations

in the electron components of the scattered spectra appeared only as a modulation of the thermal profiles. Hence, the measured spectral profile  $S(\underline{k}, \omega)$  may be considered as the sum of two parts: a thermal component  $S_{\text{Thermal}}(\underline{k}, \omega)$  as given by scattering theory and a non-thermal component  $S_1(\underline{k}, \omega)$  which is defined as

$$S_1(\underline{k}, \omega) = S(\underline{k}, \omega) - S_{\text{Thermal}}(\underline{k}, \omega)$$

It follows then  $S_1(\underline{k}, \omega)$  represents the spectrum of non-thermal density fluctuations. Fig. 6-1 and Fig. 6-2 show respectively the red-shifted and the blue-shifted sides of  $S_1(\underline{k}, \omega)$  for Case 1, and Fig. 6-3, Fig. 6-4 show the corresponding sides of  $S_1(\underline{k}, \omega)$  for Case 2. For the abscissa in these figures, two frequency scales are shown, one indicating the absolute value of the frequency shift and the other indicating the frequency shift normalized to the electron plasma frequency  $\omega_p$ . For Case 1, it is seen that  $S_1(\underline{k}, \omega)$  consists of "peaks" which occur at approximately  $\omega_p$ ,  $2\omega_p$ ,  $2.5\omega_p$ ,  $3\omega_p$  and  $4\omega_p$ , whereas for Case 2, "peaks" appear at approximately  $2\omega_p$ ,  $3\omega_p$ ,  $4\omega_p$  and  $5\omega_p$ . Thus, the present results indicate that the observed non-thermal density fluctuations are correlated with harmonics of  $\omega_p$  and when the electron density (and hence,  $\omega_p$ ) was changed, the anomalous "peaks" shifted in wavelength accordingly.

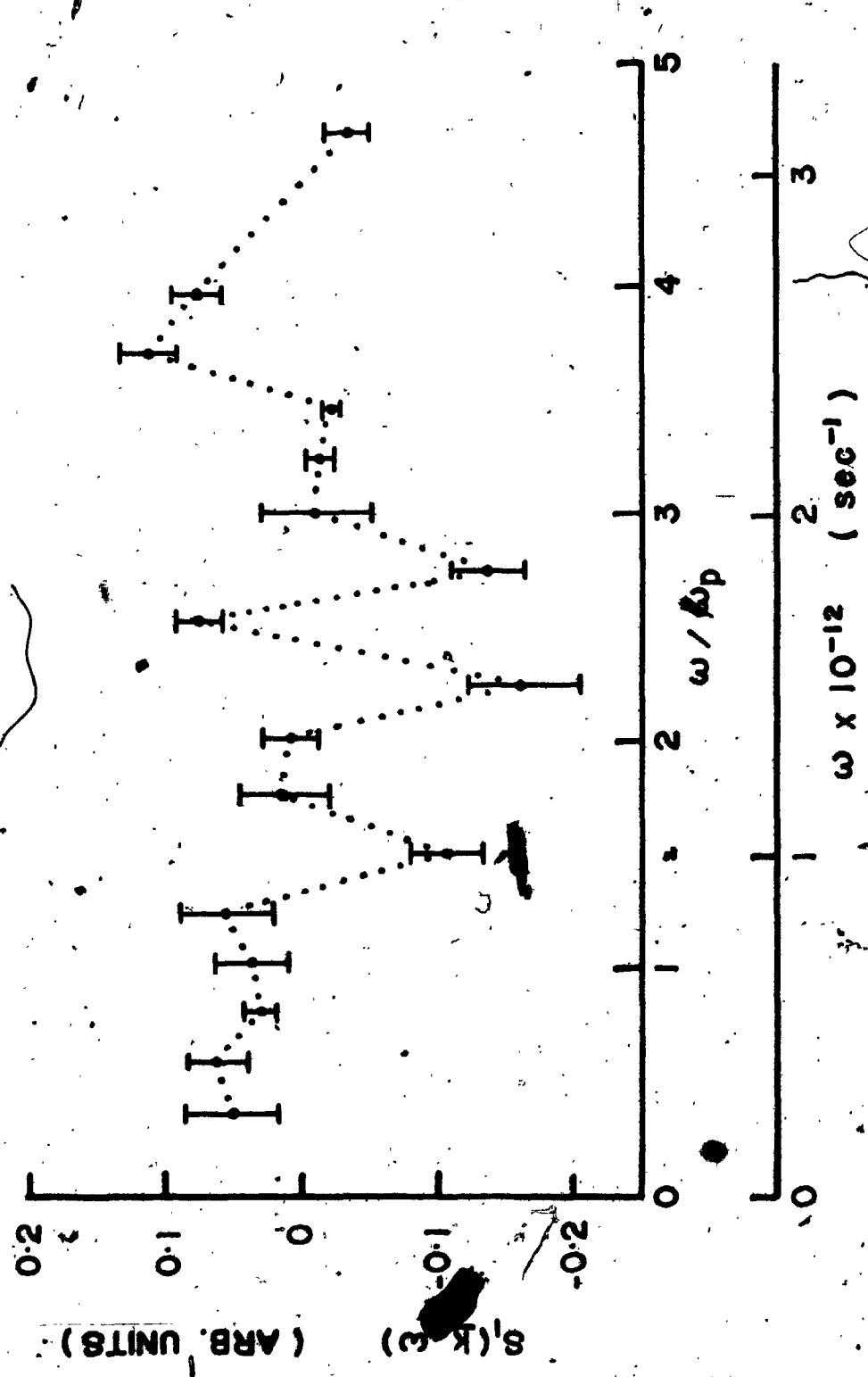


Fig. 6-1 The red-shifted side of the non-thermal component of the scattered spectrum for Case 1.

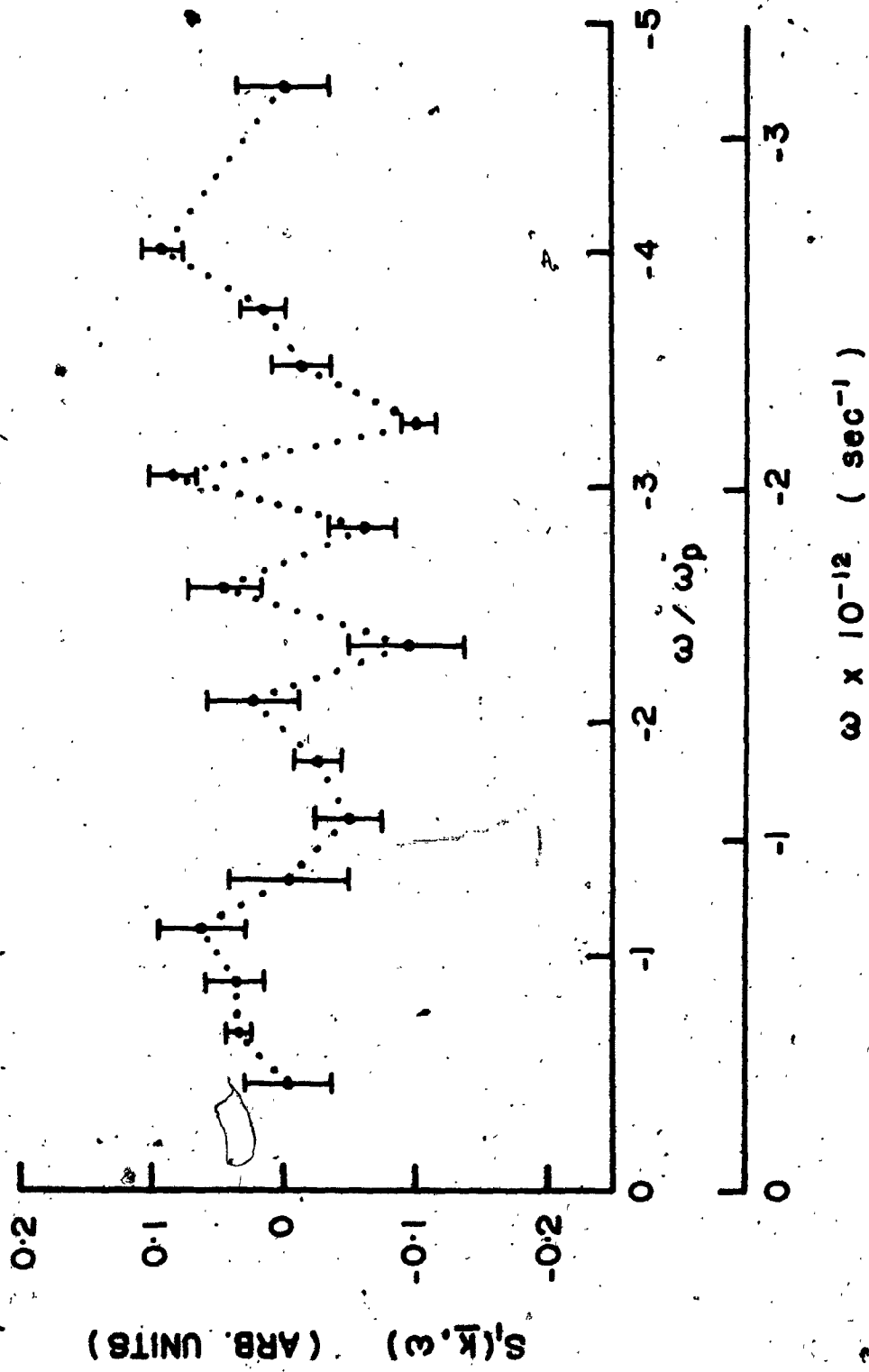


Fig. 6-2 The blue-shifted side of the non-thermal component of the scattered spectrum for Case 1.

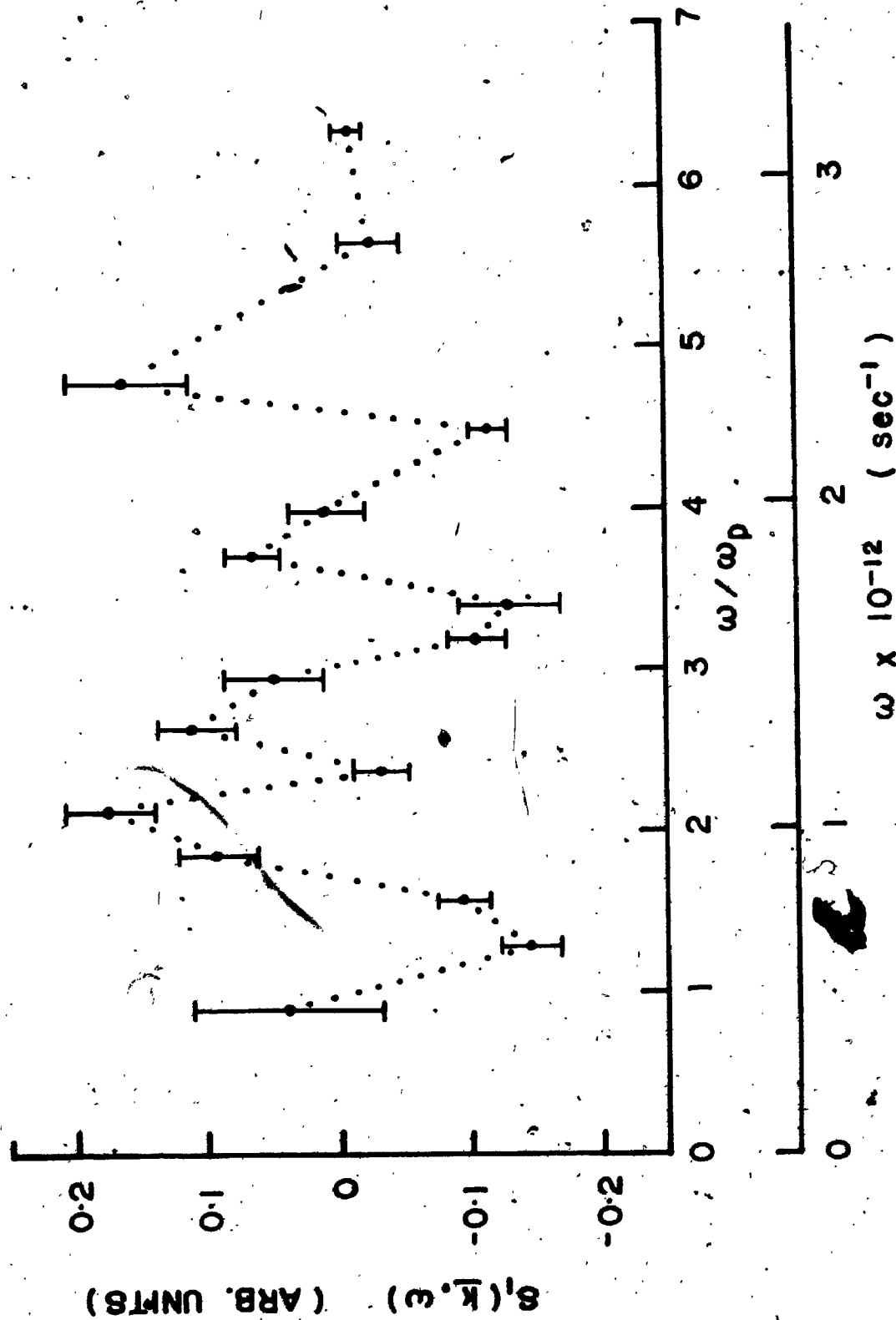


Fig. 6-3 The red-shifted side of the non-thermal component of the scattered spectrum for Case 2.

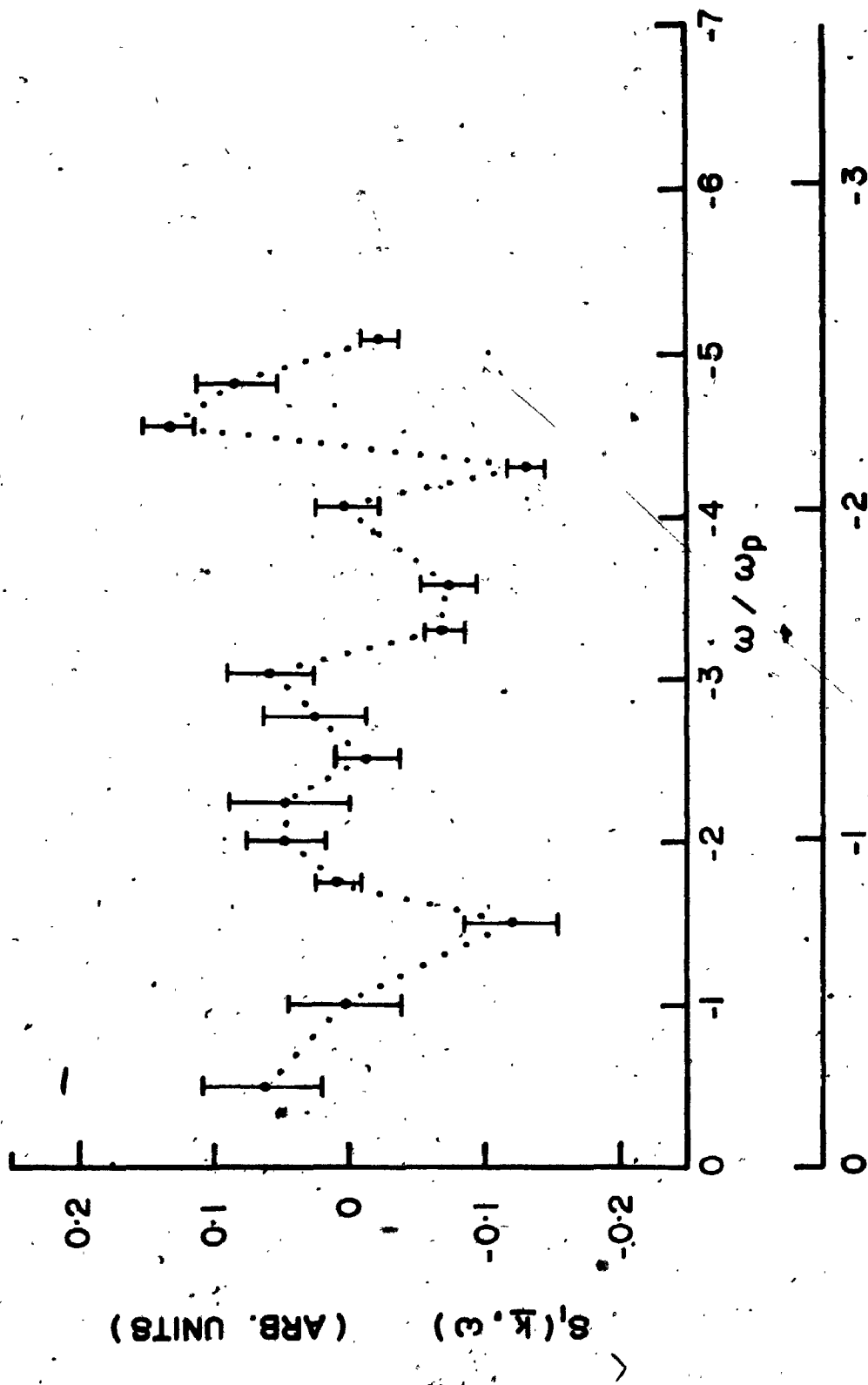


Fig. 6-4 The blue-shifted side of the non-thermal component of the scattered spectrum for Case 2.

### 6-1.2 Comparison with Arc Plasmas.

A very interesting point about the anomalous scattering phenomenon observed in this experiment is that the deviations did not appear as a single feature like a "dip" or a resonant "peak" as observed in other earlier measurements made on theta-pinch plasmas<sup>(33,34)</sup>. Instead, the anomalies are qualitatively similar to those observed in several scattered spectra measured on arc plasmas<sup>(11,27,28,29,32)</sup>. They contained multiple features and appeared as a modulation of the thermal spectrum. Quantitative correlation between these anomalies is, however, unclear. Specifically, the anomalies observed here showed, except for a single feature in Case 1, modulations at intervals of  $\omega_p$ ; results obtained by Ringler and Nodwell<sup>(27,28)</sup> indicated modulations at harmonics of  $\omega_p$ ; measurements made by Ludwig and Mahn<sup>(11)</sup> showed modulations at intervals of  $\omega_p/2$ ; Churchland and Nodwell<sup>(32)</sup> observed modulations at intervals of  $\omega_p/4$  and finally, the anomalies observed by Ludwig et al<sup>(29)</sup> seemed to be unsystematic.

Table 6-1 shows a comparison of some basic parameters characterizing these plasmas. It is interesting to note that all of these are cold, dense plasmas with very similar parameters. As indicated by the small number of electrons in the Debye volume, these plasmas are collision-dominated. By comparing the various equipartition times with the time scale of scattering measurements (typically 20-40 nsec as



Table 6-1 Comparison between the theta-pinch plasma and some arc plasmas.

PLASMA	REFERENCE	$n_e$ (cm <sup>-3</sup> )	$T_e$ (eV)	$\alpha$	$\Lambda$	$\tau_{ee}$ (sec)	$\tau_{ii}$ (sec)	$\tau_{ei}$ (sec)
Magnetically stabilized hydrogen arc plasmas.	27	$7.4 \times 10^{15}$	5.2	0.41	56	$4 \times 10^{-11}$	$2 \times 10^{-9}$	$7 \times 10^{-8}$
	28	$9.7 \times 10^{15}$	5.3	0.45	51	$3 \times 10^{-11}$	$1 \times 10^{-9}$	$5 \times 10^{-8}$
		$1.1 \times 10^{16}$	4.5	0.51	38	$2 \times 10^{-11}$	$9 \times 10^{-10}$	$4 \times 10^{-8}$
	11	$1.2 \times 10^{16}$	6.0	0.47	55	$3 \times 10^{-11}$	$1 \times 10^{-9}$	$5 \times 10^{-8}$
Carbon arc plasmas	29	$1.0 \times 10^{16}$	5.2	0.46	48	$3 \times 10^{-11}$	$1 \times 10^{-9}$	$5 \times 10^{-8}$
	32	$1.3 \times 10^{17}$	2.3	1.90	4	$9 \times 10^{-13}$	$4 \times 10^{-11}$	$2 \times 10^{-9}$
Theta-pinch plasmas.	Present work.	$1.8 \times 10^{17}$	2.5	2.20	4	$8 \times 10^{-13}$	$3 \times 10^{-11}$	$1 \times 10^{-9}$
		$1.4 \times 10^{16}$	5.1	0.55	40	$2 \times 10^{-11}$	$8 \times 10^{-10}$	$4 \times 10^{-8}$
		$7.7 \times 10^{15}$	5.1	0.41	54	$3 \times 10^{-11}$	$1 \times 10^{-9}$	$6 \times 10^{-8}$

NOTATIONS:  $\alpha = 1/k\lambda_D$  is the scattering parameter,  
 $\Lambda = n_e \lambda_D^3$  is the number of electrons in the Debye volume (20),  
 $\tau_{ee}$  = electron-electron equipartition time (53),  
 $\tau_{ii}$  = ion-ion equipartition time (53),  
 $\tau_{ei}$  = electron-ion equipartition time (53).

given by the duration of the laser pulse), it is seen that the velocity distributions of the electrons and that of the ions in these plasmas are most likely Maxwellian although the electron and ion temperatures may be different except for the carbon arc plasmas in which the electron and ion temperatures may even be equal.

In spite of the apparent quantitative inconsistencies, the qualitative similarity between the anomalies observed in the scattered spectra as well as the close similarity between these plasmas with regard to the parameters listed in Table 6-1 may indeed lead one to speculate that the anomalous scattering phenomenon is probably a fundamental and universal plasma phenomenon, at least in the case of a cold, dense plasma.

### 6-1.3 The Plasma Approximation.

In the framework of plasma kinetic theory, there is an important expansion parameter known as the plasma parameter,  $g$ , which is defined as

$$g = \frac{1}{n_e \lambda_D^3}$$

where  $n_e \lambda_D^3$  ( $=\Lambda$  as defined by Salpeter<sup>(20)</sup>) is the number of electrons in the Debye volume.

Physically, the plasma parameter is a measure of the

ratio of the mean interparticle potential energy to the mean plasma kinetic energy. An ideal gas corresponds to zero potential energy between particles. Therefore, if the plasma parameter is small, the plasma may be treated as an ideal gas of charged particles, that is, a gas with charge density and electric field but in which there is no interaction between two discrete particles. Accordingly, the plasma parameter may also be interpreted as a measure of the degree to which plasma or collective effects dominate over single-particle behaviour. The plasma state is described by equations obtained from an expansion of the exact many-body equations in powers of  $g$  and the assumption  $g \ll 1$  (or equivalently,  $\Lambda \gg 1$ ) is called the plasma approximation.

In standard scattering theories, plasma approximation is used and effects to the first order in  $g$  are considered. In Salpeter's theory<sup>(20)</sup>, this is seen explicitly in the calculation of the density fluctuation, in which only terms to the order  $g$  are retained. As for Rosenbluth and Rostoker's theory<sup>(23)</sup>, effects of the order  $g$  are obtained from a physical approach, namely, the uncorrelated dressed test-particle formalism. Corrections to the cooperative electron fluctuations when  $\Lambda (=n_e \lambda_D^3) \approx 1$  have been considered by Theimer<sup>(54)</sup>. He concludes that deviations from the normal spectra will occur when  $(4\pi/3)n_e \lambda_D^3 < 0.5$ . Measurements of coherent spectra ( $\alpha > 1$ ) including both the ion feature and

the plasma satellites have been made in the range of  $\Lambda=2-10$  by Rohr<sup>(55)</sup> and no significant deviations from the standard theory ( $\Lambda \gg 1$ ) were observed. Similar agreement with theory was obtained by Kato<sup>(56)</sup> who made measurements at  $\Lambda=2$  and  $\Lambda=12$  for  $\alpha > 1$ . However, an anomalous result for  $\Lambda \approx 7$  and  $\alpha = 0.45$  showing apparently a resonant peak in the scattered spectrum was reported by John et al<sup>(34)</sup> and it was conjectured that the standard scattering theories which assume  $\Lambda \gg 1$  and consider effects to the first order in  $1/\Lambda$  might not be appropriate when  $\Lambda$  was of that order.

For the measurements presented here,  $\Lambda=40$ ,  $\alpha=0.55$  in Case 1 and  $\Lambda=54$ ,  $\alpha=0.41$  in Case 2. Deviations were again observed even when  $\Lambda$  was almost an order of magnitude greater than that in the measurement of John et al<sup>(34)</sup>. Although the deviations in these cases consisted of multiple features rather than a single resonant feature, the present results nonetheless suggest that it is unlikely that the observed anomalous scattering phenomenon is due to the use of the plasma approximation  $\Lambda \gg 1$  ( $g \ll 1$ ) and the neglect of effects of second and higher orders in  $1/\Lambda$  ( $g$ ) in the scattering theory.

#### 6-1.4 Macroscopic Plasma Structure.

In a plasma, spatial variations of physical quantities are sources of free energy. It is a natural tendency of a nonuniform system to release the extra amount of free energy and thereby to approach a uniform state of thermal equilibrium. Ordinarily, this is achieved through collisional processes. However, the sources of free energy may also drive oscillations in the plasma or even excite plasma instabilities<sup>(57)</sup>.

As noted in Chapter 4, photographic study of the plasma shows that, at the time of scattering measurements, the plasma columns were apparently macroscopically quiescent and uniform. Furthermore, in the central region of the plasma column where scattering measurements were made, gradients associated with electron density and possibly electron temperature should be much less pronounced than those in the plasma boundary. Electron drifts, if present, should also be smaller in the central region. Since the ratio of the spatial extent of the plasma to the scattering region in Case 2 was greater than that in Case 1 by almost a factor of two, one would expect that, if the observed anomalous scattering phenomenon was due to gradients or drifts, greater degree of deviation would be present in the scattered spectrum of Case 1. Evidently, no such disparity was observed in the scattered spectra for the two cases. One may therefore conjecture that the anomaly observed here

was not caused by macroscopic nonuniformities in the plasma.

## 6-2 Other Considerations.

### 6-2.1 Effect of Laser Radiation on the Plasma.

The advantage of laser scattering as a plasma diagnostic technique is that, in general, the probing laser beam does not perturb the plasma. However, since the radiation does interact with the plasma, it is clear that at some level of laser intensity, the probing beam could exert an appreciable effect on the plasma. The laser can heat the plasma through the process of inverse bremsstrahlung<sup>(53)</sup> or the electric field of the laser light can influence the motion of the free electrons. The former can falsify the temperature value determined from the laser scattering measurements and the latter can give rise to non-thermal density fluctuations in the plasma<sup>(32)</sup>.

Assuming the electron-electron relaxation time is short compared with the duration of the laser pulse, radiation absorbed by inverse bremsstrahlung can be regarded as increasing the plasma electron temperature. The fractional increase in electron temperature under this condition and the further assumption that heat has not been conducted away during the laser pulse is given by<sup>(58)</sup>

$$\frac{\Delta T_e}{T_e} = 5.32 \times 10^{-7} \left( \frac{n_e Z}{T_e^{3/2}} \right) \lambda_i^3 \left\{ 1 - \exp\left(-\frac{h\nu_i}{T_e}\right) \right\} I_i \Delta\tau$$

where  $T_e$  is the electron temperature in eV,  $n_e$  is the electron density in  $\text{cm}^{-3}$ ,  $Ze$  is the charge on the ions,  $\lambda_i$  is the wavelength of the laser light in cm,  $h\nu_i$  is the photon energy of the laser radiation (1.79 eV for ruby laser),  $I_i$  is the laser intensity in  $\text{watts-cm}^{-2}$  and  $\Delta\tau$  is the duration of the laser pulse in sec. Accordingly, for the two cases of plasmas studied here, the fractional increase in electron temperature would be less than  $10^{-3}$ .

As for the collective effect, the maximum speed of a free electron accelerated by the electric field of the laser radiation is given by (59)

$$v_{\text{max}} = \frac{e E_i}{m \omega_i} = \frac{e}{m \omega_i} \left( \frac{2 I_i}{c \epsilon_0} \right)^{1/2} \text{ m-sec}^{-1}$$

where  $E_i$  and  $\omega_i$  are respectively the electric field and circular frequency of the incident laser light in units of  $\text{V-m}^{-1}$  and  $\text{rad-sec}^{-1}$ . In the present experiment,  $v_{\text{max}}$  was of the order of  $10^4 \text{ m-sec}^{-1}$  which was only a few percent of the thermal speed of the electrons. Since the deviations in the scattered spectra corresponded to phase velocities of the order of electron thermal velocity, collective effect should also be negligible.

## 6-2.2 Non-Maxwellian Velocity Distribution of Electrons in the Plasma.

In the framework of the scattering theory outlined in Chapter 2, a plasma is assumed such that the velocity distributions of the electrons and the ions are Maxwellian although their respective temperatures need not be equal. If the plasma further deviates from such an equilibrium state, appreciable changes in the scattered spectrum may occur. In particular, the presence of small, secondary components of cold electrons drifting in a background of hot electrons has been used to explain the anomalous scattering features in the electron spectra measured from a carbon arc plasma<sup>(32)</sup>. Modification of the spectrum  $S(\underline{k}, \omega)$  to incorporate such a non-Maxwellian distribution of electrons in the plasma is outlined in Appendix B.

As an example, Fig. 6-5 shows the convoluted theoretical profiles for a plasma in thermal equilibrium and that for a plasma with two arbitrarily imposed secondary, drifting, cold electron components. In the presence of this particular non-Maxwellian electron distribution, the scattered spectrum shows apparently periodic oscillations. Thus, it is conceivable that by incorporating appropriate components of cold, drifting electrons in the plasma, modified scattered spectra can be generated to fit the experimental data of Case 1 and Case 2 here. However, at the present, we do not understand if and why small, drifting



✓ 4

Fig. 6-5 Convolved theoretical scattered spectra for a plasma in thermal equilibrium (solid line) and for a non-Maxwellian plasma with two arbitrarily imposed, secondary, cold, drifting electron components (dotted line). Parameters of the plasmas are listed in Table 6-2.

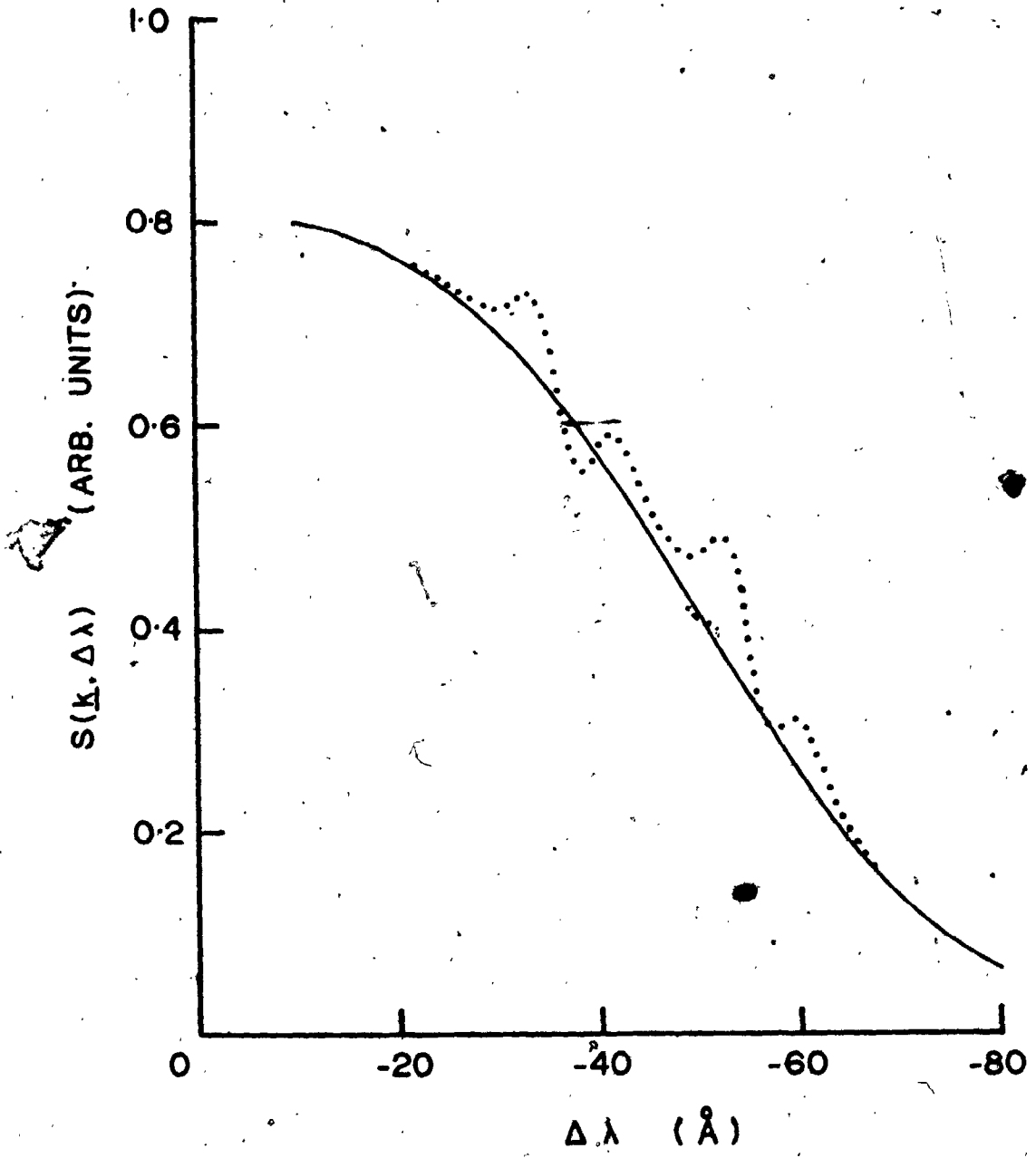


Table 6-2 Parameters of the plasmas considered  
in Fig. 6-5.

Maxwellian plasma:	$n_e = 1.4 \times 10^{16} \text{ cm}^{-3}$ $T_e = 5.1 \text{ eV}$
Non-Maxwellian plasma:	$n_{e0} = 1.4 \times 10^{16} \text{ cm}^{-3}$ $T_{e0} = 5.1 \text{ eV}$ $a = n_{e1}/n_{e0} = 0.002$ $T_{e1} = 10^{-3} T_{e0}$ $v_{D1} = 1.14 \times 10^8 \text{ cm-sec}^{-1}$ $b = n_{e2}/n_{e0} = 0.004$ $T_{e2} = 10^{-3} T_{e0}$ $v_{D2} = 1.71 \times 10^8 \text{ cm-sec}^{-1}$

components of cold electrons should exist in the plasmas studied in this experiment. The above approach of data analysis was not followed as it would seem too arbitrary. The qualitative aspect of the modification in the scattered spectrum was nonetheless considered as a valuable reference.

### 6-3 Summary and Conclusions.

A special spectrometer system has been developed which allows one to scan simultaneously the red-shifted and the blue-shifted sides of the spectrum of laser radiation scattered from a plasma. The system has also included in it density and temperature monitoring channels whereby "shot-to-shot" variations in the plasma electron density and temperature could be closely monitored, thus effectively overcoming the problem of inherent plasma non-reproducibility in point-to-point scanning measurements. Absolute values of electron density could also be determined from the density monitor. Optical arrangement of the system ensured that measurements in all channels were made on the same plasma volume. Spectral resolutions of the channels scanning the red-shifted and the blue-shifted sides of the scattered spectrum were approximately 6 Å and 5 Å respectively.

Using this spectrometer system, spectra of laser radiation scattered at  $90^\circ$  from a theta-pinch plasma have

been measured. Two plasma discharges were selected for the present study; one was formed at an initial hydrogen filling pressure of 20 milliTorr ( Case 1 ) and the other was formed at a pressure of 50 milliTorr ( Case 2 ). In each case, scattering measurements were made during the ninth half cycle of the discharge and at a time corresponding to the maximum compression of the plasma column. End-on photographs taken by an image converter camera indicated that, at the time scattering measurements were made, the plasmas studied were macroscopically quiescent and homogeneous within the scattering volume. As determined from the scattering measurements, parameters of the plasmas were, for Case 1:  $n_e = (1.40 \pm 0.14) \times 10^{16} \text{ cm}^{-3}$ ,  $T_e = (5.1_{-0.2}^{+0.3}) \text{ eV}$ , corresponding to  $\alpha = 0.55 \pm 0.04$ , and for Case 2:  $n_e = (7.7 \pm 1.1) \times 10^{15} \text{ cm}^{-3}$ ,  $T_e = (5.1 \pm 0.3) \text{ eV}$ , corresponding to  $\alpha = 0.41 \pm 0.04$ .

The measured scattered spectra contained multiple features which appeared as fine structures of oscillations superimposed on the thermal profiles. Qualitatively, these anomalies were symmetrical about the laser wavelength. Enhancement in the ion spectrum was observed only in the spectrum in Case 1. As the scattered spectrum is a measure of the spectrum of electron density fluctuations, the present results can be interpreted as an experimental observation of non-thermal density fluctuations in the plasma. It is seen that these non-thermal fluctuations are correlated with harmonics of the plasma frequency. Furthermore, the

qualitative similarity between the anomalies observed here and those reported in measurements on arc plasmas as well as the close similarity between these plasmas suggest that the anomalous scattering phenomenon could be a basic plasma phenomenon in cold, dense plasmas. The present results also suggest that the observed deviations from theory are probably not due to incompleteness of the scattering theories in which the plasma approximation is used and only effects to the order  $g$ , the plasma parameter, are considered. Finally, the photographic study of the plasma discharges indicates that the anomalous scattering was not caused by macroscopic non-uniformities in the plasma.

It was pointed out in the beginning of the thesis that the present work is a first phase of a formal investigation of the phenomenon of anomalous scattering of laser radiation by a theta-pinch plasma. With regard to future studies, there is always the possibility of improving the experimental instrumentation as well as techniques of measurement. On the other hand, it will be worthwhile to obtain and compile a greater set of  $90^\circ$ -scattered spectra measured on the theta-pinch plasma over a wide range of electron densities and electron temperatures. Such a collection of data may provide a better understanding of the dependence of non-thermal density fluctuations on basic plasma parameters. Furthermore, attempts should also be made to measure the spectra of laser radiation scattered at

angles other than  $90^\circ$ , that is, to measure the scattered spectra corresponding to different scattering wave vector  $\underline{k}$ . From this, the dispersion properties of the observed non-thermal density fluctuations may be studied, which may also lead to a better understanding of wave propagation in plasmas.

## APPENDICES

### Appendix A - Rayleigh Scattering Calibration.

#### A-1 Density Measurement in the Density Monitoring Channel.

The intensity of Rayleigh scattered light measured in the density monitoring channel ( channel 3 ) is

$$I_R = N_R \sigma_R \int I_0(\omega) T_T(\omega) d\omega$$

where  $N_R$  is the total number of scattering centres,  $\sigma_R$  is the Rayleigh scattering cross section<sup>(60)</sup>,  $T_T(\omega)$  is the transmission profile of the channel and  $I_0(\omega)$  is the spectral distribution of the laser light defined as

$$I_0 = \int I_0(\omega) d\omega,$$

$I_0$  being the laser intensity.

As the spectral width of  $I_0(\omega)$  is much smaller than that of  $T_T(\omega)$ ,

$$\int I_0(\omega) d\omega \approx T_T(\lambda_0) \int I_0(\omega) d\omega$$

$$I_R = T_T(\lambda_0) N_R I_0$$

where  $T_T(\lambda_0)$  is the transmission of the channel at the laser



wavelength  $\lambda_0$ . Thus,

$$I_R = N_R \sigma_R T_T(\lambda_0) I_0$$

For Rayleigh scattering measurement on a gas of pressure  $P_0$  at temperature  $T_0$ ,

$$N_R = \left( \frac{P_0}{K T_0} \right) V_S$$

where  $K$  is the Boltzmann constant and  $V_S$  is the scattering volume. Hence,

$$I_R(P_0) = \left( \frac{P_0}{K T_0} \right) V_S \sigma_R T_T(\lambda_0) I_0$$

From Eq. (3-1), the intensity of Thomson scattered light measured in this channel is

$$I_T(\underline{k}) = n_e V_S \sigma_T I_0 T_T \int S(\underline{k}, \omega) \Psi_T(\omega) d\omega$$

Therefore,

$$\frac{I_T(\underline{k})}{I_R(P_0)} = \left( \frac{\sigma_T}{\sigma_R} \right) \left( \frac{K T_0}{P_0} \right) \left( \frac{T_T}{T_T(\lambda_0)} \right) n_e \int S(\underline{k}, \omega) \Psi_T(\omega) d\omega$$

whereby the electron density can be determined. For nitrogen gas<sup>(18)</sup>,  $(\sigma_R/\sigma_T)=380$ .

### A-2 Density Measurement in the Scanning Channels.

Following similar arguments described in the above section, the intensity of Rayleigh scattered light measured in each of the scanning channels 1 and 2 of the spectrometer system is

$$I_R(P_0) = \left(\frac{P_0}{KT_0}\right) V_s \sigma_R T_i(\lambda_0) I_0$$

where  $i=1,2$  and  $T_1(\lambda_0)$ ,  $T_2(\lambda_0)$  are respectively the transmissions of channel 1 and channel 2 at  $\lambda_0$ .

If the transmission of the channel remains constant throughout the spectral range of the Thomson scattered spectrum, the frequency integrated intensity in the electron spectrum is

$$I_e(\underline{k}) = n_e V_s \sigma_T I_0 T_i(\lambda_0) \int S_e(\underline{k}, \omega) d\omega$$

and using Eq. (2-17),

$$I_e(\underline{k}) = n_e V_s \sigma_T I_0 T_i(\lambda_0) \left(\frac{1}{1+\alpha^2}\right)$$

Hence,

$$\frac{I_e(\underline{k})}{I_R(P_0)} = \left(\frac{n_e}{1+\alpha^2}\right) \left(\frac{\sigma_R}{\sigma_T}\right) \left(\frac{P_0}{KT_0}\right)$$

and the electron density <sup>50</sup> can be determined from:

$$\eta_e = (1 + \alpha^2) \left( \frac{\sigma_T}{\sigma_R} \right) \left( \frac{K T_0}{P_0} \right) \left( \frac{I_e(k)}{I_R(P_0)} \right)$$

Appendix B. - The Scattered Spectrum for a Plasma with Non-Maxwellian Electron Velocity Distribution.

We wish to consider a plasma in which there exists, in addition to the background electron component, two secondary, drifting and cold electron components. Accordingly, we consider an electron distribution function of the form<sup>(32)</sup>:

$$f_e(\underline{v}) = (1-a-b)f_{e0}(\underline{v}) + af_{e1}(\underline{v}-\underline{v}_{D1}) + bf_{e2}(\underline{v}-\underline{v}_{D2})$$

where  $1 > a, b > 0$ .

$$f_{e0}(\underline{v}) = n_{e0} \left( \frac{m}{2\pi K T_{e0}} \right)^{3/2} \exp\left\{-\left(\frac{m}{2K T_{e0}}\right) \underline{v}^2\right\}$$

$$f_{e1}(\underline{v}-\underline{v}_{D1}) = n_{e1} \left( \frac{m}{2\pi K T_{e1}} \right)^{3/2} \exp\left\{-\left(\frac{m}{2K T_{e1}}\right) (\underline{v}-\underline{v}_{D1})^2\right\}$$

$$f_{e2}(\underline{v}-\underline{v}_{D2}) = n_{e2} \left( \frac{m}{2\pi K T_{e2}} \right)^{3/2} \exp\left\{-\left(\frac{m}{2K T_{e2}}\right) (\underline{v}-\underline{v}_{D2})^2\right\}$$

where  $\underline{v}_{D1}$ ,  $\underline{v}_{D2}$  are the drift velocities of the two secondary components;  $n_{e0}$ ,  $n_{e1}$ ,  $n_{e2}$  are the densities of the three components and  $T_{e0}$ ,  $T_{e1}$ ,  $T_{e2}$  are the temperatures of the components.

Using this form of  $f_e(\underline{v})$ , the screening integral  $G_e(\omega/k)$  can be written as<sup>(32)</sup>

$$G_e(\omega/k) = (1-a-b)G_{e0}(\omega/k) + aG_{e1}(\omega/k) + bG_{e2}(\omega/k)$$

where

$$G_{e0}(\omega/k) = \frac{4\pi e^2}{mk^2} \int \frac{\underline{k} \cdot \nabla_{\underline{v}} f_{e0}(\underline{v})}{\underline{k} \cdot \underline{v} - \omega} d\underline{v}$$

$$G_{e1}(\omega/k) = \frac{4\pi e^2}{mk^2} \int \frac{\underline{k} \cdot \nabla_{\underline{v}} f_{e1}(\underline{v}-\underline{v}_{D1})}{\underline{k} \cdot \underline{v} - \omega} d\underline{v}$$

and 
$$G_{e2}(\omega/k) = \frac{4\pi e^2}{mk^2} \int \frac{\underline{k} \cdot \nabla_{\underline{v}} f_{e2}(\underline{v}-\underline{v}_{D2})}{\underline{k} \cdot \underline{v} - \omega} d\underline{v}$$

Thus, the scattered spectrum  $S(k, \omega)$  can be calculated using Eq. (2-9).

## REFERENCES

1. S.E. Schwarz, Proc. IEEE 51, 1362 (1963).
2. T.H. Maiman, Nature 187, 495 (1960).
3. D.E. Evans and J. Katzenstein, Rep. Prog. Phys. 32, 207 (1969).
4. T.S. Brown and D.J. Rose, J. Appl. Phys. 37, 2709 (1966).
5. J.H. Williamson and M.E. Clark, J. Plasma Phys. 6, 211 (1971).
6. See, for example, D.F. Dubois and V. Gilinski, Phys. Rev. 133, 1317 (1964); M.S. Grewal, Phys. Rev. 134, A86 (1964).
7. V.C. Pineo, D.P. Hynek and G.H. Millman, J. Geophys. Res. 68, 2695 (1963).
8. L. Kellerer, Z. Phys. 239, 147 (1970).
9. D.E. Evans and P.G. Carolan, Phys. Rev. Lett. 25, 1605 (1970).
10. D.G. Carolan and D.E. Evans, Plasma Phys. 13, 974 (1971).
11. D. Ludwig and C. Mahn, Phys. Lett. 35A, 191 (1971).
12. D.E. Evans, M.J. Forrest and J. Katzenstein, Nature 212, 21 (1966).
13. J.P. Baconnet, G. Cesari, A. Coudeville and J.P. Watteau, Phys. Lett. 29A, 19 (1969).

14. J.P. Baconnet, G. Cesari, A. Coudeville and J.P. Watteau, Proc. Int. Conf. Ioniz. Phenomena Gases, 9th, Bucharest, Rumania, p643. Edituura Academic Republicii Socialiste Romania.
15. D.E. Evans and M.J. Forrest, Proc. Int. Conf. Ioniz. Phenomena Gases, 9th, Bucharest, Rumania, p646. Edituura Academic Republicii Socialiste Romania.
16. B. Kronast and Z.A. Pytrzk, Phys. Rev. Lett. 26, 67 (1971).
17. S.A. Ramsden, "Physics of Hot Plasmas", edited by B.J. Rye and J.C. Taylor, Plenum Press, New York, 1970, Chapter 3.
18. A.W. DeSilva and G.C. Goldenbaum, "Methods of Experimental Physics", 9A, edited by H.R. Griem and R.H. Lovberg ( Academic Press, New York, 1971 ) Chapter 3.
19. H.J. Kunze, "Plasma Diagnostics", edited by W. Lochte-Holtgreven, North Holland Publishing Company, Amsterdam, 1968, Chapter 9.
20. E.E. Salpeter, Phys. Rev. 120, 1528 (1960).
21. J.A. Fejer, Can. J. Phys. 38, 1114 (1960).
22. J.P. Dougherty and D.T. Farley, Proc. R. Soc. A 259, 79 (1960).
23. M.N. Rosenbluth and N. Rostoker, Phys. Fluids 5, 776 (1962).
24. I.B. Bernstein, S.K. Trehan and M.P. Weenink, Nucl. Fusion 4, 61 (1964).

25. D.E. Evans, M.J. Forrest and J. Katzenstein, Nature 211, 23 (1966).
26. R. Seimon and J. Benford, Phys. Fluids 12, 249 (1969).
27. H. Ringler and R.A. Nodwell, Phys. Lett. 29A, 151 (1969).
28. H. Ringler and R.A. Nodwell, Phys. Lett. 30A, 126 (1969).
29. D. Ludwig, C. Mahn, A. Eschlwech and P. Voigt, Plasma Phys. 16, 69 (1974).
30. C.R. Neufeld, Phys. Lett. 31A, 19 (1970).
31. J. Meyer and V. Potocnik, Phys. Lett. 45A, 129 (1973).
32. M.T. Churchland and R.A. Nodwell, Can. J. Phys. 52, 655 (1974).
33. A.M. Gondhalekar, B. Kronast and R. Benesch, Phys. Fluids 13, 2623 (1970).
34. P.K. John, J. Irisawa and K.H. Ng, Phys. Lett 36A, 277 (1971).
35. See, for example, J.D. Jackson, "Classical Electrodynamics", John Wiley & Sons, Inc., New York, 1962.
36. See, for example, D.K.C. MacDonald, "Noise and Fluctuations", New York, Wiley, 1962.
37. H.A.B. Bodin, T.S. Green, G.B.F. Niblett and N.J. Peacock, Proc. IV International Conference on Ionization Phenomenon in Gases, 1959, p1065.
38. See, for example, B.A. Lengyel, "Lasers", second edition, Wiley-Interscience, New York, 1971, Chapter 4.



39. See, for example, S.L. Marshall, "Laser Technology and Applications", McGraw-Hill, Inc., New York, 1968, Chapter 4.
40. R.G. Meyerand, Jr. and A.F. Haught, Phys. Rev. Lett. 11, 401 (1963).
41. For Fabry-Perot type multi-channel spectrometers, see: J.G. Hirschberg, J. Opt. Soc. Am. 50, 514 (1960); G.G. Shepherd, C.W. Lake, J.R. Miller and L.L. Cogger, App. Opt. 4, 267 (1965); M.J. Forrest, Culham Lab. Rept. CLM-P 116 (1966); P.K. John and K.H. Ng, J. Phys. E.: Sci. Instr. 5, 325 (1972).
42. For grating type multi-channel spectrometers, see: E. Glock, Pro. VII Int. Conf. Phen. Ionized Gases, Beograd, 1965, Gradevinska Publishing House, Beograd, Yugoslavia, Volume III, p194 (1966); A.D. Beach, J. Sci. Instrum. 44, 690 (1967).
43. S.A. Pollack, Appl. Opt. 5, 1749 (1966).
44. P. Jacquinet, J. Opt. Soc. Am. 44, 761 (1954).
45. R.C.A. 7265 Multiplier Phototube Data, Electron Tube Division, Harrison, N. J. (1958).
46. P.K. John and K.H. Ng, J. Phys. E: Sci. Instr. 5, 325 (1972).
47. Interference Filter 6948  $\text{\AA}$  Data Sheet, Corion Corporation, Holliston, Massachusetts.
48. R.H. Huddleston and S.L. Leonard, "Plasma Diagnostic Techniques", Academic Press, New York, 1965, Chapter 2.

49. See, for example, I.F. Kvartskhava, K.N. Kervalidze and Yu.S. Gvaladze, Sov. Phys. JETP 11, 1182L (1960), and T. Uchida, M. Sato and S. Hamada, Nuclear Fusion 2, 70 (1962).
50. R.H. Dixon, D.F. Duchs and R.C. Elton, Phys. Fluids 16, 1762 (1973).
51. W.H. Kegel, Phys. Lett. 29A, 681 (1969).
52. W.H. Kegel, Plasma Phys. 12, 295 (1970).
53. L. Spitzer, Jr., "Physics of Fully Ionized Gases", Interscience Publishers, New York, 1967, Chapter 5.
54. O. Theimer, Phys. Lett. 20, 639 (1966).
55. H. Rohr, Z. Phys. 209, 295 (1968).
56. M. Kato, Phys. Fluids 15, 460 (1972).
57. S. Ichimaru, "Basic Principles of Plasma Physics", W.A. Benjamin, Inc., Reading, Massachusetts, 1973, Chapter 8.
58. H.J. Kunze, Z. Naturf. A 20, 801 (1965).
59. J. Sheffield, "Plasma Scattering of Electromagnetic Radiation", Academic Press, New York, 1975, Chapter 4.
60. Lord Rayleigh, Phil. Mag. 47, 375 (1899).
61. D. Bohm and E.P. Gross, Phys. Rev. 75, 1851 (1949).
62. L. Landau, J. Phys. U.S.S.R. 10, 25 (1946).